CORTICAL AND SUBCORTICAL CORRELATES OF ORORHYTHMIC BEHAVIORS

BY

Meredith E. Estep

Submitted to the graduate degree program in Neuroscience
and the Graduate Faculty of the University of Kansas
in partial fulfillment of the requirements for the degree of
Doctor of Philosophy.

_____
Steven M. Barlow, Ph.D., Chairperson

Committee members*

_____*
Edward T. Auer, Ph.D.

_____*
Cary R. Savage, Ph.D.

_____*
Paul D. Cheney, Ph.D.

_____*
Jeffrey Searl, Ph.D.

Date Defended: December 2nd 2009

The Dissertation Committee for Meredith E. Estep certifies
that this is the approved version of the following dissertation:

CORTICAL AND SUBCORTICAL CORRELATES OF ORORHYTHMIC BEHAVIORS

Committee:

_____
Steven M. Barlow, Ph.D., Chairperson*

_____
Edward T. Auer, Ph.D.

_____
Cary R. Savage, Ph.D.

_____
Paul D. Cheney, Ph.D.

_____
Jeffrey Searl, Ph.D.

Date Approved: December 2nd 2009

CORTICAL AND SUBCORTICAL CORRELATES OF ORORHYTHMIC BEHAVIORS

Meredith E. Estep

Abstract. Although the healthy adult possesses a large repertoire of coordinative strategies for oromotor behaviors, a range of nonverbal, speech-like movements including cyclic jaw motion and lip pursing can be observed during speech. The extent of overlap among sensorimotor speech and nonspeech central neural correlates is unknown. The purpose of this study was to determine the spatial extent of unique and shared neural bases subserving task- and rate-specific ororhythmic behaviors utilizing a randomized block design fMRI study with an audiovisual motor stimulus paradigm to record neural correlates of suck and unvoiced syllabic speech performed at 1 or 3 Hz by a group of healthy adults. A functionally defined region of interest analysis provided (1) descriptive analysis of individual clusters, and (2) quantitative analysis of the extent of activation differences between conditions. Both factors (task and rate) were shown to significantly affect BOLD signal changes at the cortical, subcortical, and brainstem levels.

ACKNOWLEDGEMENTS

This work was supported in part by the National Institutes of Health grants (NIH R01 DC003311, NIH P30 HD02528, NIH P30 DC005803), University of Kansas (KU) General Research Fund, and the KU Research Fellowship Award. Access to facilities and equipment was made possible in part by the Hoglund Brain Imaging Center of the KU Medical Center in Kansas City, and the Perceptual Neuroscience Laboratory and Communication Neuroscience Laboratories on the KU campus in Lawrence, Kansas.

Particular appreciation is extended to the members of my dissertation committee and other faculty who have been particularly instrumental in my learning and development including, Steven M. Barlow PhD., Edward T. Auer PhD., Cary R. Savage PhD., Paul D. Cheney PhD., and Jeffrey Searl PhD. I am also grateful to members of the Communication Neuroscience Laboratories for their friendship and encouragement. I would also like to express gratitude to my family for their endless support and kind words.

My mentor briefly mentioned the following statement to me that has helped foster my motivation for a career in scientific research:

"Just remember, every day is important and offers something interesting."

-Dr. Steven M. Barlow

TABLE OF CONTENTS

LIST OF TABLES

LIST OF FIGURES

ABBREVIATION KEY

ACC……Anterior cingulate cortex

BGTC……....……Basal ganglia thalamocortical

BOLD…….Blood-oxygenation level dependent

CPG……Central pattern generator

FFX……. ……Fixed effects

fMRI…….. ……Functional magnetic resonance imaging

GLM……...……General linear model

GUI…….Graphical user interface

HDR ……..… Hemodynamic response

MI…….. Primary motor cortex

PD……...Parkinson's disease

RFX……Random effects

ROI ……Region of interest

SMA ……...Supplementary motor area

SPM ……Statistical parametric map

CHAPTER 1: INTRODUCTION

The brain has been studied using functional neuroimaging to provide insight into cortical, subcortical, and brainstem regions encoding sensorimotor mechanisms of healthy adult ororhythmic behaviors including mastication (Foki, Geissler, Gartus, Pahs, Deecke, et al., 2007) and speech production (Gracco, Tremblay, & Pike, 2005; Riecker, Wildgruber, Dogil, Grodd, & Ackermann, 2002). Identifying and making inferences about regionally specific effects in the healthy brain provide comparative measures for changes in brain functioning underlying clinical symptoms of sensory processing deficits of trigeminal afferent input (Kubina, Ristic, Weber, Stracke, Forster, et al., 2009; Obermann, Pleger, de Greiff, Stude, Kaube, et al., 2009; Stankewitz, Voit, Bingel, Peschke, & May, 2009) and motor deficits affecting rhythmic jaw, tongue, or lip movements (Foki et al., 2007; Hanakawa, Parikh, Bruno, & Hallett, 2005; Hesselmann, Sorger, Lasek, Guntinas-Lichius, Krug, et al., 2004). The present report provides data on the encoding of speech and nonspeech behaviors in the central nervous system among a group of healthy adults. The methods of this functional neuroimaging study were designed to be easily adapted for future investigations aimed at understanding how brain function is disrupted by damage or disease, reorganized by the emergence of adaptive processes, or plasticity and recovery as a function of sensorimotor rehabilitation.

Motivation for the current study was two-fold: (1) to contribute to our understanding of the role of neural correlates that are shared or unique among healthy adult ororhythmic behaviors, and (2) to initiate a comprehensive line of programmatic research in the functional connectivity of cortical-subcortical neural networks and brainstem pattern generators subserving human orofacial sensorimotor encoding.

Specific Aim

Assess the spatial extent of neural substrate that encodes the intersegmental rate (1 and 3 Hz) of speech (unvoiced /da/) and nonspeech (suck) ororhythmic tasks performed by healthy adults. Region of interest analysis was used for two purposes, including: (1) descriptive – individual cluster analyses, and (2) quantitative – areas that were differentially and commonly correlated across the two tasks and two rates were identified by general linear model (GLM) analyses and conjunction analysis.

Background, Significance, & Rationale

Central encoding & patterning of human ororhythmic behaviors

Muscles of the anterior oral cavity and lower face including lips, cheeks, and tongue are collectively referred to as 'orofacial musculature' and their movements are controlled by the central nervous system. Each muscle is innervated by a group of neurons projecting from a central motoneuron pool. For craniofacial muscles, the motoneuron pools are organized in columns (i.e., motor nuclei) within the brainstem and are critical control points in the motor system as they are the final common pathway for neural impulses to reach the orofacial muscles. Human ororhythmic behaviors rely on a combination of many different "driving" signals affecting the timing and amplitude of neural impulses sent to orofacial musculature for articulating speech (e.g., spoken, whispered, or silently mouthed phonemes) and nonspeech (e.g., suck, mastication, isolated tongue movements) behaviors.

Distinct cortical projections to the pontomedullary motor nuclei and periaqueductal gray of the brainstem reticular formation are hypothesized to play a role in producing speech and nonspeech behaviors (Corfield, Murphy, Josephs, Fink, Frackowiak, et al., 1999; Iriki, Nozaki, & Nakamura, 1988; Lund & Kolta, 2006a; Nozaki, Iriki, & Nakamura, 1986). Cortically originating signals are directly linked with brainstem motor nuclei by monosynaptic corticobulbar connections, or indirectly linked through polysynaptic interneuronal systems referred to as central pattern generators (CPGs). These premotor dynamic networks are (1) capable of producing rhythmic output and the basic features of ongoing behaviors, and (2) are responsive to both descending modulatory inputs and peripheral feedback systems that adapt the oromotor behavior to the state of the internal and external environments during simple speech tasks, mastication, and suck (Barlow, Lund, Estep, Kolta, 2010; Estep & Barlow, 2007; Hidaka, Morimoto, Masuda, Kato, Matsuo, et al., 1997; Lund & Kolta, 2006b; Takahashi, Miyamoto, Terao, & Yokohama, 2007; Zimmerman & Barlow, 2008).

Cerebral control systems utilize multiple CPGs at the brainstem level subserving a wide variety of periodic behavioral patterns and coordinating parts of integrated motor acts in mammals and lower vertebrates (Hamdy, Xue, Valdez, & Diamant, 2001; Menard, Auclair, Bourcier-Lucas, Grillner, & Dubuc, 2007; Menard & Grillner, 2008; Saitoh, Menard, & Grillner, 2007). While the mechanisms supporting the pattern generating circuitry for suck and mastication have been explored in animal and human studies (Iriki et al., 1988; Moore, Smith, & Ringel, 1988; Nakamura & Katakura, 1995), less is known of the role of CPGs in the sensorimotor control of speech production (Dronkers, 1996; Hickok, 2001; Wise, Green, Buchel, & Scott, 1999). The alternating movements of synergists driving certain speech movements are

hypothesized to benefit from dynamically assembled CPGs relegating portions of the patterned behavior to brainstem reticular nuclei and therefore reducing cortical load (Barlow & Estep, 2006; Lund & Kolta, 2006a).

Network flexibility & connectivity

Distributed networks are composed of anatomically and/or functionally connected cortico-cortical, cortico-subcortical-brainstem, and thalamocortical—brainstem motor areas (Grillner, Hellgren, Menard, Saitoh, & Wikstrom, 2005; Morecraft, Stilwell-Morecraft, & Rossing, 2004) that are temporally correlated or exert influence over one another in a variety of combinations and contexts. Variable connectivity patterns are facilitated by dynamic links of converging and diverging neural signaling mechanisms among brain regions. As a result, distributed networks are robust and provide a large repertoire of adaptive functional interactions among remote brain regions (Buchel & Friston, 2001; McIntosh, Rajah, & Lobaugh, 2003; Tononi, Sporns, & Edelman, 1999).

In the present context, the composition of a "network" is considered a plastic phenomenon manifest by the ability of neurons to not only modulate within a single network (Menard et al., 2007), but also fractionate and recombine with different CPGs (Grillner, 1991; Hooper & Moulins, 1989; Meyrand, Simmers, & Moulins, 1991, 1994). This flexibility allows for different muscle subgroups to cooperate in variable fashions to modify a motor pattern (Zelenin, Grillner, Orlovsky, & Deliagina, 2003) or produce more than one form of behavior (Islam, Zelenin, Orlovsky, Grillner, & Deliagina, 2006). More specifically, different sets of motoneurons can receive rhythmic synaptic inputs from common premotor (e.g.,

interneuronal/CPG) networks, resulting in behavioral modifications (Mentel, Cangiano, Grillner, & Buschges, 2008; Mentel, Krause, Pabst, El Manira, & Buschges, 2006). In agreement with this notion, elements of the masticatory CPG brainstem circuitry have been hypothesized to also participate in the control of human speech (Lund & Kolta, 2006a).

Motor control theories

Extensive connections between brain areas allow for the effective online control of limb and orofacial movement parameters. A functional-anatomic hierarchy exists across interconnected brain areas that are differentially recruited for limb action planning and movement execution (Grafton & Hamilton, 2007; Johnson-Frey, Newman-Norlund, & Grafton, 2005; Tunik, Rice, Hamilton, & Grafton, 2007), direction, and speed (Johnson & Ebner, 2000). The basal ganglia and cerebellum are integral components of interconnected loops (e.g., basal ganglia-thalamo-motor loop and cerebello-cerebral loop) that influence motor functions and monitor the rate of force change during rhythmic sequences of human limb movement (Hwang & Shadmehr, 2005; Pope, Wing, Praamstra, & Miall, 2005). Overall, the limb motor control literature supports the idea that a subset of areas is discretely activated to regulate kinematic parameters within a larger motor control network (Rocca, Gatti, Agosta, Tortorella, Riboldi, et al., 2007; Schaal, Sternad, Osu, & Kawato, 2004).

Similar to limb studies, the control of oromotor performance rate is thought to be subserved by interconnected brain areas (i.e., distributed networks including the cortex, basal ganglia, thalamus, and cerebellum) that are differentially recruited for aspects of speech preparation and execution processes (Bohland & Guenther, 2006; Rieker, Mathiak, Wildgruber,

Erb, Hertrich, et al., 2005) and nonspeech tasks (Dresel, Castrop, Haslinger, Wohlschlaeger, Hennenlotter, et al., 2005). Strong support for the existence of separate and distinct mechanisms for speech and nonspeech coordination in adults has been provided from biomechanical recordings and clinical findings that the coordinative organization of mature speech is distinct from that of any extant motor behavior or nonspeech precursor (Kent, Mitchell, & Sancier, 1991; Ostry & Munhall, 1994). Alternatively, the notion of an organizational hierarchy, similar to that described in the limb motor control literature, for oromotor behaviors is based on common coordinative organization and models of speech production that incorporate the function of CPGs (Grillner, 1981). It is yet to be functionally determined if a subset of areas within a larger network encodes the kinematics of speech and nonspeech behaviors.

These classic viewpoints (i.e., separate/unique vs. interconnected/shared neural substrates) and the notion of a flexible neural substrate hypothesized to produce variable pattern combinations are further defined below within the context of adult speech and nonspeech ororhythmic behaviors.

1. Functionally specific central control of speech and nonspeech behaviors

The notion of separate sensorimotor control mechanisms among speech and nonspeech motor acts (Weismer, 2006; Ziegler, 2003) is based on experimental observations of kinematic outputs including specific ensembles of muscles and joints (Kelso & Tuller, 1983; Moore et al., 1988; Tuller & Kelso, 1984). A speech motor control network has been hypothesized to be dedicated to generating motor control signals and/or processing sensory input including sensorimotor cortex, basal ganglia, thalamus, and inferior right cerebellum (Dronkers, 1996;

Riecker et al., 2005; Ziegler, 2002). Less is known of the networks encoding human nonspeech behaviors.

Related clinical research supports the notion that nonspeech orofacial kinetics provide little insight into the underlying physiology of neuromotor speech disorders such as dysarthria, and training on nonspeech oral behaviors may not be effective in enhancing speech production (McAuliffe, Ward, Murdoch, & Farrell, 2005; Solomon, Robin, & Luschei, 2000; Weismer, 2006). Functional neuroimaging research of human speech and nonspeech central motor control may provide insight to why nonverbal therapies often do not facilitate speech recovery (Dworkin, Abkarian, & Johns, 1988) or inform the bases of motor speech disorders (Ziegler, 2003).

2. Common coordinative organization across speech and nonspeech behaviors

Clinical applications of nonspeech tasks that closely mimic actual speech movements for assisting in diagnosis of neurologic disease have been supported (Ballard, Robin, & Folkins, 2003; Folkins, Moon, Luschei, Robin, Tye-Murray, et al., 1995) on the basis of speech being encoded by a broader network of brain regions than nonspeech behaviors (Clark, 2003; Donnan, Carey, & Saling, 1999; Ray, 2003). Human verbal utterances are subserved by motor pathways including: (1) extensive connections among frontal lobe areas, basal ganglia, and cerebellum (cortico – subcortical loops), and (2) monosynaptic connections from frontal motor areas to brainstem cranial nuclei (Jurgens, 2002; Kuypers, 1958). This latter motor pathway is thought to heavily influence the fast articulatory gestures of human speech production. It is further

assumed that the coordinative organization afforded by these neural circuits would be beneficial for both speech and nonspeech behaviors.

3. Basic motor infrastructure with variable and interactive pattern combinations

Grillner and Wallen (2004) have proposed that the majority of voluntary motor tasks are derived from the same general motor infrastructure that is flexible and subject to learning. A basic motor infrastructure that is parsed for different behaviors could encompass an extensively variable behavioral repertoire. In support of this notion are findings that corticospinal systems used for accurate positioning of the limb during locomotion involve circuits overlapping with those used during reaching in the cat (Drew, 1993; Drew, Prentice, & Schepens, 2004) and nonhuman primates (Grillner, Georgopoulos, & Jordan, 1997).

The notion of motor systems being interactive and hierarchical implies, (1) a large range of substrate flexibility for pattern combinations, and (2) varying levels of control for numerous behaviors based on relatively stereotyped motor patterns. For example, volitional swallowing can be modified only to a limited degree, while chewing is extremely adaptive and modifiable through learning. Flexibility of neural substrate is hypothesized to enable variable movement-pattern combinations for speech production (Grillner & Wallen, 2004), such as the differential lip and tongue movements utilized to achieve different lingual-alveolar tasks (McGuigan & Winstead, 1974). The reliance of speech and nonspeech behaviors on shared neurophysiologic infrastructure (i.e., shared musculoskeletal systems and flexible neural connectivity) supports the notion of an organizational hierarchy based on a common coordinative framework of ororhythmic behaviors.

Health relevance

Assessing healthy brain activity correlated to specific oromotor kinematics is a significant first step to understanding abnormalities such as slowness associated with a variety of central motor disorders resulting from cerebral stroke, cerebral palsy associated with hypoxic ischemic injury, cerebellar infarcts and disease, or Parkinson's disease (PD). These patients often have difficulty initiating speech, progressing through an utterance or switching from one utterance to another (Ackermann, Grönem, Hoch, & Schönle, 1993; Spencer & Rogers, 2005; Svensson, Henningson, & Karlsson, 1993). Specific timing deficits include, delayed initiation of speech articulatory gestures in apraxia of speech (Ziegler & von Cramon, 1986a,b), decreased syllable repetition rates and/or increased syllable duration are demonstrated in patients with chorea (Ziegler & von Cramon, 1986c), spastic dysarthria (Ludlow, Connor, & Bassich, 1987), and dysarthria related to cerebellar syndromes (Ackermann, Hertrich, & Hehr, 1995; Duffy, 2005; Gentil, 1990).

Dysfunction between various components of the central motor system such as the frontoponto-cerebellar pathways (Ackermann, 2008; Ackermann, Mathiak, & Ricker, 2007; Alexander, Naeser, & Palumbo, 1990; Kent, Duffy, Slama, Kent, & Clift, 2001), corticobulbar tracts (Lo & Ratnagopal, 2007), basal ganglia interconnections (Caligiuri, 1987; Ciucci, Barkmeier-Kraemer, & Sherman, 2008; Forrest, Weismer, & Turner, 1989), and loops between basal ganglia and cerebellum (Garraux, McKinney, Wu, Kansaku, Nolte, et al. 2005; Middleton & Strick, 2000; Taniwaki, Okayama, Yoshiura, Togao, Nakamura, et al., 2006) rather than abnormalities within areas may give rise to different articulatory system deficits in different patient populations (Ackermann et al., 1993, 1995).

Brain lesions localized near the left face representation of primary motor cortex can result in severe dysarthria (slow, effortful speech, lacking normal prosody), with only mild deficits in tongue movement (Terao, Ugawa, Yamamoto, Sakurai, Masumoto, et al., 2007). Apraxia of speech has been clinically demonstrated to manifest slowing of speech that is not correlated to nonspeech behavior rate. Such observations imply apraxia of speech may affect the control of speech rate at variable degrees, while nonspeech faculties can remain relatively unimpaired (Ricci, Magarelli, Todino, Bianchini, Calandriello, et al., 2008; Ziegler, 2002) or impaired (Hageman, Robin, Moon, & Folkins, 1994; McNeil & Kent, 1990).

It remains unclear to what extent task-specific oromotor performances share central neural circuitry and the extent they utilize different physiological mechanisms for different tasks. Study of common and task-specific central activations correlated to the healthy encoding of speech and nonspeech movements may provide insight to why some lesions and diseases differentially affect oromotor performances. Functional neuroimaging studies of both healthy and clinical populations offer an approach to better understand the central mechanisms encoding oromotor kinematics, functional connectivity of neural networks subserving oromotor behaviors, and have the potential to provide greater precision in diagnoses and guidance for more effective oromotor therapy techniques.

Perspectives from functional neuroimaging studies

From a neuroimaging viewpoint, functional activations correlated with speaking are likely to at least partially overlap with correlates of nonspeech motor control. Commonalities and differences in neural activity correlated with speech and nonspeech behaviors (Bonilha,

Moser, Rorden, Baylis, & Fridriksson, 2006; Kimura & Watson, 1989; Terumitsu, Fujii, Suzuki, Kwee, & Nakada, 2006) support the notion of widely separated brain regions with temporally correlated activity as interdependent substrates that can be modulated with changes in task demands (Greicius, Supekar, Menon, & Dougherty, 2008; Haughton & Biswal, 1998; Lowe, Dzemidzic, Lurito, Mathews, & Phillips, 2000). Increased stimulus or task complexity engages the speech production system by recruiting areas beyond the primary sensorimotor cortices that are involved in nonspeech motor sequencing (e.g., left hemisphere inferior frontal sulcus and posterior parietal cortex, as well as bilateral anterior insula and frontal operculum, the basal ganglia, thalamus, and cerebellum). The recruitment of additional brain regions is presumably due to increased neural demand (Bohland & Guenther, 2006; Guenther, 2006; Guenther, Ghosh, & Tourville, 2006; Soros, Sokoloff, Bose, McIntosh, Graham, et al., 2006).

Functional MRI studies have provided observations of distributed oromotor networks activated by speech and nonspeech tasks such as speaking a single syllable (Riecker, Ackermann, Wildgruber, Meyer, Dogil, et al., 2000), syllable trains produced at different frequencies (Riecker et al., 2005), whistling (Dresel et al., 2005), and opening the mouth altered with protruding the lips (Soros et al., 2006). The notion of bilateral cortical representation of midline muscles engaged in oromotor behaviors (Muellbacher, Artner, & Mamoli, 1999) is supported by consistent findings of bilateral activation in the face area of primary motor cortex (MI) and supplementary motor area (SMA) correlated with speech production (Murphy, Corfield, Guz, Fink, Wise, et al., 1997; Riecker et al., 2005) and orofacial movements (Dresel et al., 2005; Soros et al., 2006). Similarly, a bilateral network of cortical (sensorimotor, SMA, insula) and subcortical (thalamus, cerebellum) have been indicated in studies of nonspeech

including tongue movement (Corfield et al., 1999; Hesselmann et al., 2004; Komisaruk, Mosier, Liu, Criminale, Zaborszky, et al., 2002; Salmelin & Sams, 2002) and mastication (Onozuka, Fujita, Watanabe, Hirano, Niwa, et al., 2002). Bilateral brainstem nuclei show increased activation correlated with smiling and lip puckering (facial nuclei, Komisaruk et al., 2002) and tongue movement (hypoglossal nuclei, Corfield et al., 1999; Komisaruk et al., 2002). To our knowledge, no published functional imaging studies exist that have been designed to investigate the correlates of suck in humans.

The sequential and temporal encoding of orofacial articulators are critical to fluent oromotor performances. Auditory and somatosensory feedback engage a complex network of cortical and subcortical areas that are presumed to continuously evaluate the quality of speech output and update the speech motor plan (Levelt, 1989; Schiller, 2005). Task dynamics and complexity reveals differential patterns of brain activation. For example, increases in regional activation of bilateral medial premotor areas including SMA and cingulate correlated with the encoding and articulation of syllable sequences (Alario, Chainay, Lehericy, & Cohen, 2006). Bilateral activation of the cerebellar hemispheres, left-lateralized anterior insula, and posterior inferior temporal gyrus is correlated with encoding subsyllabic aspects of verbal utterances such as onset complexity (e.g., CCV versus CV, Riecker, Brendel, Ziegler, Erb, & Ackermann, 2008). Bilateral activation of medial premotor areas and basal ganglia is correlated with complex syllable sequences (Bohland & Guenther, 2006) and is attributed to greater task demands and the monitoring of potential response errors (Fu, Morgan, Suckling, Williams, Andrew, et al., 2002). Detection and correction of speech production errors is hypothesized to rely on general performance monitoring instead of a language-specific process (Ganushchak & Schiller, 2006;

Hartsuiker & Kolk, 2001; Holroyd & Coles, 2002; Masaki, Tanaka, Takasawa, & Yamazaki, 2001; Schiller, 2005).

The complexity of a verbal task can be modified by increasing the difficulty of syllable sequences or syllable composition. The former experimental manipulation performed by Bohland and Guenther (2006) resulted in increased bilateral activity in cerebellum, thalamus, basal ganglia, and frontal operculum, left-lateralized activity in premotor and prefrontal areas and extending along the inferior frontal sulcus, anterior insula, posterior parietal lobe, and inferior posterior temporal lobes. Right-lateralized activity correlated to more complex syllable sequences includes the right inferior cerebellum (Bohland & Guenther, 2006). Other investigators have demonstrated the effect of altering the syllabic composition. Simple tasks such as speaking a single vowel are correlated with posterior paravermal activation. Encoding accurate timing of more complex polysyllabic utterances is correlated with activity in the anterior paravermal region, left cerebellar lobe, left caudate, and right putamen (Garraux et al., 2005; Soros et al., 2006).

Functional neuroimaging study design considerations

1. Challenges to imaging oromotor behaviors

When designing a neuroimaging study of oromotor behaviors, head and jaw movements of overt responses must be carefully managed (Birn, Bandettini, Cox, & Shaker, 1999; Gracco et al., 2005; Munhall, 2001). Decreased signal-to-noise ratio and anatomical distortions may result from orofacial movements occurring while the scanner is collecting data. Movement during overt articulation and the effects of background scanner noise introduce potentially confounding

effects on activation (Birn, Bandettini, Cox, Jesmanowicz, & Shaker, 1998). Researchers have avoided such artifacts by switching off the gradients during periods of movement and then switching them back on for image acquisition.

The innovative clustered sequence (Eden, Joseph, Brown, Brown, & Zeffiro, 1999; Edmister, Talavage, Ledden, & Weisskoff, 1999; Hall, Haggard, Akeroyd, Palmer, Summerfield, et al., 1999) allows for oromotor tasks to be performed within 'silent' intervals between image acquisitions, and therefore, while the participant is not moving (Gracco et al., 2005; Rimol, Specht, Weis, Savoy, & Hugdahl, 2005). This sequence capitalizes on the sluggish hemodynamic response (HDR) that is delayed by ~2 seconds following stimuli onset, peaks ~3 to 5 seconds after stimulus onset for a single event (Glover, 1999), and is delayed ~2 seconds after the offset for ongoing behaviors (Frackowiak, Friston, Frith, Dolan, & Mazziotta, 1997; Riecker et al., 2005). In relation to repetitive oromotor movements, a 5 second offset (Birn, Cox, & Bandettini, 2004; Handwerker, Ollinger, & D'Esposito, 2004) between oromotor response and the midpoint of data acquisition are appropriate to detect blood-oxygen level dependent (BOLD) signal changes that are indirectly linked to brain activity, at the peak or close to the peak of the HDR curve (Soros et al., 2006).

2. Designing appropriate task and baseline conditions

Functional MRI experimental design involves the manipulation of selected tasks to maximally detect the neuronal process of interest while minimizing non-task related variance that may influence or affect that process of interest. Blocked designs are most efficient for estimating the size of the HDR and appropriate selection of tasks, such as parametrically varying task difficulty, increases the reliability of correctly estimating the HDR function. Appropriate baseline conditions are hypothesized to activate all but the processes of interest. Any implicit processing occurring in the baseline task reduces the difference between the activation task and the baseline task (Price, Wise, & Frackowiak, 1996).

The goal of the current investigation is to characterize the neural activity correlated with task and rate encoding of ororhythmic control. The selected speech task is an unvoiced /da/ (to minimize auditory feedback and somatosensory feedback, and sensorimotor control associated with vocal fold vibration) and the nonspeech task is Suck, both cued visually. The rhythmic performance rate of 1 Hz or 3 Hz is cued by repetitive audio click. During the baseline condition the participant simply observes the audiovisual stimuli while not performing any ororhythmic task. To compare each of the four experimental states (Suck 1 Hz; Suck 3 Hz; Unvoiced /da/ 1 Hz; Unvoiced /da/ 3 Hz) to a baseline state within one simple model, we chose Listen 1 Hz + Listen 3 Hz as the baseline condition from which to compare the experimental conditions collapsed across task (e.g., Suck 1 Hz + Suck 3 Hz > Listen 1 Hz + Listen 3 Hz) or rate (e.g., Suck 1 Hz + Unvoiced /da/ 1 Hz > Listen 1 Hz + Listen 3 Hz).

3. Analytical approaches to fMRI data

Statistical analyses based on GLM principles address the BOLD signal in terms of both intensity and spatial extent of regional activation. This method accounts for the predicted response of one paired comparison relative to another and sources of non-task related variability. GLM based statistical analyses allow for flexibility in modeling the predicted signal response attributed to the experimental task while removing effects of no interest. The basic equation is $Y = XM + \varepsilon$ where Y is the acquired time-series data; X is the design matrix which models the independent variables (i.e., explanatory variables); M is the vector of parameter estimates representing contrasting explanatory variables to estimate predicted response amplitude; and ε is the residual variance in the data not explained in the model.

Two GLM statistical approaches commonly used to analyze fMRI data treat the subject variable as either a fixed effect or a random effect. Fixed effects (FFX) analyses have a large number of degrees of freedom resulting in artificially high detection ability (i.e., power or sensitivity), but do not take into account the between-subject variability and thus inferences are limited to only those subjects chosen for the analysis. In the present study, FFX GLM was used for single-subject analyses to collapse multiple runs of one participant into one data set. Because the FFX activation maps do not allow inferences about the population and require additional validation due to their sensitivity to extreme effects, Random effects (RFX) analyses are used for group-level analyses.

RFX analyses provide more reliable results and take into account sampling variability (i.e., between-subject variability), allowing inferences about the population from which the subjects were drawn to be made. The RFX multi – study design matrix is constructed from a

series of single – study design matrices that are based on separate sets of predictors for each subject. The RFX approach has become a standard in fMRI analysis and was used in the present study to collapse across participants at the group level of analysis. Conservative estimates of sample size for RFX analysis of fMRI experiments indicate that 80% power can be achieved using a threshold of 0.05 with approximately 10 subjects (Desmond & Glover, 2002).

Results are displayed by plotting the mean signal time courses of the most significant voxel detected within each BOLD cluster. It should be noted that plotting the signal of only the most significant voxel within the cluster is expected to improve between group differences, but may not represent the cluster region well. For this reason, average BOLD signal characteristics are provided in table format for each activated cluster.

4. Voxel-wise time series analysis & statistical threshold selection

In a typical fMRI data analysis, signal from the task condition and signal from the baseline condition are averaged separately and then compared to determine if the two conditions are significantly different. A test statistic (e.g., t-statistic) relating to the magnitude of contrast between conditions is then computed per voxel. The overall results of the statistical tests of the GLM at each voxel across the entire image volume are presented as a statistical parametric map (SPM), which is color coded based on a threshold criterion. SPM threshold selection is arbitrary when evaluating across the whole image volume and there is currently no agreed consensus how to best threshold a statistical map.

The goal of the current investigation was to detect the overall pattern and spatial extent of activation correlated with ororhythmic behaviors in a group of healthy adult participants. First, a

whole-brain mapping approach was implemented to provide insight to our hypothesis of activated regions at the cortical, subcortical, and brainstem levels. Next, a pontomedullary brainstem mask was created by segmenting the participants' high resolution anatomical image volumes to separately investigate the voxel time courses from a smaller area (compared to whole – brain mapping approach) in order to increase statistical power and spatial correspondency across subjects. This separate analysis was motivated by the knowledge that, (1) there is high anatomical variability in brainstem anatomy and functional localization of brainstem sensorimotor nuclei, and (2) region of interest (ROI) analyses are statistically more powerful than evaluating across the whole brain.

It is important to note the disadvantages of ROI analysis include, (1) demarcating regions can be subjective, and (2) only pre-selected regions are evaluated and other task-relevant regions may be missed. Our brainstem mask was demarcated using prominent anatomical landmarks identified across subjects and in order to not downplay the role of other coactivated areas by narrowly focusing on the pre-selected mask we are performing this analysis after the whole-brain analysis.

Summary & Area in the Literature this Study was Intended to Enhance

Recent studies have shown healthy speakers to demonstrate common and unique activations between repeated nonspeech oral movements and syllabic speech behaviors (Bonilha et al., 2006; Terumitsu et al., 2006). These studies suggest that at the syllable production level, there are commonalities and differences in the neural substrates involved in speech and nonspeech oral behaviors. It is generally accepted that rate is an appropriate outcome measure for examining the relations between changes in oromotor function and brain function (Ludlow, Hoit, Kent, Ramig, Shrivastav, et al., 2008). This parameter is especially relevant to studies of ororhythmic control as differential deficits in oromotor timing are have been identified across various central motor disorders (Ricci et al., 2008; Terao et al., 2007). Few studies have incorporated rate as a variable associated with the dynamic functional organization of the cortico – subcortical loops related to speech and nonspeech movements with similar kinetics.

To our knowledge, there are no published accounts of fMRI investigations of suck and unvoiced syllabic speech performed at varying rates. In this investigation of the putative neural subsystems that encode the intersegmental rate of ororhythmic tasks, suck and unvoiced syllabic speech (/da/) were chosen as the nonspeech and speech tasks (based on their similar kinetics) to be performed by participants. Our overarching contribution to the literature regards the extent of common and unique brain substrates involved in kinematic parameter encoding (specifically, intersegmental rate) of healthy adult speech and nonspeech behaviors. Our findings will be discussed in context of what is known of the spatial and networking attributes of the neural substrate responsible for oromotor control.

Overall purpose

To identify and assess the task-specific network activations and modulations among cortical and subcortical regions encoding intersegmental rate of ororhythmic (suck and unvoiced syllabic speech) behaviors of healthy adults *in vivo.*

Salient measures

Cortical and subcortical neural activations were measured by the BOLD signal intensity based on the HDR function over time. We were looking for differences in regional brain activity (magnitude and spread) between tasks in addition to looking for either an overlap of activation maps across conditions *or* condition-specific differences in temporal correlations of activated brain regions.

CHAPTER 2: METHOD

Formal Hypothesis

H_0: The spatial extent of active neural substrate among cortical and subcortical structures which encodes the rate of unvoiced syllabic speech is a subset of neural resources that also drive functional synergies involved in the production of suck.

H_A: The spatial extent of active neural substrate among cortical and subcortical structures which encodes the rate of unvoiced syllabic speech does not utilize shared neural resources that also drive some of the functional synergies involved in the production of suck.

Study Design: Multifactorial, Repeated-Measures

Due to the nature of the fMRI signal (no absolute zero point), repeated- measures designs are often implemented to increase the precision for comparing condition effects. One advantage of this study design is the ability to exclude between-subjects variability from the experimental error. This is achieved by having each subject serve as their own control. Independent repetition and randomization of the order of conditions for each participant minimizes interference effects that could arise in the situation of having specified placements within the condition presentation order. At the random-effects level, i.e. group – level statistical analysis, these issues are

assumed to be solved since the data is collapsed for each condition at the first – level statistical analysis.

The multifactorial, repeated-measures design of the current study consisted of two experimental factors and one group of healthy adult participants. Each participant received all experimental conditions in an order specified by random permutation. Two within-subjects factors: task (2 conditions: Suck or Unvoiced /da/, cued by words presented visually) and rate (2 conditions: 1 Hz or 3 Hz, cued by auditory click sounds) were simultaneously investigated to obtain information about their combined effects on the fMRI BOLD signal in cortical, subcortical, and brainstem regions. All combinations of the factor levels were included in this 2 x 2 = 4 factor-level study (i.e. Suck 1 Hz, Suck 3 Hz, Unvoiced /da/ 1 Hz, Unvoiced /da/ 3 Hz). An audiovisual baseline was created by presenting the word 'Listen' with the 1 Hz or 3 Hz click sound (2 baseline conditions: Listen 1 Hz or Listen 3 Hz). This baseline condition was designed to provide stimuli that match the experimental condition stimuli without cueing the participant to move. It was of interest if the main effects of both task and rate factors explained changes in the dependent variable (i.e., percent signal change in fMRI BOLD response).

Hardware & Software Engineering

To record the participant's ororhythmic pneumatic compression gestures, a silicone pacifier was secured orally at midline and instrumented with a 1/8" ID polyethylene tube (orange line) with pressure transducer (Honeywell, 1 psi full scale) input to the data acquisition system (-3dB LP f_c @ 50 Hz, 200 sps, 16-bits, P_{cal}: 10 cmH_2O = 1.18 volts, full compression = 40 cmH_2O) (Figure 1, p. 25). A software application developed using LabVIEW 8.6 provided a graphical user interface (GUI), and real-time target and recording of nipple compression pressure in cmH_2O. A Pentium 4 computer equipped with a National Instruments PCI 6052E multifunction DAQ was used to sample pacifier nipple compression pressure. This provided a record of changes in the nipple cylinder intraluminal pressure produced during the participant's pneumatic compression gestures cued by audiovisual stimuli. To ensure subject compliance, the investigator monitored the audiovisual stimuli and real-time pacifier nipple compression pressure signal recording of the participant's ongoing performance via PC outside of the MRI suite.

The software presented audio and visual stimuli to cue the rate (1 Hz or 3 Hz) and task (Suck or Unvoiced /da/) of the participant's ororhythmic mouthing movements, respectively. To deliver the audiovisual stimuli to the participant, audio and video cables connected the investigator's PC to the LCD projector and participant's earphones, respectively. Audio cues were generated by DAC0, amplified and delivered through MR compatible ear buds. For verification purposes, each time an audio cue waveform was generated, a pulse was sent from DAC1 as analog input to ACH3 (Figure 1, p. 25). The real-time pressure signal was displayed with the LCD projector to both the participant and investigator only during the practice session

(detailed in the following section). During the scanning session (detailed in the following section), the stimulus presentation window computer XVGA graphics interface to a back-display projector to present visual stimuli (words only, not real-time pressure signal) to the participant positioned within the bore of the scanner.

Two behavioral recording sessions constituted an entire study session. During the practice session, a pacifier positioned in the participant's mouth provided input to channel 1 of a model 225 bridge amplifier (Biocommunication Electronics, LLC) with gain of 2000, lowpass filter cutoff at 50 Hz, and DC coupled. The practice session compression signal was then output to analog input channel 1 on a BNC-2090 (National Instruments) break-out box. The trigger pulse for initiating the software was generated by the break-out box digital output and input to the trigger input (PFi0/TRIG1) during the practice session. During the experiment session, a pacifier positioned in the participant's mouth provided input to analog channel 2 of the bridge amplifier with identical gain, lowpass filter, and coupling as used for channel 1 during the practice session. The experiment session compression signal was then output to analog channel 2 on the break-out box. An optical pulse trigger originating from the scanner was input to the synchronization box and sent to the break-out box trigger input (PFi0/TRIG1) during the experiment session.

Figure 1. Hardware connections for software initiation and pneumatic compression signal reception/amplification

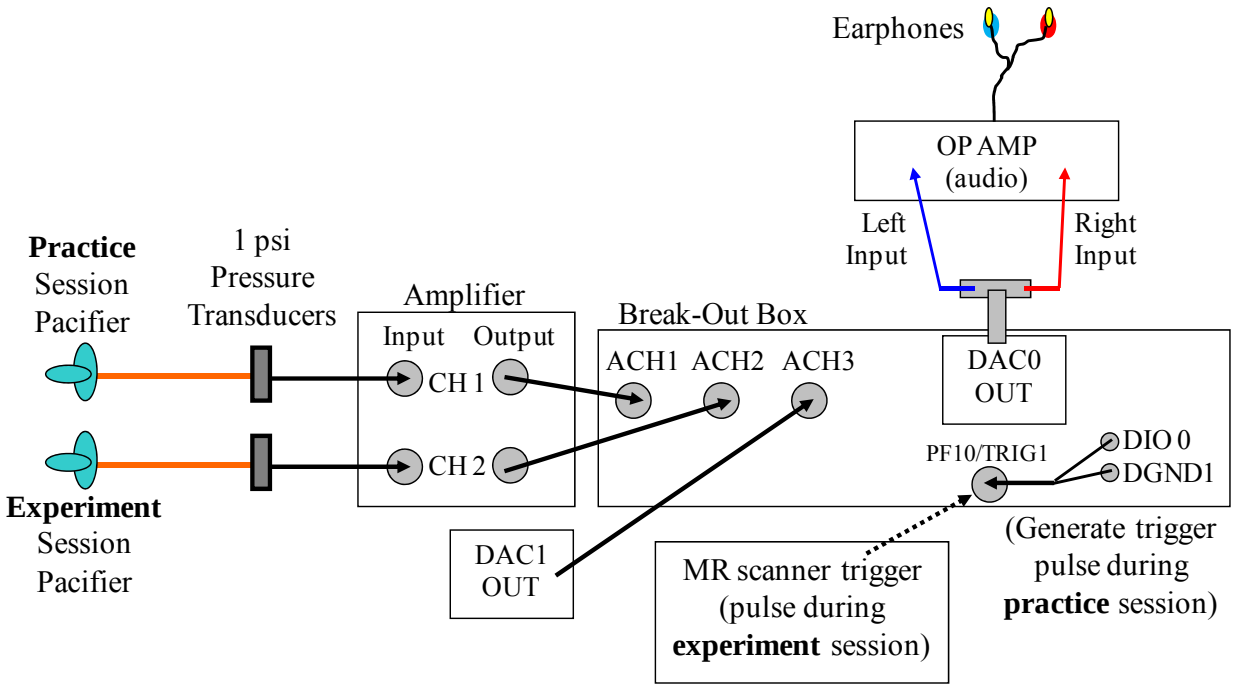

Participants, Practice Session & Experimental Session

Written informed consent was obtained prior to enrollment in the study. Each participant was informed of the purpose and duration of the study, and took part in the required practice session before allowed to enter the MRI suite and participate in the neuroimaging session (i.e., experimental session). Participants were right-handed (based on the Edinburgh Handedness Inventory, average score = +85.1) male and female adults (N=10, 5 females) between the ages of 20-35 years (mean age = 25.95 years) who had no known neuropsychiatric or speech disorders, or abnormal findings on physical examinations.

The required practice session took place in a consultation room outside of the MR scanner suite. The purpose of the practice session was to allow each participant to become familiar with the tasks and rates they would be instructed to perform while in the scanner if they proved to be eligible for the experimental session. A sterile silicone Soothie™ pacifier was positioned in the participant's mouth at midline and connected to the data acquisition system. The audiovisual stimuli were presented via PC to the investigator and the participant. Unique to the practice session, a visual feedback graphic showed the compression signal rise and fall in accordance with the participant's mouthing movements. This graphic was used to demonstrate to the participant the effect of their mouthing movements. The investigator discouraged the participant from performing tongue movements or jaw/teeth clenching unrelated to the ororhythmic tasks.

During the practice session, the investigator described the articulations related to each task to the participant using the following statements: "your goal is to match the rate of your

repetitive suck or unvoiced /da/ oral movements with the rate of the clicking sound. For the suck task, strip the tip of your tongue along the length of the nipple cylinder while creating negative intra-oral pressure with your upper and lower lips sealed around the base of the pacifier shield. For the unvoiced /da/ task, mouth the word 'da' as if you are trying to silently communicate with someone across the room. For the listen task, simply listen to the audio cues. When you see the word STOP, you are to complete any mouthing movement you may have already begun, and remain still." The participant was visually primed for the upcoming task by the words "SUCK" (to cue the suck task), "DA" (to cue the unvoiced /da/ task) or "LISTEN" (to cue the control condition). The onset of task performance was signaled by the word "GO" accompanied by the auditory cue (1 Hz or 3 Hz click sound, approximately 50 msec in duration) delivered by MR-compatible ear buds to signal the rate at which the participant was to perform the visually cued task. This resulted in four task conditions (Suck 1 Hz; Suck 3 Hz; Unvoiced /da/ 1 Hz; Unvoiced /da/ 3 Hz) and two control conditions (Listen 1 Hz; Listen 3 Hz) randomly cued throughout each practice session.

Following the practice session, the investigator evaluated the digitized pneumatic compression signal to determine if the participant was eligible to participate in the experimental session. Participants who demonstrated suck- and unvoiced /da/ - related pneumatic compressions reaching 25% of full nipple compression (i.e., 10 cmH_2O), 2 – 4 gestures within the 3.25 second epoch for the 1 Hz condition and 6 – 10 gestures within the 3.25 second epoch for the 3 Hz condition were deemed eligible to participate in the following experimental session. If the participant failed to achieve satisfactory performance, s/he was not eligible to participate in the following experimental session.

Prior to the experimental session, eligible participants were interviewed by an MRI technologist regarding routine questions associated with safety screening, general health status, and the duration of the data acquisition runs. Once all questions had been addressed, a sterile silicone pacifier was positioned orally at midline and the MRI-compatible earbuds were inserted into the participant's right and left ear canals. The MRI technologist assisted the participant into the MRI suite and onto the scanner bed (supine). Circumaural muffs with attached microphone were then placed over the participant's ears for added protection and to allow two-way communication between the participant in the scanner and the investigator and MRI technologist outside of the scanner suite. MRI standard foam padding was used to restrict major head movements. After the participant confirmed they could see the visual cues on the back-projector and hear the audio cues delivered through the ear buds, the scanner bed was positioned in the scanner.

During the scanning period, the participant was instructed to perform the cued ororhythmic tasks as they had during the practice session, but without the visual feedback of their compression signal. While lying in the MR scanner, the participant was presented with visual (words only) and audio stimuli via back-projector and MR-compatible ear buds, respectively. The four task conditions (Suck 1 Hz; Suck 3 Hz; Unvoiced /da/ 1 Hz; Unvoiced /da/ 3 Hz) and two control conditions (Listen 1 Hz; Listen 3 Hz) were randomized across participants to avoid confounding order effects. The control conditions allowed us to subtract the audiovisual stimuli effects from the motor conditions during the analysis stage.

Synchronized Neuroimaging Data Acquisition & Stimuli Presentation

The software allowed the investigator to develop a series of randomized block design neuroimaging protocols synchronized to an optical pulse produced peripherally by the Siemens Allegra 3T scanner prior to each sparse sampling volume acquisition (i.e., one brain volume recorded per optical pulse). The pulse triggered the initiation of the audiovisual stimuli for the upcoming block and allowed for real-time and post-experiment segmentation of the nipple compression pressure, visual cues, and audio waveforms that were acquired continuously starting from the first synchronization pulse and ending approximately 10 seconds after the last synchronization pulse. Each block (Figure 2, p. 30) was a total of 10 seconds in duration and contained a 3 second sparse sampling volume acquisition and a 7 second silent interval in which the participant was cued by audiovisual stimuli via MR compatible earbuds and back-projector, respectively, to perform an ororhythmic task for 3.25 seconds. To avoid movement artifact, participants were cued to perform the behavioral tasks during the silent interval and then instructed to remain completely still for the duration of the sparse sampling volume acquisition. The onset of movement was cued 5.5 seconds prior to the midpoint of the data acquisition in order to time the data acquisition to the evolution of the peak HDR (Handwerker et al., 2004).

Figure 2. Example of one experimental block

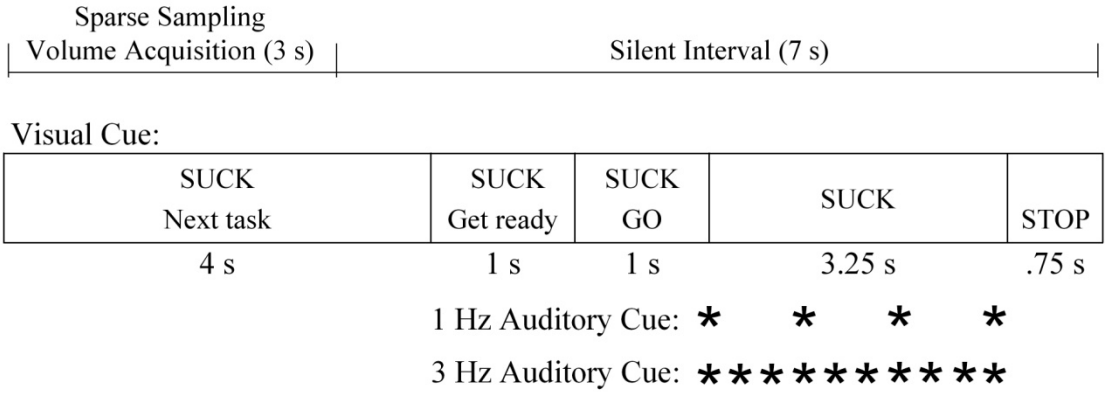

The anatomical scanning was done with a T1-weighted MPRAGE pulse sequence (208 slices). Sparse sampling was used to acquire the functional data set of 85 BOLD EPI measurements (brain volumes) per run. Each brain volume consisted of 35 axial slices at the voxel resolution of 3.75 x 3.75 x 3.00 mm^3 and 0.5 mm gap, TR=10 s (delay TR=7 s), TE=30 ms, interslice time = 78 ms, interleaved slice order, field of view = 240, matrix size = 64. To avoid T_1 –saturation effects, the first two brain volumes were dropped from the set of saved functional data and were not counted in the 85 BOLD EPI measurements. Because one brain volume was recorded following the completion of each condition, the first data point of each run was skipped in order to match each scanner acquisition volume to the participant's preceding performance. Thus, each run yielded 84 data points (14 data points/task) in 14.33 min. Each experiment session included three runs and yielded 252 data points (42 data points/condition) in 42.99 min of functional scanning time.

Behavioral Data Processing & Analysis

Behavioral data processing included: (1) baseline calculation – determined by averaging the data between 3.1 – 5.1 seconds after the trigger. To be accepted, blocks must have had a standard deviation ≤ .05 cmH_2O of the average. (2) Peak identification – peak detection algorithm implemented thresholds for peak amplitude (≥ 10 cmH_2O) and width (≥ 0.175 s). After peaks were located, the minimum value between each peak was determined. If this value was greater than the acceptable minimum (9 cmH_2O), the detected peak following the minimum was thrown out. This eliminated false peaks where there were multiple small peaks at the top of one peak.

Blocks were included in analysis if the performance rate was within an acceptable range for the cued rate of 1 Hz (0.2 – 1.8 cmH_2O/sec) or 3 Hz (2.2 – 3.8 cmH_2O/sec), and the successful completion of an acceptable number of peaks (2 – 4 peaks for 1 Hz task; 6 – 10 peaks for 3 Hz task). Task condition blocks were discarded if the participant failed to achieve the cued rate, or produced too few or too many peaks. Baseline condition blocks were discarded if the participant generated one or more peaks greater than 20 cmH_2O, or generated more than 2 peaks during the baseline condition block.

Neuroimaging Data Processing

Before the functional data were statistically analyzed, the following processing steps were performed: (1) image reconstruction from k-space into a two-dimensional image via Fourier transformation followed by application of an 8 mm spatial filter at the time of data acquisition, (2) raw data conversion from DICOM file format to a more readable format (i.e., <experiment name_subject ID_series_volume _image>) recommended for BrainVoyager 1.9, (3) functional data from each session were screened for motion and/or magnet artifacts with cine-loop animation.

To improve the quality of the data, 3D motion correction using 6 transformational parameters was applied to align each functional volume for a given participant to the first functional volume of the first functional data set. The second and third runs were referenced to the first volume of the first run's functional data project. If a participant moved more than 3 mm during a run that participant was then excluded from further analyses. In the case that the participant moved less than 3 mm over each run, their data were further analyzed. Due to the nature of sparse sampling data acquisition (not acquired continuously as in typical box-car design), no further spatiotemporal filtering, global mean normalization, nor hemodynamic response function convolutions were applied to the functional data.

Anatomical brain images were isovoxel formatted to 1x1x1 mm^3, transformed into BrainVoyager standard sagittal orientation, and morphed into Talairach space (Talairach & Tournoux, 1988) for whole-brain analyses (~ 1,614,717 anatomical voxels, Figure 3, p. 34). To analyze brainstem correlates, a separate native space brainstem analysis was run using a mask

segmented from one of the participants (18,210 anatomical voxels, Figure 4, p. 34). Functional data were superimposed either on each individual's T_1 weighted anatomical scan (for single-subject analysis), or on a mean structural image derived from all individuals (for group analysis). The combined functional and anatomical data served as 4-dimensional datasets for each run, each participant, and the study group. Statistical comparisons (ANOVAs) are being made within approximately 38,275 functional voxels for the whole-brain analysis and within approximately 432 functional voxels for the brainstem mask analysis.

Figure 3. T1 weighted anatomical average (N=10) for whole-brain analyses, with applied Talairach transformation

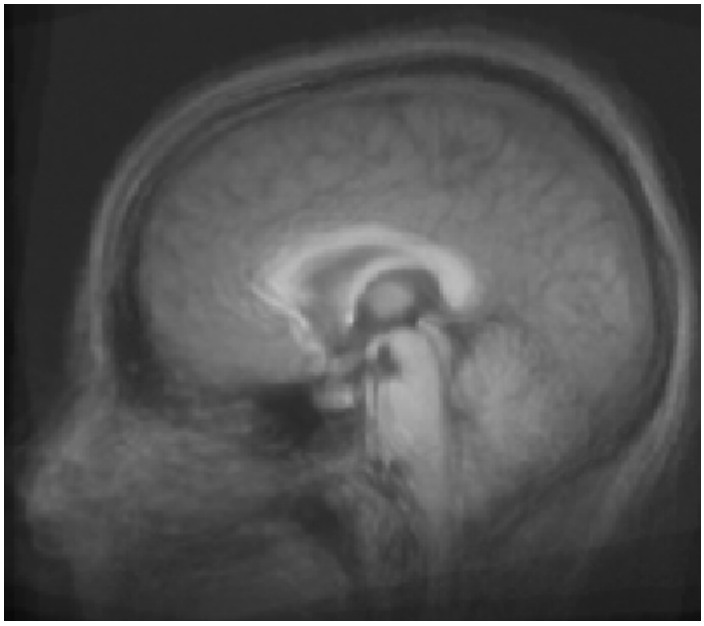

Figure 4. T1 weighted anatomical average (N=10) for brainstem analyses, without Talairach transformation

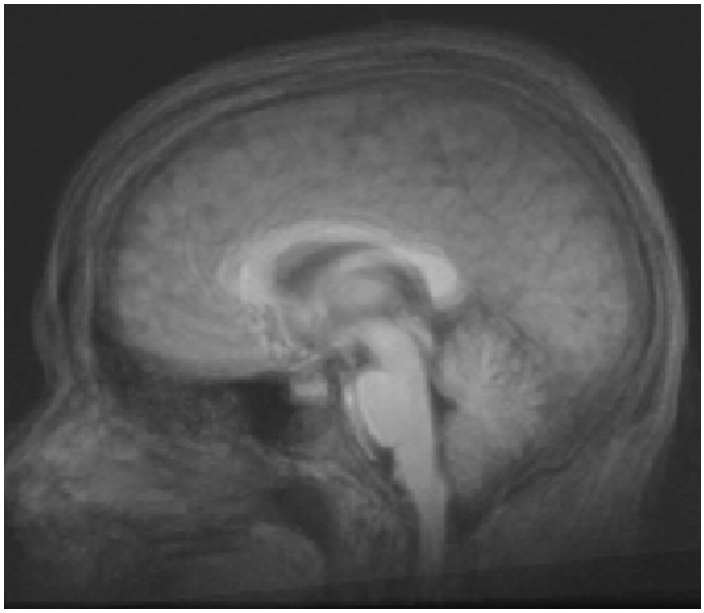

Neuroimaging Data Analysis

GLM principles were applied for single-subject and group analyses to identify cortical, subcortical, and brainstem regions that manifested activity significantly correlated with ororhythmic task and/or rate. *A priori* ROI of (bilateral sensorimotor cortex, cingulate, insula, basal ganglia, thalamus, superior and inferior cerebellum, and pontomedullary regions were defined based on findings from published oromotor fMRI studies (Ackermann, 2008; Ackermann & Riecker, 2004; Bohland & Guenther, 2006; Fu et al., 2002; Riecker et al., 2005) and areas we found as significantly correlated to one or more of the four task conditions across at least 70% of participants in our single-subject analyses (Table 3, p. 51).

Single-study design matrices were specified for each participant and ultimately referenced to the group-level multi-study design matrix. Our multi-study design matrix was constructed as an RFX analysis using a separate set of predictors for each subject. RFX statistical maps were generated to provide information of task and rate main effects. Areas of significant activation were then assessed by applying the two-way, within-subjects factor model to compare regional activations to baseline. These follow-up contrasts were run in *a priori* ROI with ≥ 4 contiguous significantly active voxels. The activation in these areas was characterized relative to baseline using an RFX ROI approach. For each region, coordinates of the voxel of maximum significance, and the anatomic location maxima were determined by superimposing the data on an average of the group's anatomy.

Imaging data were modeled as a single-factor design at all levels of analysis for testing overall main effects. The list of model conditions contained the factor-level combinations of

Suck 1 Hz; Suck 3 Hz; Unvoiced /da/ 1 Hz; Unvoiced /da/ 3 Hz as the four main predictors. The control conditions (Listen 1 Hz and Listen 3 Hz) were not included in the model and served as the baseline condition (i.e., Listen 1 Hz + Listen 3 Hz). Contrasts were specified by including the same predictors for all subjects (Table 1, p. 36). The data were processed using a percent signal change transformation and the resulting contrast maps (F statistic) represented the comparison of the individual betas of all subjects.

Table 1. Contrasts analyzed

Contrast Type & Name	Baseline	Predictors	Contrasts
Task-specific activation (collapsed across rate) Suck > Unvoiced /da/	Listen 1 Hz + Listen 3 Hz	Suck 1 Hz Suck 3 Hz Da 1 Hz Da 3 Hz	+Suck 1 Hz +Suck 3 Hz - Da 1 Hz - Da 3 Hz
Rate-specific activation (collapsed across task) 3 Hz > 1 Hz	Listen 1 Hz + Listen 3 Hz	Suck 1 Hz Suck 3 Hz Da 1 Hz Da 3 Hz	- Suck 1 Hz +Suck 3 Hz - Da 1 Hz +Da 3 Hz

Single-Subject Analysis

Prior to including functional data into the single-subject neuroimaging analyses, blocks with unacceptable behavioral performance were excluded and each participant's data were evaluated to confirm reasonable signal-to-noise ratio. The functional imaging data were then analyzed for each run separately per participant using a single-study GLM model based on a single-factor design matrix with four predictors (Suck 1 Hz; Suck 3 Hz; Unvoiced /da/ 1 Hz; Unvoiced /da/ 3 Hz) and two baseline conditions (Listen 1 Hz; Listen 3 Hz). A multi-study design matrix was then created for each participant by combining their single-study design matrices (collapsing across runs) enabling an GLM analysis to be performed for each participant. The following four contrasts were assessed by collapsing across each factor and comparing the BOLD signal of each condition with baseline:

Contrast 1: [Suck > Baseline] = Suck 1 Hz + Suck 3 Hz > Listen 1 Hz + Listen 3 Hz.

Contrast 2: [Unvoiced /da/ > Baseline] = Unvoiced /da/ 1 Hz + Unvoiced /da/ 3 Hz > Listen 1 Hz + Listen 3 Hz.

Contrast 3: [1 Hz > Baseline] = Suck 1 Hz + Unvoiced /da/ 1 Hz > Listen 1 Hz + Listen 3 Hz.

Contrast 4: [3 Hz > Baseline] = Suck 3 Hz + Unvoiced /da/ 3 Hz > Listen 1 Hz + Listen 3 Hz.

Statistically significant BOLD signal changes were depicted on SPM t-maps, corrected for multiple comparisons at the threshold of $p(Bonf) < 0.05$. Significant main effects were assessed across runs of each participant separately.

Group Analysis: Part 1

Whole-Brain RFX GLM & Conjunction Analyses

To identify regions across the whole brain with main effects of the task and rate factors, a multi-study design matrix (constructed from the series of single-study design matrices) was analyzed using an RFX GLM. This analysis used a summary-statistic approach, i.e. using the average of the estimated beta weight values of each participant and condition from the single-subject analysis where, (1) the model was fit for each subject using a subject-separable GLM (first-level group analysis), (2) main effects were defined and contrast maps were calculated to demonstrate the contrast of the parameter estimates at each voxel, and (3) the contrast images were then fed into a GLM that implemented a one-sample t-test (second-level group analysis). The resulting contrast map represented a comparison of the individual betas of all subjects.

To initially assess the overlapping substrates by task or rate, two simple SPM map overlays (one for overlapping tasks, one for overlapping rates) were computed and visually assessed for shared correlates. To formally determine the minimal network correlates, i.e., shared correlates, for the production of, a) the Suck and Unvoiced /da/ tasks, and b) the 1 Hz and 3 Hz rates, a conjunction analysis was based on the multi-study design matrix. Conjunction maps were calculated between multiple contrasts of the conditions compared to baseline (Friston, Penny, & Glasser, 2005). The conjunction map produced was obtained at each voxel by computing a new statistical value as the minimum of the statistical values obtained from the defined contrasts listed below.

Contrast 1: [Suck > Baseline] = Suck 1 Hz + Suck 3 Hz > Listen 1 Hz + Listen 3 Hz.

Contrast 2: [Unvoiced /da/ > Baseline] = Unvoiced /da/ 1 Hz + Unvoiced /da/ 3 Hz > Listen 1 Hz + Listen 3 Hz.

Contrast 3: [1 Hz > Baseline] = Suck 1 Hz + Unvoiced /da/ 1 Hz > Listen 1 Hz + Listen 3 Hz.

Contrast 4: [3 Hz > Baseline] = Suck 3 Hz + Unvoiced /da/ 3 Hz > Listen 1 Hz + Listen 3 Hz.

The conjunction of (Contrast 1 + Contrast 2) revealed significant clusters of activity shared by the tasks. The conjunction of (Contrast 3 + Contrast 4) revealed significant clusters of activity shared by rates. Significant clusters of ≥ 4 contiguous significantly active voxels were considered to represent shared correlates of the two contrasts specified. A GLM of ROIs was then run as described above (i.e., second-level group analysis) to compare the activity levels to baseline.

Group Analysis: Part 2

Brainstem RFX GLM & Conjunction Analyses

A native space brainstem analysis was run using a mask segmented from one of the participants (Figure 5, p. 41) chosen as having the most anatomically representative brainstem of the group. Each participant's anatomical and functional data sets were aligned with the representative brainstem mask. All brainstems were aligned to the following landmarks: rostral pons passing dorsally through the decussation of superior cerebellar peduncles, bulbopontine sulcus, and the pyramidal decussation extending to the most inferior point shared by the functional data sets. These landmarks were defined based on published brainstem atlas (Paxinos & Huang, 1995) to encompass brainstem motor and sensory nuclei, reticular formation, and periaqueductal gray. Anatomical landmarks included rostral pons, bulbopontine sulcus, and most inferior point shared by the functional data sets. Functional data were overlaid on a native space average anatomical data set created from aligning the brainstems.

To initially assess the overlapping substrates by task or rate, two simple SPM map overlays (one for overlapping tasks, one for overlapping rates) were computed and visually assessed for shared correlates within the masked brainstem region. To formally determine the minimally shared areas among (a) the suck and unvoiced /da/ tasks, and (b) the 1 Hz and 3 Hz rates limited to the masked brainstem region, a conjunction analysis was performed withing the masked region. The conjunction steps from Group Analysis: Part 1 were repeated within the masked brainstem region only.

Figure 5. Brainstem mask landmarks

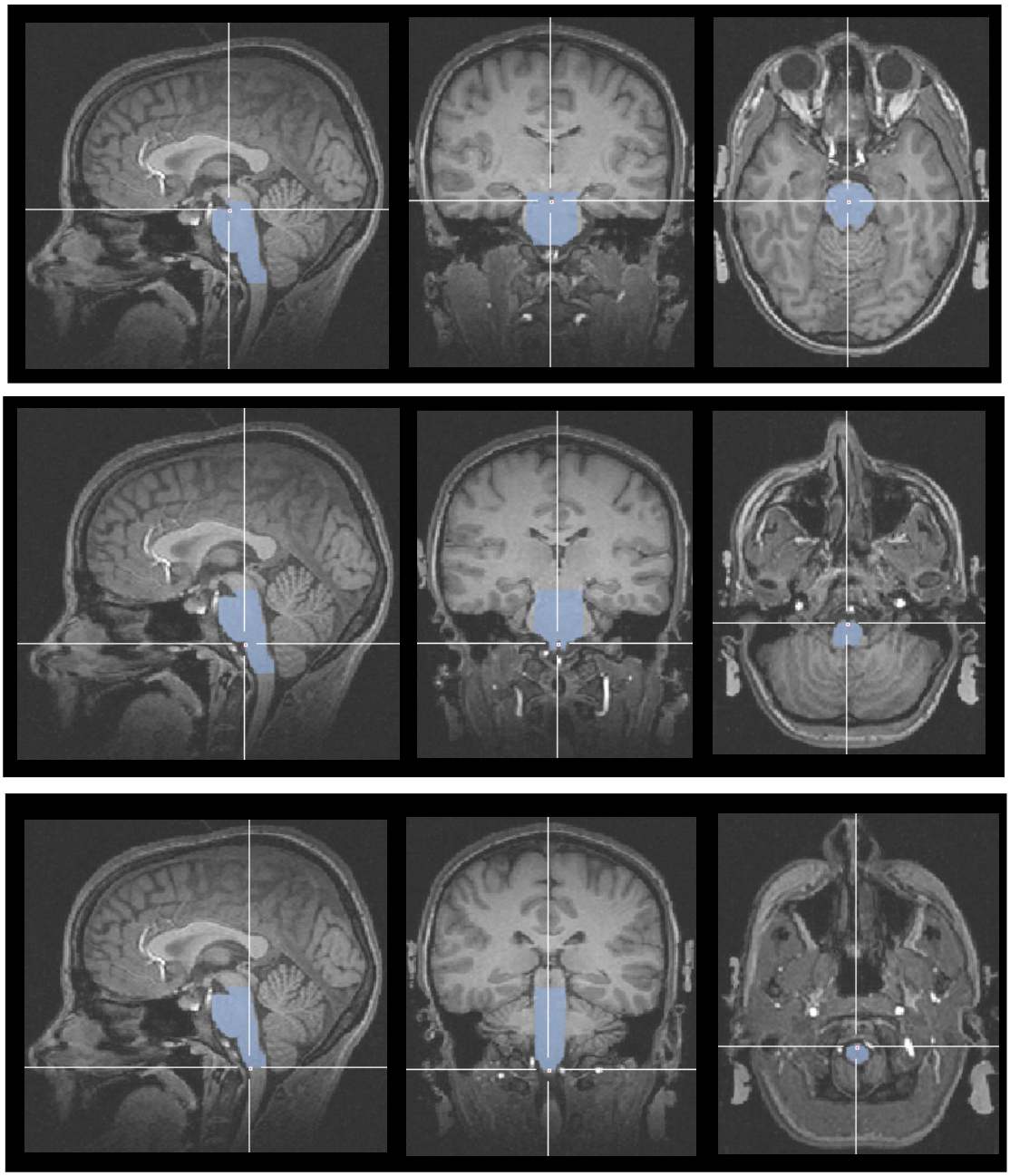

CHAPTER 3: RESULTS

Behavioral Results

A total of N=10 subjects participated. Three runs were collected and analyzed from each participant with the exception of one run being discarded due to unacceptable subject compliance. A total of 29 runs were included in the behavioral and neuroimaging analyses. The following percentages of data were excluded from Suck 1 Hz, Suck 3 Hz, Unvoiced /da/ 1 Hz, Unvoiced /da/ 3 Hz: 3.69%, 1.97%, 3.69%, 0.99%, respectively, due to unacceptable subject performance.

Rate was found to be quite stable across the four task conditions (Table 2, p. 42), with an overall higher variability in task found at the higher performance rate (3 Hz) compared to the lower performance rate (1 Hz). Mean amplitude was stable within each task, with the Unvoiced /da/ condition being performed at slightly higher mean amplitude compared to the Suck condition across rate. The Unvoiced /da/ task had 20% steeper slopes found for both performance rates compared to the Suck task. An example of a pressure and click recording of a participant performing the randomized tasks is shown in Figure 6 (p. 43).

Table 2. Mean (SD) for Pressure Signals per run

Condition	# of Data Points	Rate (Hz)	Amplitude (cm H_20)	Slope (cm H_2O/s)
Suck 1 Hz	13.48 (0.99)	1.12 (0.22)	23.73 (2.21)	197.06 (55.53)
Suck 3 Hz	13.72 (0.75)	2.88 (0.35)	23.19 (2.21)	254.04 (55.72)
Unvoiced /da/ 1 Hz	13.48 (0.83)	1.12 (0.27)	24.89 (2.27)	266.57 (69.52)
Unvoiced /da/ 3 Hz	13.86 (0.44)	2.93 (0.40)	24.65 (2.30)	320.70 (68.43)

Figure 6. Sample pressure trace from participant's mouthing movements during data collection

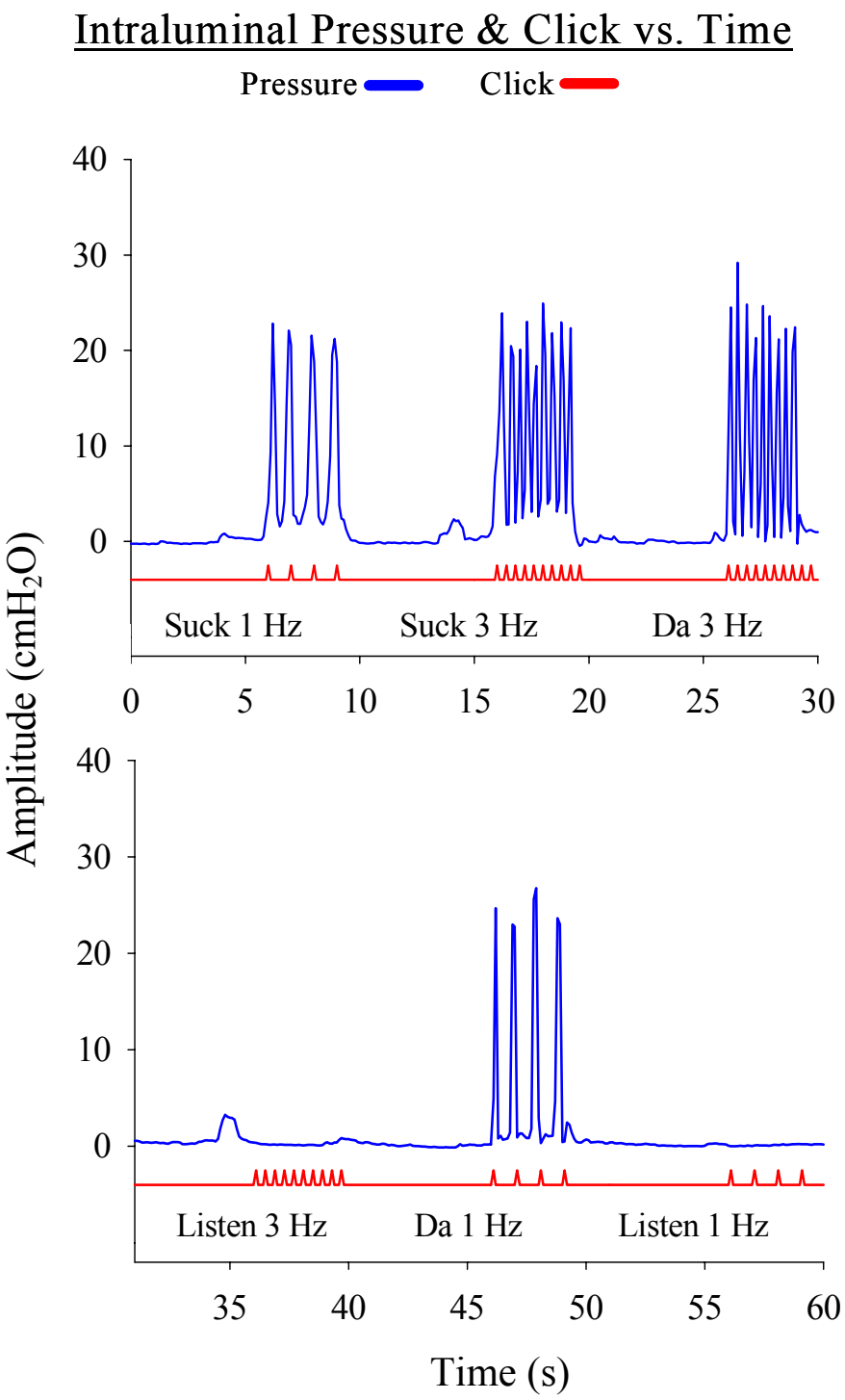

Neuroimaging Results

Single-subject findings

Eight of the ten participants moved less than 3 mm throughout the entire experimental session. Two participants moved less than 5 mm, however, much of this movement appears to have occurred between runs. Because no subject moved more than 3 mm during any of the functional runs, all ten participants' data were included and analyzed at the single-subject and group levels.

An example of GLM single-subject findings at the single-study and multi-study levels are depicted in SPM maps (Talairach coordinates shown: 0, -19, -19) from Participant 01 in Figures 7a-d (pp. 45-48) and 7e-f (pp. 49-50), respectively. The main effect of each task condition (Contrasts 1 and 2) was determined by collapsing across rate and comparing the activation to the baseline. Figure 7a (p. 45) represents areas that were more active during the Suck task condition compared to baseline. Figure 7b (p. 46) represents areas of activation more active during the Unvoiced /da/ task condition compared to baseline. The main effect of each rate condition (Contrasts 3 and 4) was determined by collapsing across task and comparing the activation to the baseline. Figure 7c (p. 47) represents areas that were more active during the 1 Hz rate condition compared to baseline. Figure 7d (p. 48) represents areas of activation more active during the 3 Hz rate condition compared to baseline. Figures 7e and 7f (pp. 49-50) represent the task-specific and rate-specific activation after the three single-study design matrices (one per run) were combined into one multi-study design matrix.

Figure 7 a. Single-study GLM analysis (Suck > Baseline)

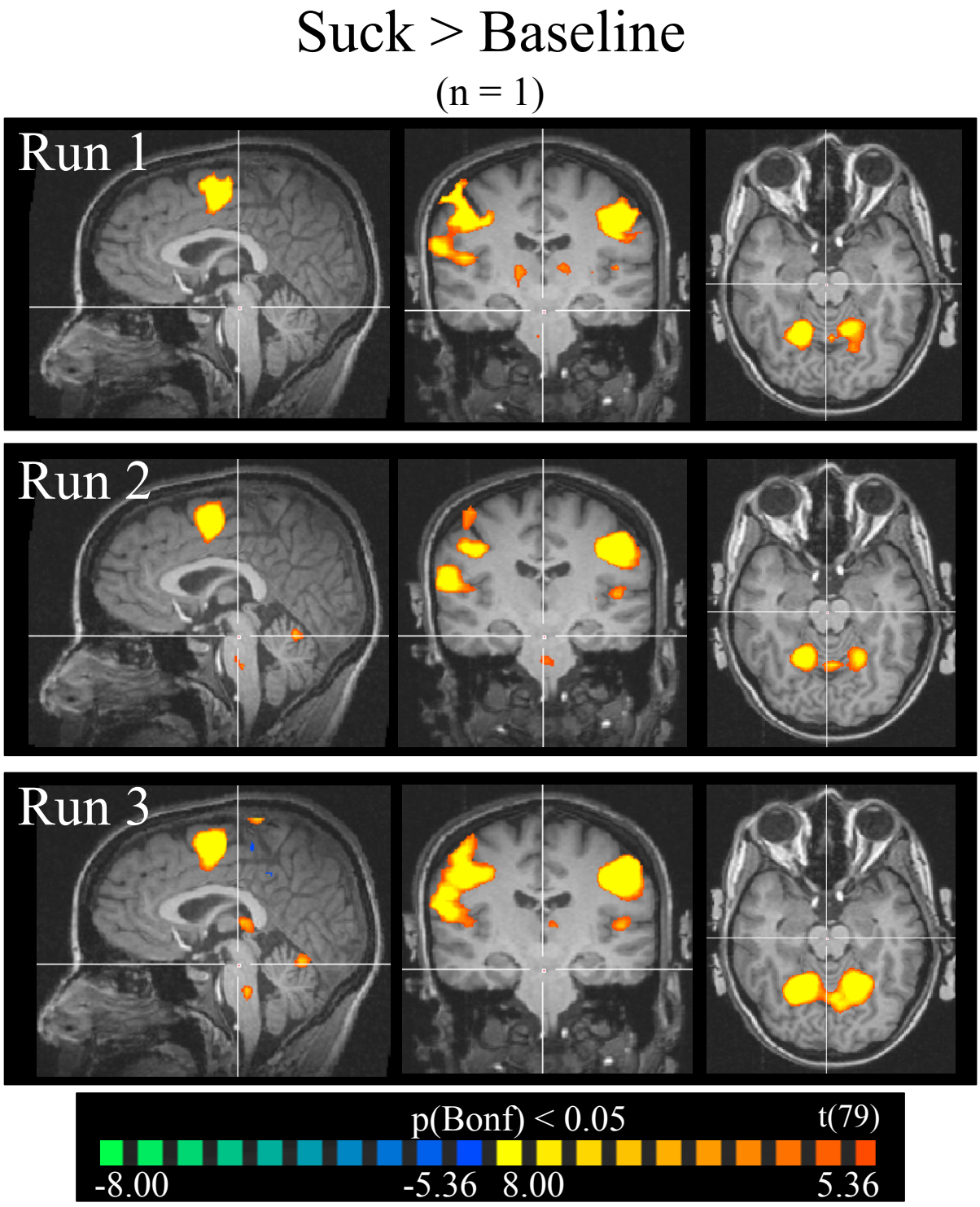

Figure 7 b. Single-study GLM analysis (Unvoiced /da/ > Baseline)

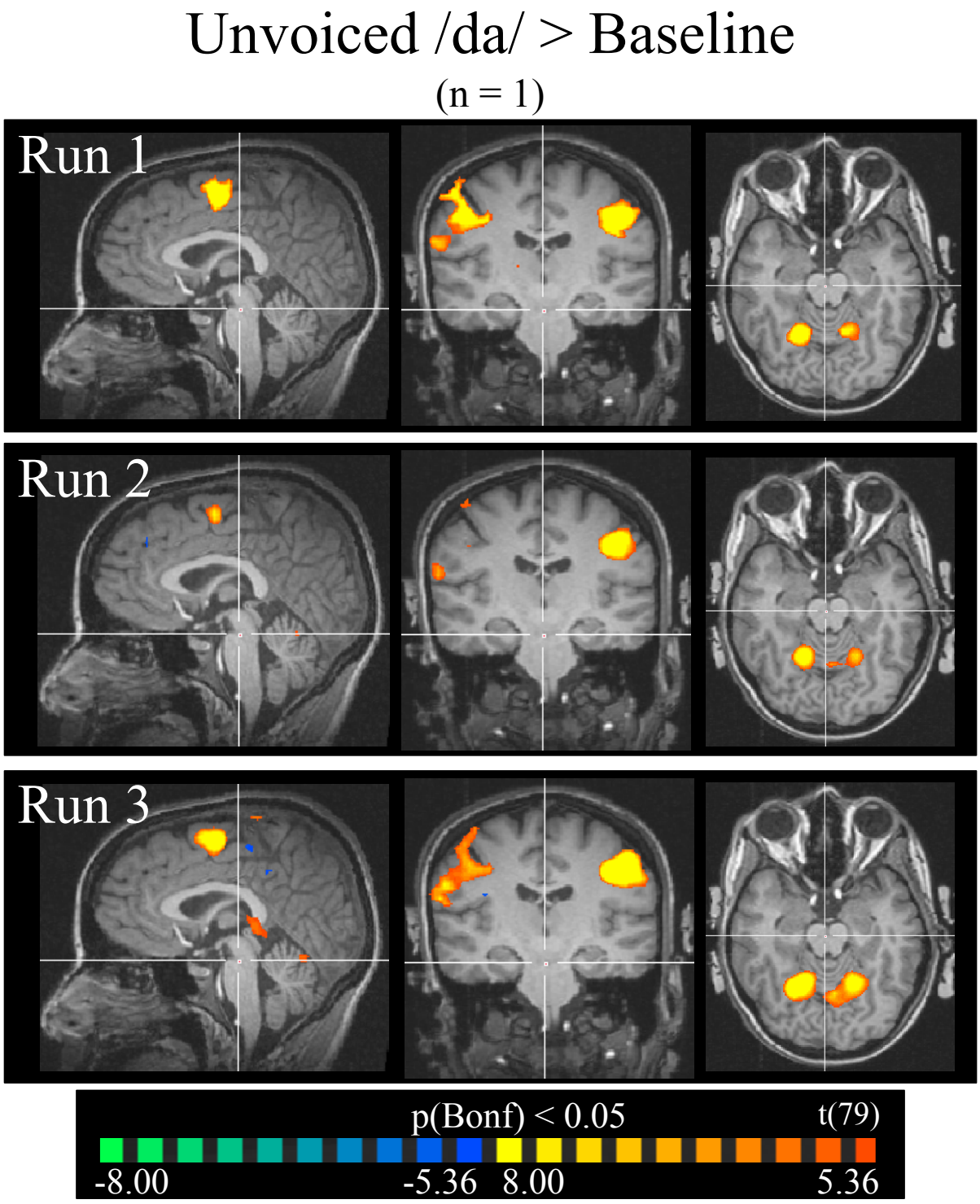

Figure 7 c. Single-study GLM analysis (1 Hz > Baseline)

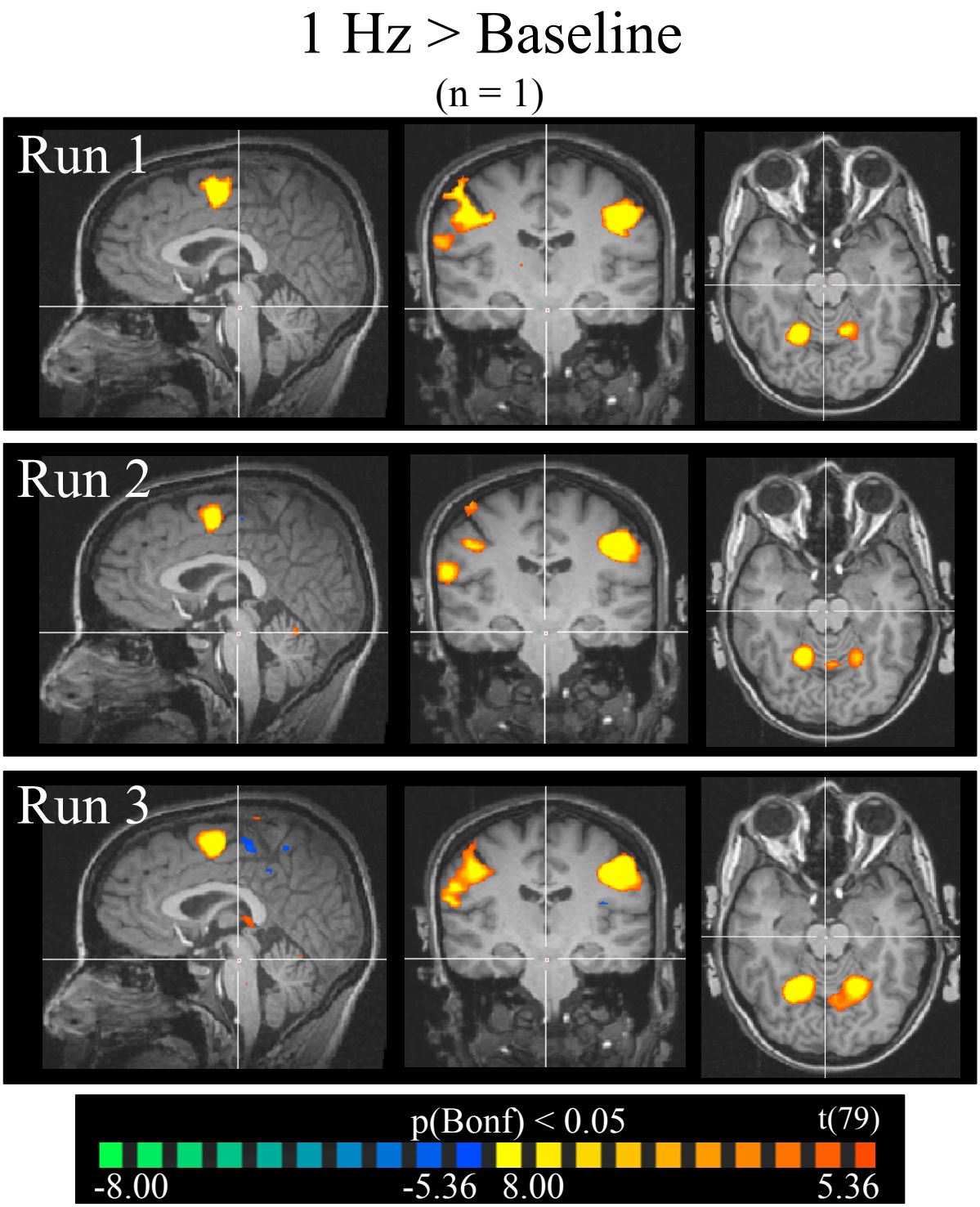

Figure 7 d. Single-study GLM analysis (3 Hz > Baseline)

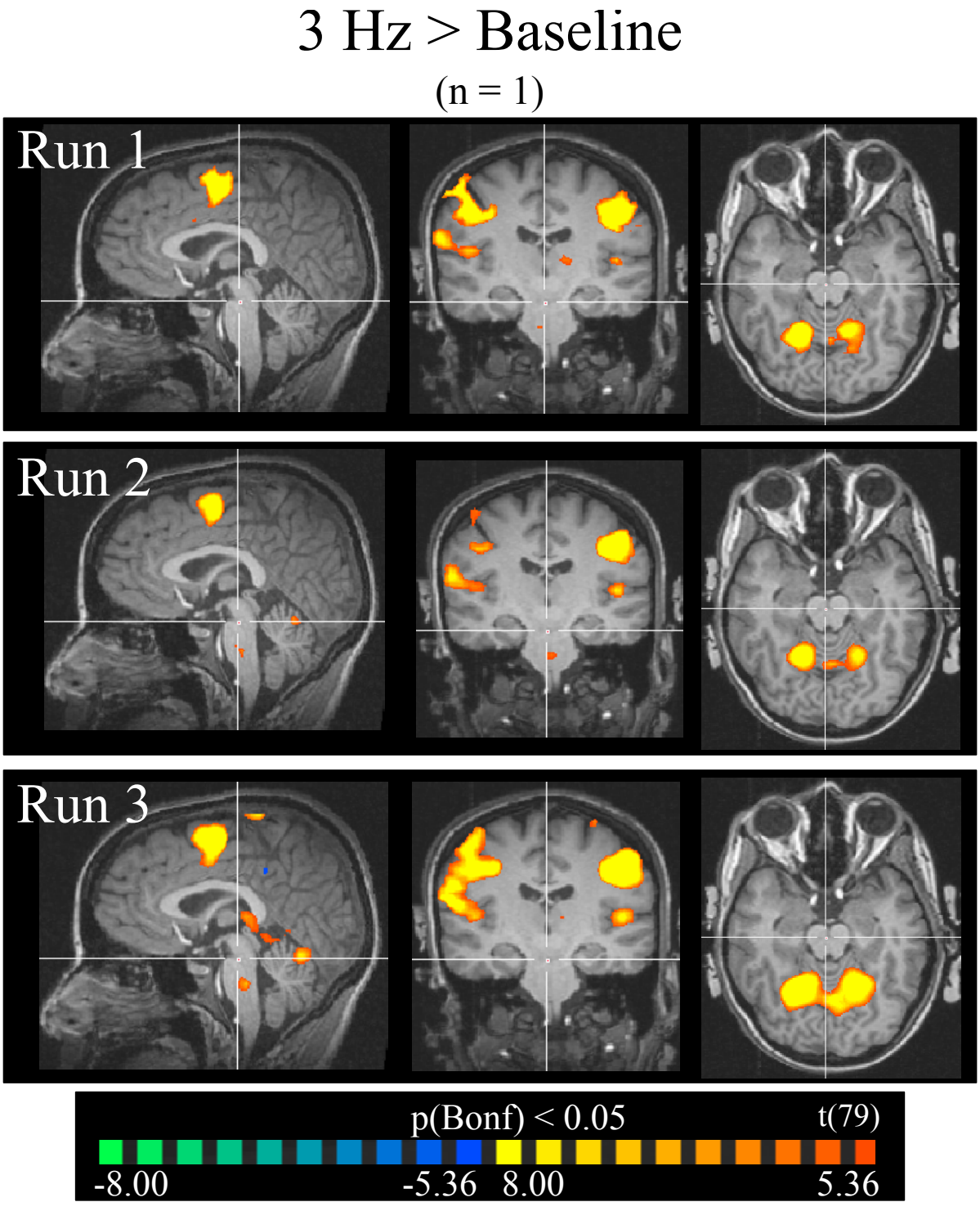

Figure 7 e. Multi-study GLM analysis (Task-correlated activity)

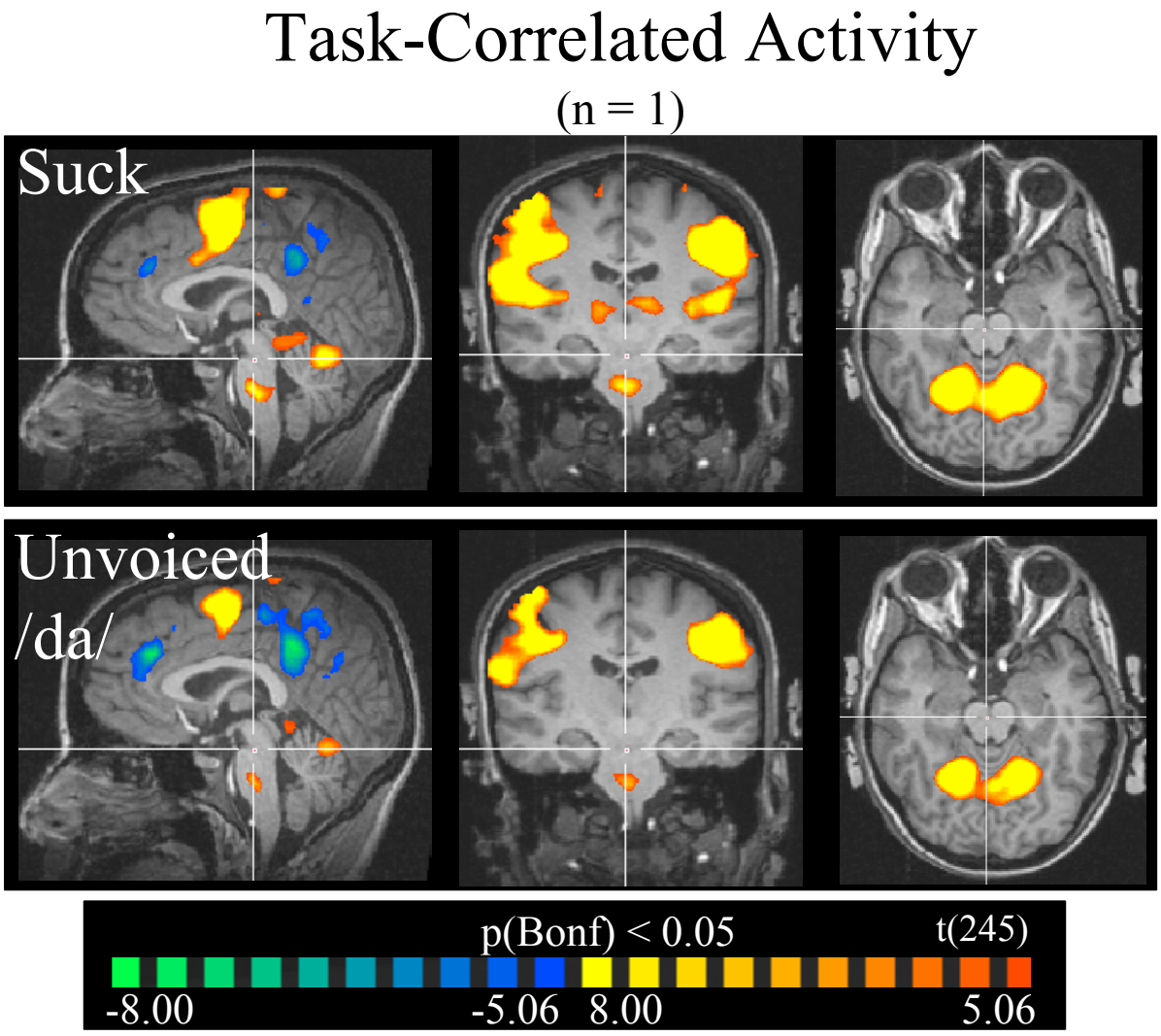

Figure 7 f. Multi-study GLM analysis (Rate-correlated activity)

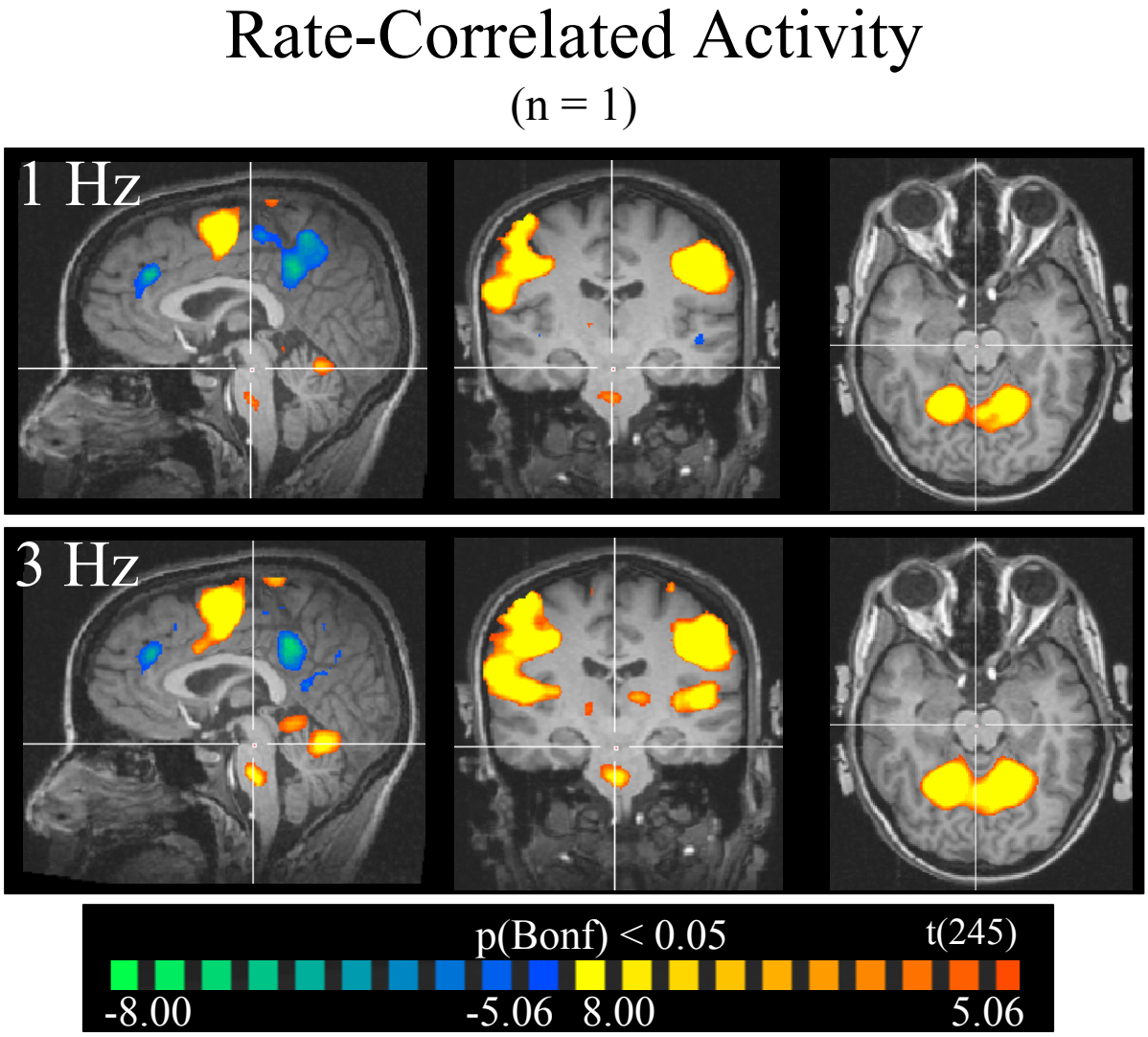

Consistent regions of activation observed in the multi-study GLM analyses of each participant included bilateral activation of inferiolateral pre- and postcentral gyri and superior cerebellum. The majority (70%) of participants showed bilateral activity in insulae, thalamic nuclei, basal ganglion, and pontomedullary regions correlated with at least one of the task or rate conditions (Table 3, p. 51). These functional areas, supported by literature as correlated with production of oromotor behaviors, were chosen as our *a priori* ROIs for group analyses.

Table 3. *A priori* ROIs for group analysis

# of Participants with Task or Rate Correlated Activity
p(Bonf) < 0.05

	Task		Rate	
ROI	Suck	Unvoiced /da/	1 Hz	3 Hz
Bilateral S1M1	10	10	10	10
R. cingulate	7	6	6	7
L. cingulate	8	6	7	7
R. insula	9	9	9	9
L. insula	9	9	9	9
R. basal ganglia	7	6	6	7
L. basal ganglia	8	8	9	9
R. thalamus	9	7	8	9
L. thalamus	8	7	8	8
Bilateral sup. cerebellum	10	10	10	10
R. inf. cerebellum	8	6	6	8
L. inf. cerebellum	7	5	6	6
R. pontomedullary	8	3	4	7
L. pontomedullary	8	3	1	6

Group findings

Overlapping and unique areas of activation identified as a function of task or rate were identified and reported at uncorrected statistical thresholds. The current study is limited in statistical power due to the small sample size (N=10). Therefore, the results presented were interpreted and discussed as preliminary findings. Whole-brain RFX analyses were reported at $p < 0.0005$; brainstem mask analyses were reported at $p < 0.0001$ (FFX) and $p < 0.001$ (RFX).

Part 1a: Whole Brain: RFX analysis, main effect of task

To determine the main effect of task, a multi-subject RFX GLM analysis including all participants, separate subject predictors, and percent signal transform was performed. To identify *a priori* ROIs actively correlated with the ororhythmic task conditions, the contrast [Suck > Unvoiced /da/] was applied and the data were thresholded at $p < 0.0005$. Table 8a (p. 54) lists the statistical details for the resulting *a priori* ROIs in bold text and post hoc ROIs in plain text. Table 8b (p. 57) lists the average magnitude of signal compared to baseline for the Suck and Unvoiced /da/ task conditions collapsed across the rate condition for the resulting *a priori* ROIs in bold text and post hoc ROIs in plain text. Figures 8a-f (pp. 60-65) include SPM maps representing some of the *a priori* ROIs that significantly differ as a function of task followed by bar graphs indicating the mean percent signal change of the task conditions compared to baseline.

Areas found to be more active in the Suck compared to Unvoiced /da/ task conditions included: bilateral basal ganglia (Figure 8a, p. 60), and thalamic nuclei; right cerebellar vermis, cortex, and deep nuclei (Figures 8c-d, pp. 62-63); and bilateral sensorimotor cortices that extended into rolandic operculi, insulae, and temporal gyri (Figure 8f, p. 65, white circles indicate a single region of activation spread across mutliple cortical areas). Further inspection ($p < 0.00005$) revealed distinct cortical areas of activation in right-lateralized rolandic operculum; bilateral insula, and sensorimotor cortex; and left supramarginal gyrus (Tables 9a-b, Figures 9a-c, pp. 66-71). No pontomedullary correlates were identified as a function of task.

Table 8 a. Multi-Subject RFX GLM, main effect of task

ROI	Cluster Region	BA	# of voxels	Peak Voxel				
				x	y	z	t value	p value
1	R. precentral gyrus	4	49	54	-10	22	6.994	0.000064
2	L. precentral gyrus (spread to rolandic operculum & insula)	6, 44, 13	3697	-54	2	13	11.790	0.000001
3	R. globus pallidus	N/A	131	21	2	1	6.255	0.000149
4	L. putamen	N/A	16	-33	2	-2	6.029	0.000195
5	L. thalamus (VPM n.)	N/A	16	-6	-19	10	5.960	0.000213
6	L. thalamus (centromedial n.)	N/A	9	-12	-16	10	5.616	0.000327
7	R. thalamus (dorsomedial n.)	N/A	190	9	-16	7	6.957	0.000066
8	R. thalamus (centromedian n.)	N/A	13	15	-22	1	6.386	0.000127
9	R. thalamus (STn.)	N/A	12	9	-10	-2	7.573	0.000034
10	R. thalamus (VPm n.)	N/A	14	9	-19	-2	6.632	0.000096
11	R. deep cerebellum (dentate n.)	N/A	24	9	-55	-32	6.968	0.000065
12	R. lat. cerebellum (ant. lobe)	N/A	19	21	-52	-20	5.886	0.000233
13	R. vermis (proximal to post. lobe)	N/A	5	3	-67	-23	6.169	0.000165
14	R. med. cerebellum (ant. lobe)	N/A	91	6	-55	-17	6.682	0.000090

15	R. inf. frontal sulcus	9	16	36	14	31	-6.459	0.000117
16	R. cingulate sulcus	31	41	21	-28	40	-5.913	0.000225
17	R. intraparietal sulcus	40	8	42	-22	34	5.761	0.000273
18	R. post. insula (spread to rolandic operculum & STG)	13, 40, 22	2438	45	-10	7	9.382	0.000006
19	R. transverse temporal gyrus & supramarginal gyrus	41, 40	1012	42	-25	19	8.124	0.000020
20	R. red n.	N/A	12	6	-22	-5	7.096	0.000057
21	R. cuneus (spread to lingual gyrus)	17	339	6	-58	-5	8.582	0.000013
22	R. cuneus	17	6	3	-70	1	5.802	0.000259
23	R. cuneus	17	5	3	-73	-2	5.698	0.000295
24	R. cuneus	18	45	9	-94	4	6.067	0.000187
25	L. superior parietal gyrus	7	4	-12	-73	40	5.491	0.000385
26	L. supramarginal gyrus	40	119	-60	-28	28	9.383	0.000006
27	L. supramarginal gyrus	40	96	-45	-31	22	8.099	0.000020
28	L. superior temporal sulcus	37	67	-39	-55	-2	7.627	0.000032
29	L. collateral sulcus (ant.)	N/A	19	-27	-46	-8	5.948	0.000216
30	L. lateral occipital sulcus	19	22	-39	-73	-17	7.176	0.000052

31	L. cuneus	18	4	-9	-70	7	5.615	0.000328
32	L. lingual gyrus	19	20	-9	-55	-8	5.775	0.000268
33	L. lingual gyrus	18	26	-18	-79	-20	5.833	0.000249

Table 8 b. RFX GLM of ROIs

ROI	Region	Contrast	df	mean	se	t value	p value
1	R. precentral gyrus	Suck	9	3.830	0.543	7.056	0.000059*
		Unvoiced /da/	9	3.126	0.512	6.101	0.000179*
2	L. precentral gyrus (spread to rolandic operculum & insula)	Suck	9	1.560	0.091	17.212	0.000000*
		Unvoiced /da/	9	1.089	0.092	11.785	0.000001*
3	R. globus pallidus	Suck	9	1.556	0.138	11.305	0.000001*
		Unvoiced /da/	9	0.837	0.190	4.393	0.001738
4	L. putamen	Suck	9	0.792	0.083	9.572	0.000005*
		Unvoiced /da/	9	0.423	0.083	5.087	0.000656
5	L. thalamus (VPm n.)	Suck	9	1.359	0.231	5.876	0.000236*
		Unvoiced /da/	9	0.893	0.187	4.767	0.001020
6	L. thalamus (centromedial n.)	Suck	9	1.435	0.164	8.748	0.000011*
		Unvoiced /da/	9	1.056	0.147	7.171	0.000052*
7	R. thalamus (dorsomedial n.)	Suck	9	1.197	0.150	7.978	0.000023*
		Unvoiced /da/	9	0.860	0.131	6.561	0.000104*
8	R. thalamus (centromedian n.)	Suck	9	0.599	0.143	4.184	0.002361
		Unvoiced /da/	9	0.355	0.123	2.882	0.018127
9	R. thalamus (STn.)	Suck	9	0.481	0.358	1.342	0.212423
		Unvoiced /da/	9	0.014	0.320	0.042	0.967074
10	R. thalamus	Suck	9	0.893	0.135	6.598	0.000099*

	(VPm n.)	**Unvoiced /da/**	**9**	**0.523**	**0.120**	**4.367**	**0.001804**
11	**R. deep cerebellum (dentate n.)**	**Suck**	**9**	**0.532**	**0.157**	**3.380**	**0.008121**
		Unvoiced /da/	**9**	**0.338**	**0.166**	**2.034**	**0.072487**
12	**R. lateral cerebellum (ant. lobe)**	**Suck**	**9**	**2.044**	**0.388**	**5.274**	**0.000511**
		Unvoiced /da/	**9**	**1.559**	**0.349**	**4.462**	**0.001574**
13	**R. vermis (proximal to post. lobe)**	**Suck**	**9**	**1.204**	**0.380**	**3.167**	**0.011416**
		Unvoiced /da/	**9**	**0.981**	**0.374**	**2.619**	**0.027873**
14	**R. medial cerebellum (ant. lobe)**	**Suck**	**9**	**1.277**	**0.180**	**7.114**	**0.000056***
		Unvoiced /da/	**9**	**1.035**	**0.174**	**5.950**	**0.000215***
15	R. inf. frontal sulcus	Suck	9	-0.272	0.100	-2.719	0.023630
		Unvoiced /da/	9	0.019	0.093	0.202	0.844111
16	R. cingulate sulcus	Suck	9	-0.190	0.081	-2.341	0.043925
		Unvoiced /da/	9	-0.029	0.070	-0.415	0.688003
17	R. intraparietal sulcus	Suck	9	2.202	0.393	5.611	0.000330*
		Unvoiced /da/	9	1.694	0.350	4.845	0.000915
18	R. post. insula (spread to rolandic operculum & STG)	Suck	9	2.165	0.298	7.265	0.000047*
		Unvoiced /da/	9	1.435	0.281	5.114	0.000633
19	R. transverse temporal gyrus & supramarginal gyrus	Suck	9	1.533	0.069	22.185	0.000000*
		Unvoiced /da/	9	1.024	0.072	14.154	0.000000*
20	R. red n.	Suck	9	0.689	0.159	4.323	0.001925
		Unvoiced /da/	9	0.422	0.156	2.715	0.023800
21	R. cuneus (spread to lingual gyrus)	Suck	9	1.023	0.274	3.736	0.004652
		Unvoiced /da/	9	0.667	0.292	2.284	0.048207
22	R. cuneus	Suck	9	1.004	0.365	2.754	0.022343

		Unvoiced /da/	9	0.536	0.365	1.468	0.176197
23	R. cuneus	Suck	9	0.941	0.254	3.697	0.004941
		Unvoiced /da/	9	0.466	0.287	1.621	0.139392
24	R. cuneus	Suck	9	0.451	0.390	1.155	0.277731
		Unvoiced /da/	9	-0.295	0.377	-0.782	0.454466
25	L. superior parietal gyrus	Suck	9	-0.014	0.179	-0.081	0.937201
		Unvoiced /da/	9	-0.357	0.194	-1.841	0.098806
26	L. supramarginal gyrus	Suck	9	2.040	0.374	5.450	0.000406*
		Unvoiced /da/	9	1.593	0.347	4.590	0.001310
27	L. supramarginal gyrus	Suck	9	0.828	0.138	6.001	0.000202*
		Unvoiced /da/	9	0.519	0.119	4.345	0.001864
28	L. superior temporal sulcus	Suck	9	0.056	0.141	0.395	0.701810
		Unvoiced /da/	9	-0.199	0.141	-1.419	0.189640
29	L. collateral sulcus	Suck	9	-0.233	0.191	-1.221	0.252953
		Unvoiced /da/	9	-0.544	0.205	-2.659	0.026071
30	L. lateral occipital sulcus	Suck	9	0.575	0.254	2.261	0.050123
		Unvoiced /da/	9	-0.137	0.246	-0.557	0.591350
31	L. cuneus	Suck	9	0.974	0.222	4.381	0.001768
		Unvoiced /da/	9	0.48	0.215	2.234	0.052328
32	L. lingual gyrus	Suck	9	1.217	0.223	5.454	0.000404*
		Unvoiced /da/	9	0.793	0.187	4.238	0.002182
33	L. lingual gyrus	Suck	9	0.429	0.200	2.143	0.060684
		Unvoiced /da/	9	-0.311	0.208	-1.498	0.168369

* Significantly different from baseline

Figure 8 a. Right globus pallidus (ROI #3) & left putamen (ROI #4)

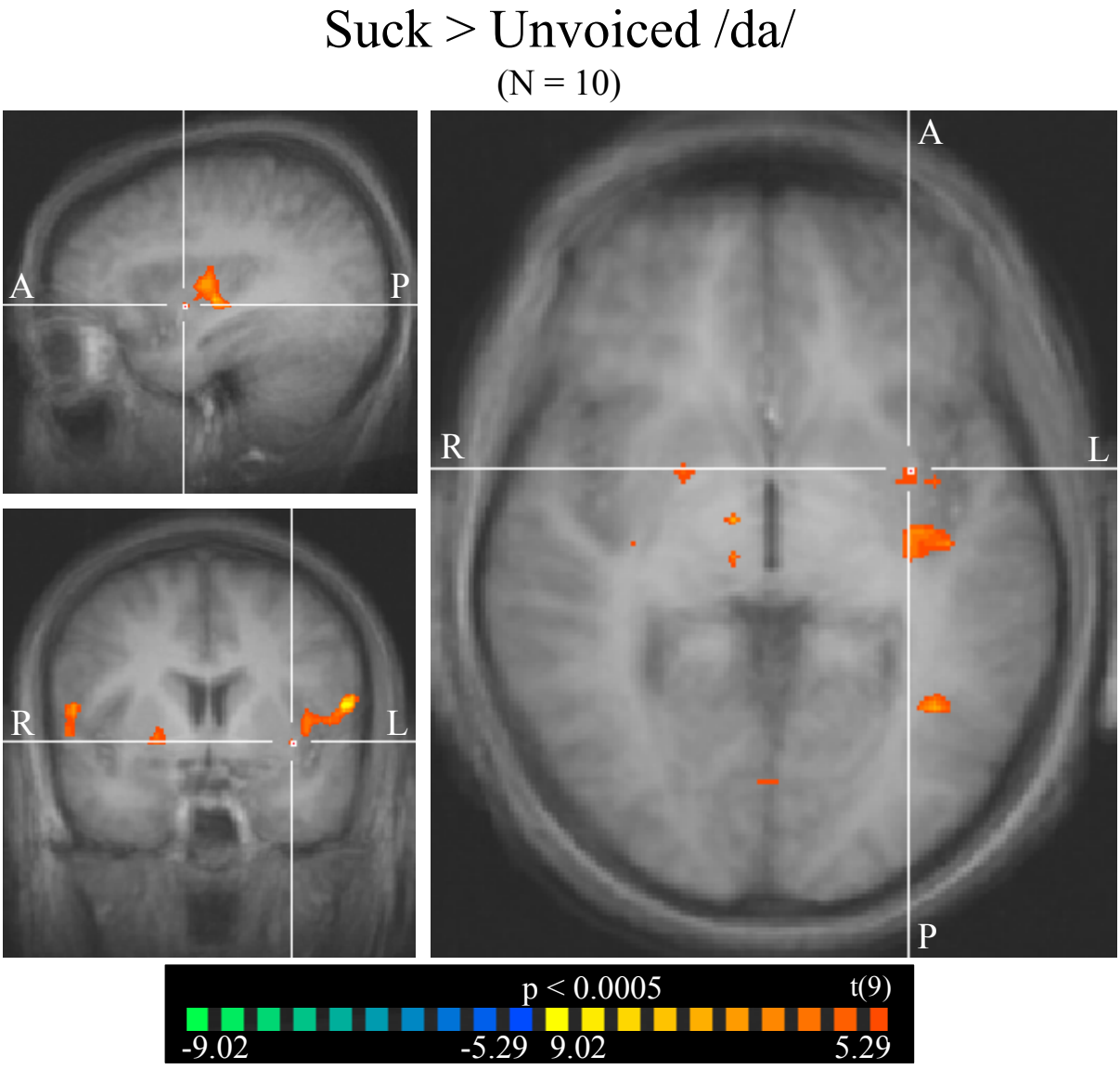

(TC pictured: -33, 2, -2)

Figure 8 b. Mean % signal change compared to baseline

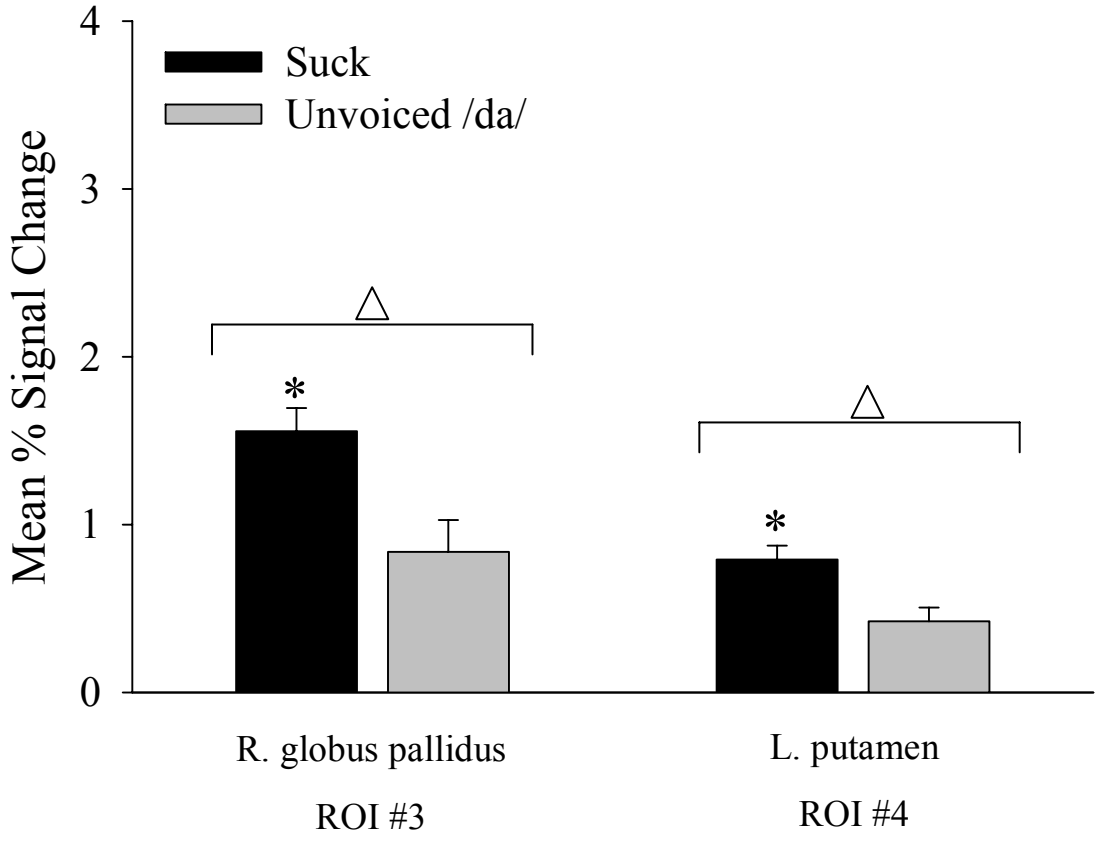

△ Significant main effect of task

* Significantly different from baseline

Figure 8 c. Right lateral cerebellum, anterior lobe (ROI #12)

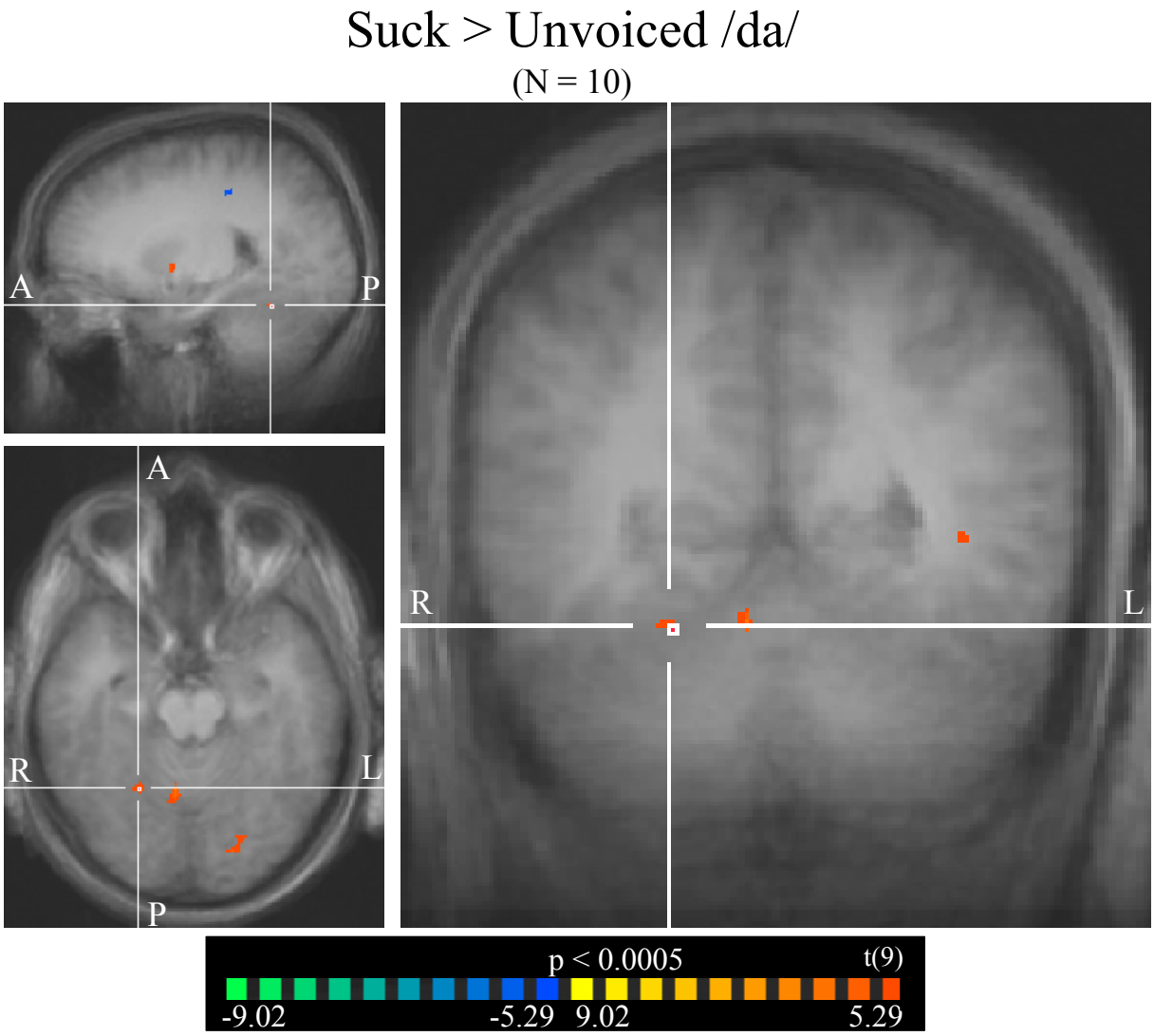

(TC pictured: 22, -52, -20)

Figure 8 d. Right deep cerebellum, dentate n. (ROI #11)

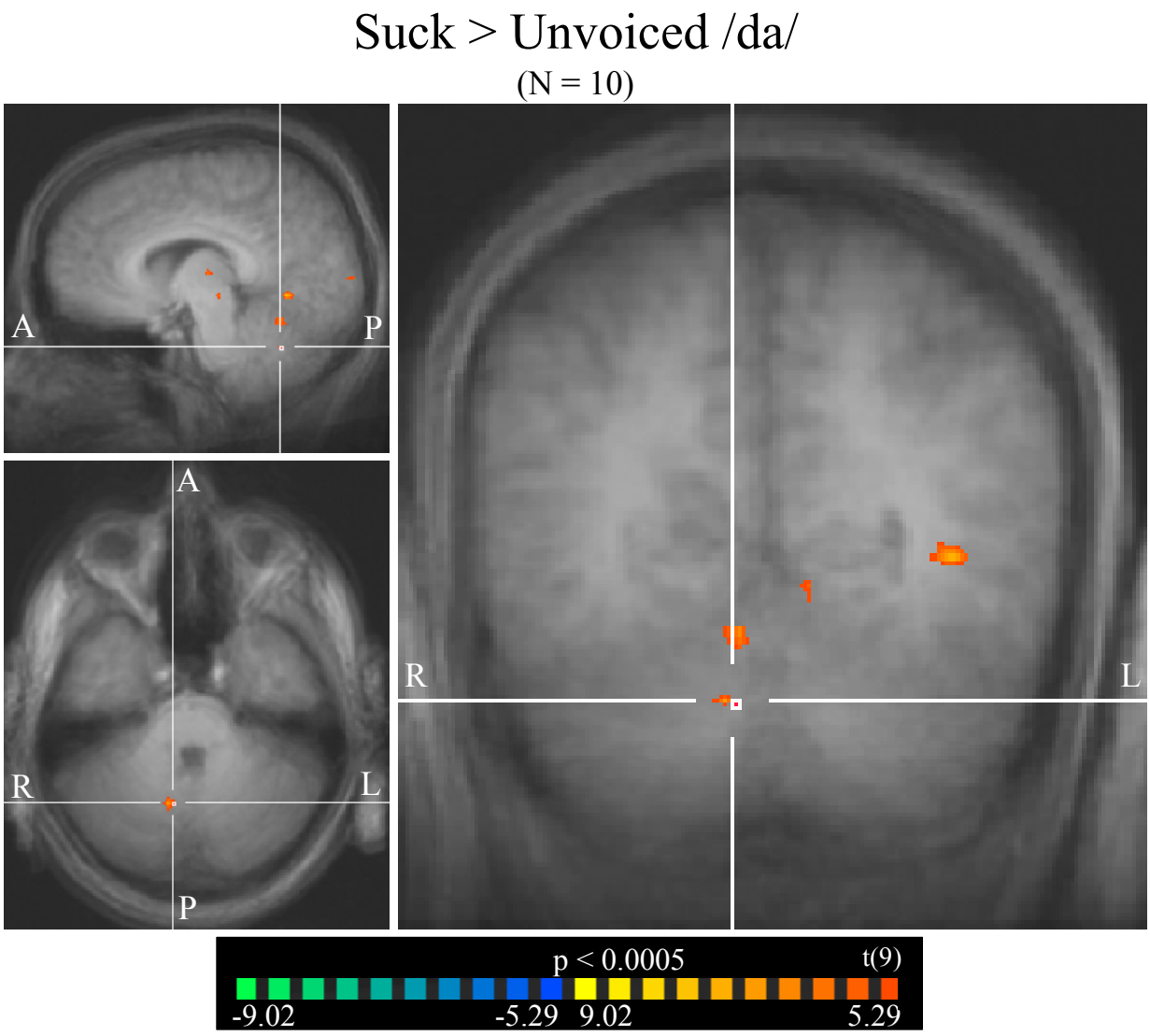

(TC pictured: 7, -55, -32)

Figure 8 e. Mean % signal change compared to baseline

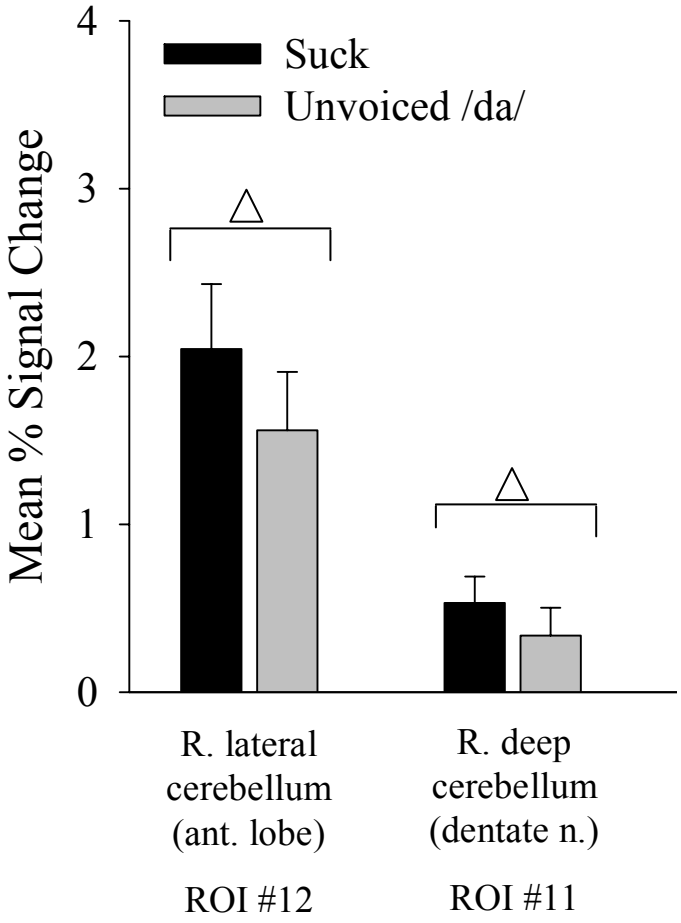

△ Significant main effect of task

* Significantly different from baseline

Figure 8 f. Left precentral gyrus spread to other cortical areas (ROI #2)

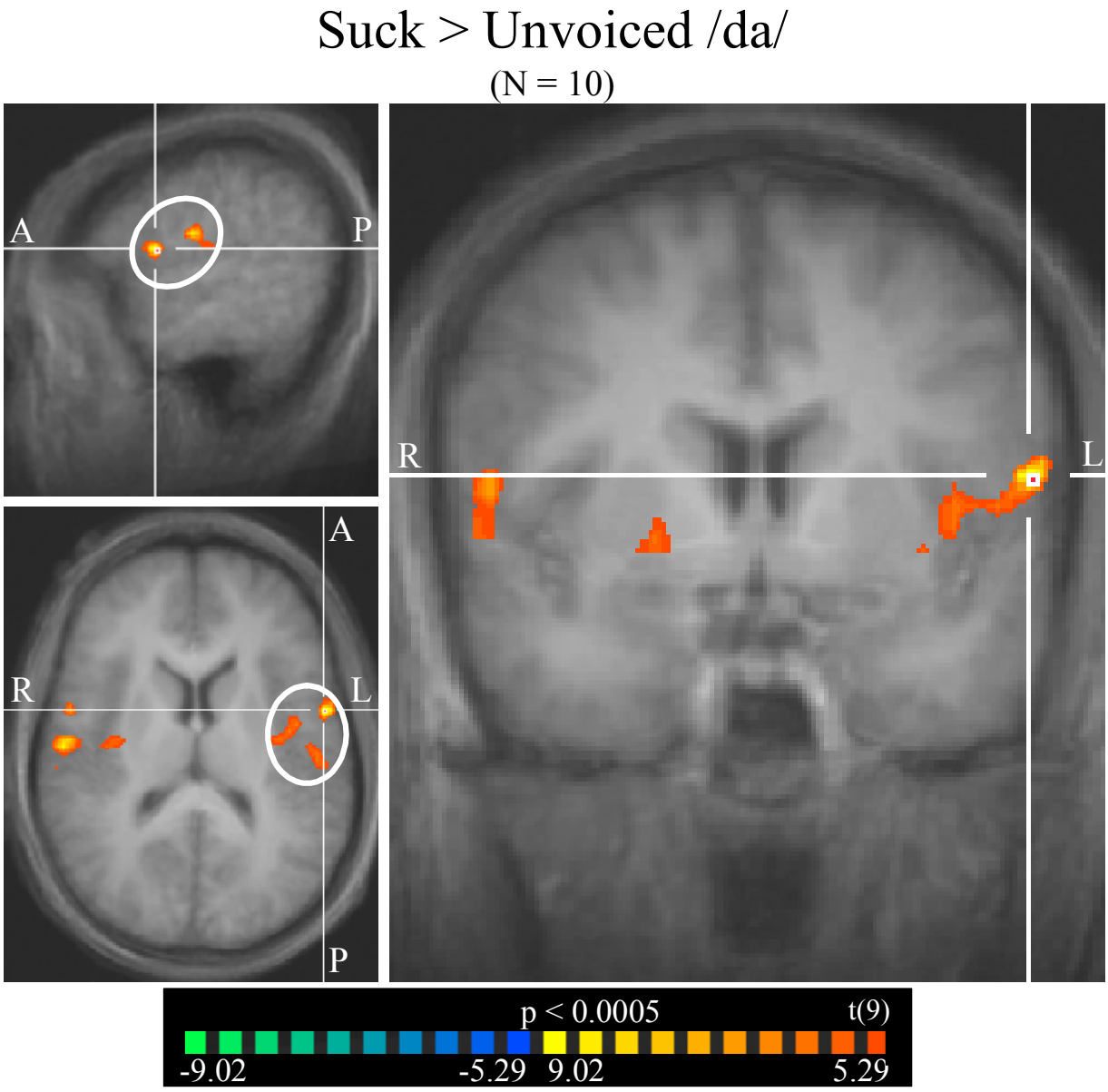

(TC pictured: -54, 2, 13)

Table 9 a. Multi-Subject RFX GLM, main effect of task

ROI	Cluster Region	BA	# of voxels	Peak Voxel				
				x	y	z	t value	p value
2	**L. precentral gyrus**	**4**	**75**	**-54**	**2**	**13**	**11.790**	**0.000001**
34	**R. postcentral gyrus**	**3**	**13**	**48**	**-13**	**22**	**9.166**	**0.000007**
35	**L. postcentral gyrus**	**2**	**16**	**-54**	**-13**	**19**	**9.307**	**0.000006**
36	**L. postcentral gyrus**	**2**	**4**	**-51**	**-19**	**16**	**7.566**	**0.000034**
37	**R. putamen**	**N/A**	**8**	**33**	**-19**	**4**	**8.359**	**0.000016**
38	**R. insula**	**13**	**5**	**42**	**-25**	**19**	**8.124**	**0.000020**
39	**L. insula**	**13**	**555**	**-39**	**-1**	**7**	**10.959**	**0.000002**
40	R. rolandic operculum	44	45	57	-13	13	9.285	0.000007
41	R. rolandic operculum	44	4	54	2	13	7.313	0.000045
42	R. transverse temporal gyrus	41	138	45	-10	7	9.382	0.000006
43	R. cuneus	17	11	6	-58	-5	8.582	0.000013
44	L. supramarginal gyrus	40	11	-60	-28	28	9.383	0.000006
45	L. supramarginal gyrus	40	4	-45	-31	22	8.099	0.000020

Table 9 b. RFX GLM of ROIs

ROI	Region	Contrast	df	mean	se	t value	p value
2	**L. precentral gyrus**	**Suck**	**9**	**2.168**	**0.248**	**8.738**	**0.000011***
		Unvoiced /da/	**9**	**1.534**	**0.250**	**6.141**	**0.000171**
34	**R. postcentral gyrus**	**Suck**	**9**	**1.688**	**0.156**	**10.855**	**0.000002***
		Unvoiced /da/	**9**	**1.334**	**0.147**	**9.072**	**0.000008***
35	**L. postcentral gyrus**	**Suck**	**9**	**2.833**	**0.569**	**4.975**	**0.000764**
		Unvoiced /da/	**9**	**2.429**	**0.568**	**4.280**	**0.002051**
36	**L. postcentral gyrus**	**Suck**	**9**	**1.728**	**0.266**	**6.499**	**0.000112**
		Unvoiced /da/	**9**	**1.247**	**0.265**	**4.703**	**0.001115**
37	**R. putamen**	**Suck**	**9**	**0.489**	**0.104**	**4.697**	**0.001126**
		Unvoiced /da/	**9**	**0.102**	**0.109**	**0.933**	**0.375141**
38	**R. insula**	**Suck**	**9**	**0.986**	**0.332**	**2.970**	**0.015702**
		Unvoiced /da/	**9**	**0.565**	**0.303**	**1.864**	**0.095216**
39	**L. insula**	**Suck**	**9**	**1.679**	**0.129**	**12.999**	**0.000000***
		Unvoiced /da/	**9**	**1.200**	**0.119**	**10.109**	**0.000003***
40	R. rolandic operculum	Suck	9	2.427	0.192	12.633	0.000000*
		Unvoiced /da/	9	1.762	0.197	8.961	0.000009*
41	R. rolandic operculum	Suck	9	1.658	0.225	7.372	0.000042*
		Unvoiced /da/	9	1.126	0.187	6.021	0.000197
42	R. transverse temporal gyrus	Suck	9	1.503	0.087	17.277	0.000000*
		Unvoiced /da/	9	0.981	0.086	11.350	0.000001*
43	R. cuneus	Suck	9	0.868	0.276	3.152	0.011704

		Unvoiced /da/	9	0.558	0.277	2.015	0.074760
44	L. supramarginal gyrus	Suck	9	1.956	0.365	5.358	0.000458
		Unvoiced /da/	9	1.523	0.342	4.461	0.001575
45	L. supramarginal gyrus	Suck	9	0.645	0.170	3.791	0.004278
		Unvoiced /da/	9	0.430	0.159	2.708	0.024060

* Significantly different from baseline

Figure 9 a. Right precentral gyrus (ROI #34)

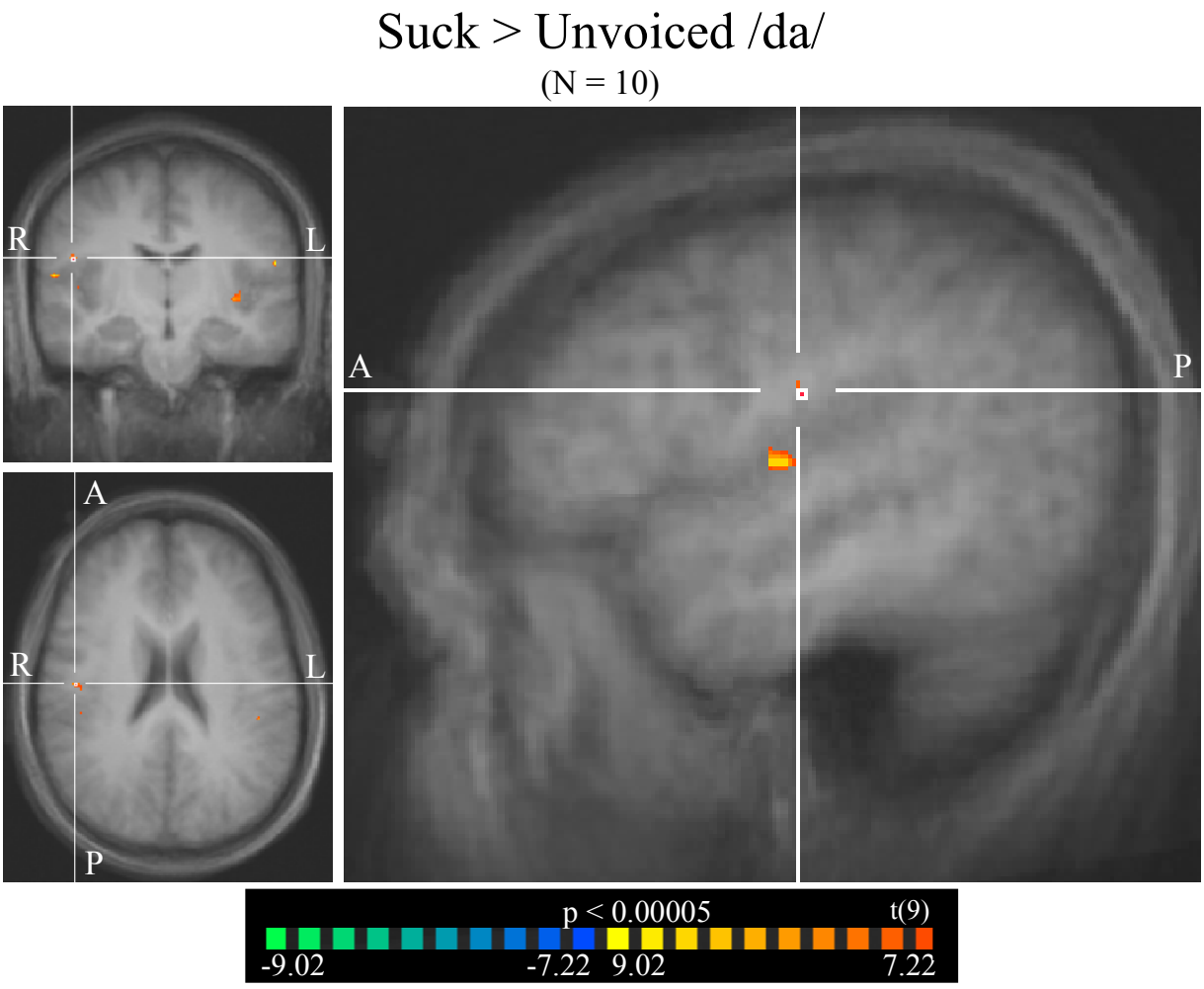

(TC pictured: 48, -13, 22)

Figure 9 b. Left pre- (ROI #2) & postcentral (ROI #35) gyri

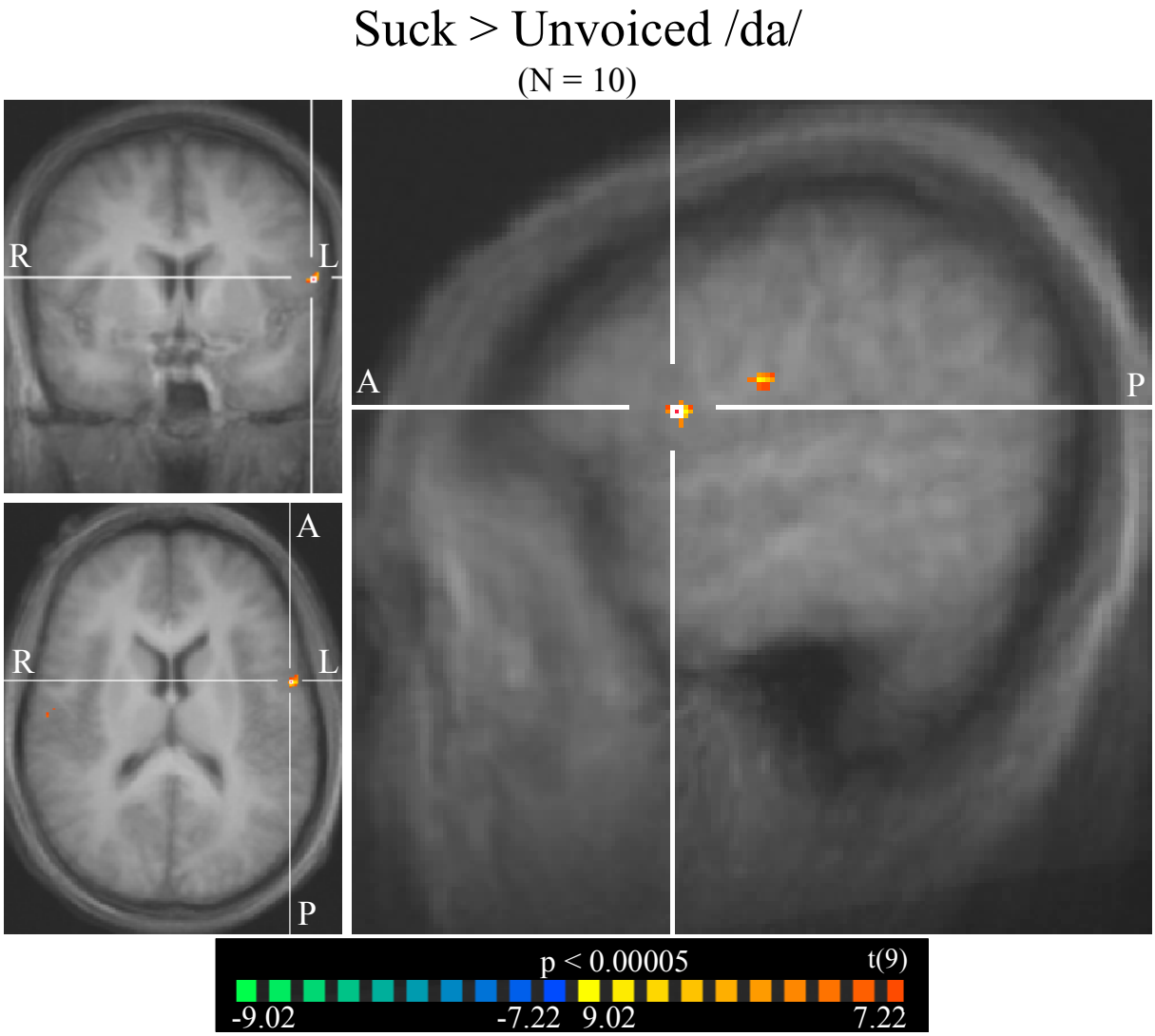

(TC pictured: -54, 3, 14)

Figure 9 c. Mean % signal change compared to baseline

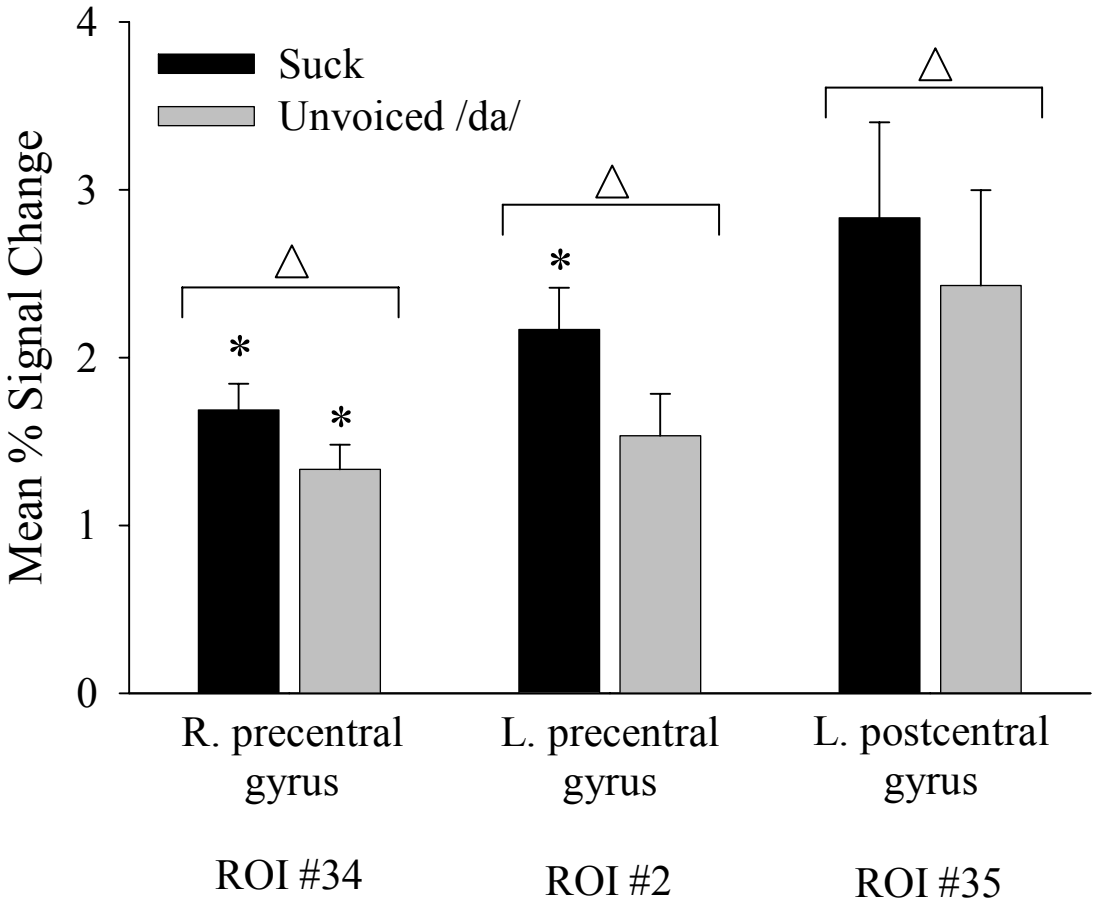

△ Significant main effect of task

* Significantly different from baseline

Part 1b: Whole Brain: Conjunction analysis, main effect of task

To initially assess the overlapping substrates by task or rate, two simple SPM map overlays (one for overlapping tasks, one for overlapping rates) were computed, thresholded at FDR < 0.01, and visually assessed for shared correlates (Figures 10a-c, pp. 73-74). To formally determine the minimally shared brain areas correlated to both task conditions, a conjunction of contrasts 1 [Unvoiced /da/ > baseline] and 2 [Suck > baseline] was performed and data were thresholded with $p < 0.0005$. Table 11a (p. 75) lists the statistical details for *a priori* ROIs in bold text and post hoc ROIs in plain text. Table 11b (p. 76) lists the average magnitude of signal compared to baseline for the Suck and Unvoiced /da/ task conditions collapsed across rate for *a priori* ROIs in bold text and post hoc ROIs in plain text. Figures 11a-e (pp. 78-82) include bar graphs and SPM maps representing the mean percent signal change of the task conditions compared to baseline for some of the *a priori* ROIs.

Areas found to be active in both Unvoiced /da/ and Suck task conditions were: bilateral sensorimotor cortices that extended into rolandic operculi, insulae, temporal gyri, and basal ganglia, cingulate, distinct insular areas (Figures 11a-c, pp. 78-80), anterior cerebellar lobes (Figures 11d-e, pp. 81-82), and a bilateral thalamic spread. Further inspection ($p < 0.00005$) revealed distinct areas of activity in the bilateral thalamic nuclei and basal ganglia (Tables 12a-b, Figures 12a-d, pp. 83-89). No pontomedullary correlates were identified in the conjunction analysis of task.

Figure 10 a. Overlapping substrates as a function of task (cortical)

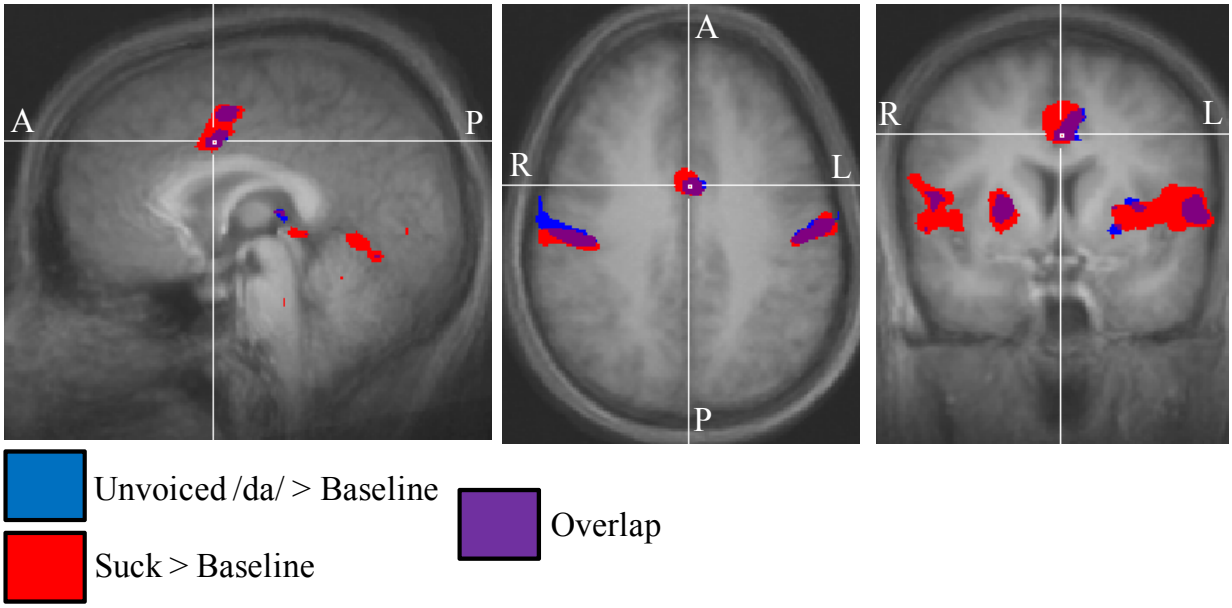

Figure 10 b. Overlapping substrates as a function of task (brainstem)

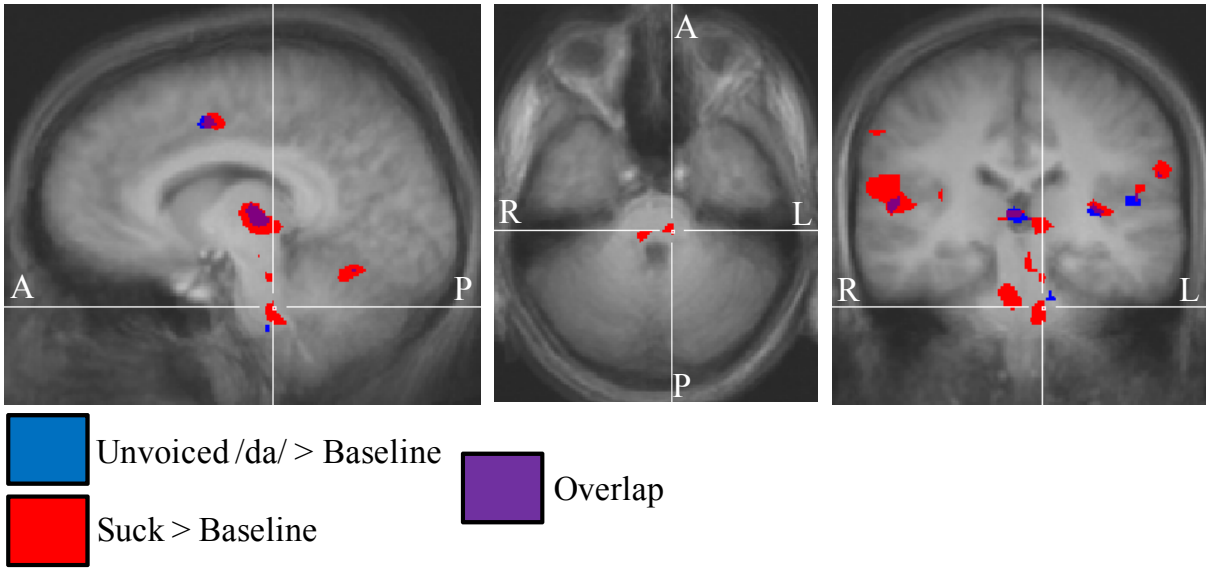

Figure 10 c. Overlapping substrates as a function of task (subcortical)

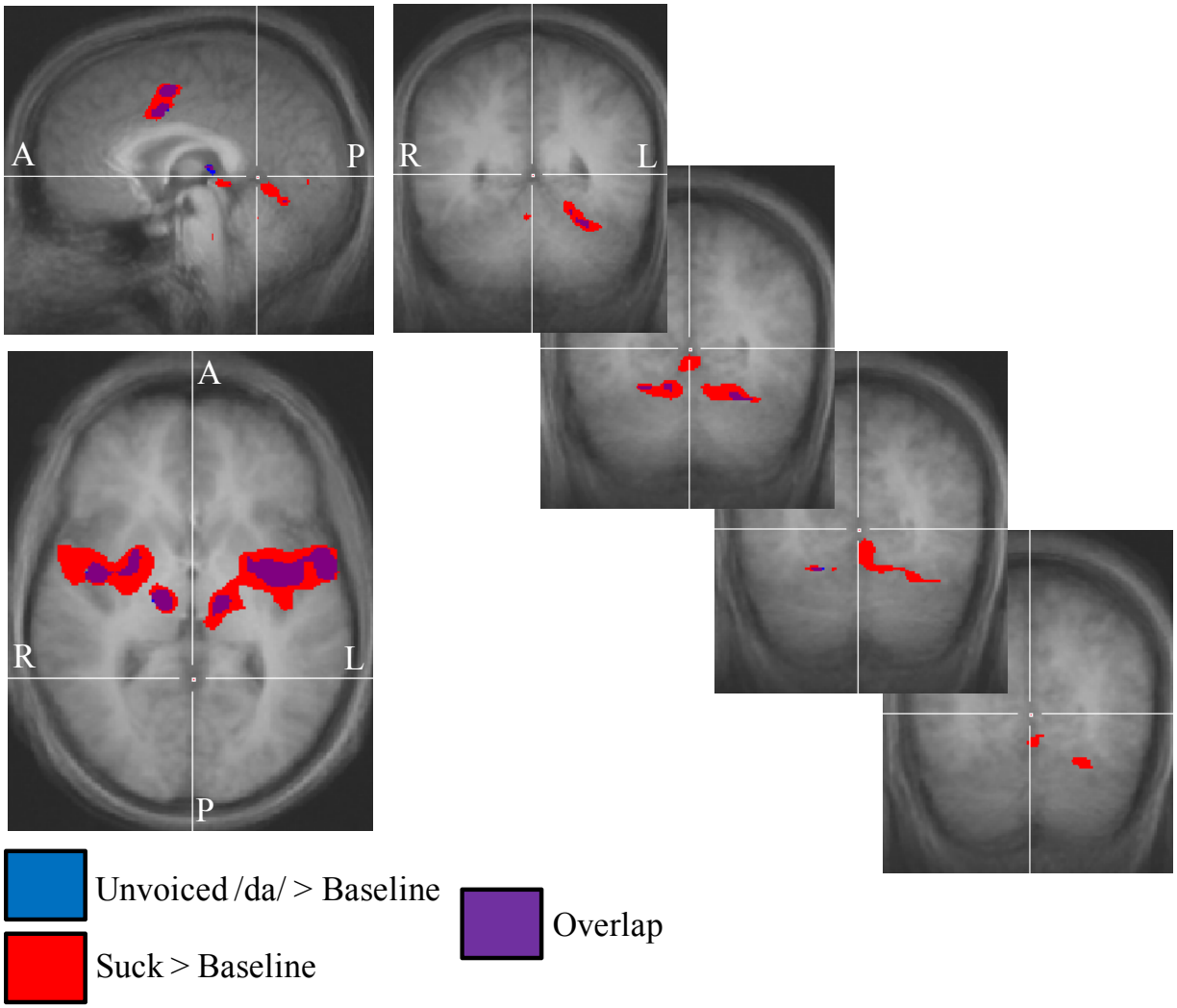

Table 11 a. Multi-Subject RFX GLM, conjunction of task conditions

ROI	Cluster Region	BA	# of voxels	Peak Voxel				
				x	y	z	t value	p value
46	**R. insula, transverse temporal & precentral gyri, & supramarginal cortex**	**4, 41, 13, 40**	**4069**	**42**	**-7**	**7**	**16.211**	**0.000000**
48	**L. precentral & inf. frontal gyri, insula, putamen, globus pallidus**	**4, 44, 13**	**4251**	**-48**	**-16**	**31**	**13.284**	**0.000000**
60	**R. thalamus (VL n.)**	**N/A**	**259**	**12**	**-16**	**1**	**9.549**	**0.000005**
61	**L. thalamus (VL n.)**	**N/A**	**194**	**-12**	**-16**	**1**	**10.091**	**0.000003**
62	**R. putamen**	**N/A**	**72**	**27**	**-4**	**-2**	**9.047**	**0.000008**
63	**R. putamen**	**N/A**	**494**	**24**	**2**	**7**	**10.535**	**0.000002**
64	**L. putamen**	**N/A**	**4**	**-24**	**-1**	**7**	**7.480**	**0.000038**
65	**Midline cingulate**	**24**	**18**	**0**	**-1**	**46**	**7.746**	**0.000029**
66	**L. cingulate**	**24**	**214**	**-6**	**-2**	**40**	**7.215**	**0.000050**
67	R. inf. frontal gyrus	44	57	51	2	10	9.632	0.000005
68	L. superior temporal gyrus	38	7	-60	-7	4	7.626	0.000032
58	L. superior temporal sulcus	19	5	-45	-67	22	-7.722	0.000029

Table 11 b. RFX GLM of ROIs

ROI	Region	Contrast	df	mean	se	t value	p value
46	R. insula, transverse temporal & precentral gyri & supramarginal cortex	Suck	9	1.988	0.045	44.012	0.000000*
		Unvoiced /da/	9	1.509	0.060	25.015	0.000000*
48	L. precentral & inf. frontal gyri, insula, putamen, globus pallidus	Suck	9	2.176	0.077	28.124	0.000000*
		Unvoiced /da/	9	1.695	0.096	17.631	0.000000*
60	R. thalamus (VL n.)	Suck	9	1.206	0.110	10.959	0.000002*
		Unvoiced /da/	9	0.922	0.097	9.504	0.000005*
61	L. thalamus (VL n.)	Suck	9	1.236	0.096	12.841	0.000000*
		Unvoiced /da/	9	0.962	0.105	9.194	0.000007*
62	R. putamen	Suck	9	1.527	0.125	12.174	0.000001*
		Unvoiced /da/	9	1.018	0.105	9.685	0.000005*
63	R. putamen	Suck	9	1.239	0.102	12.189	0.000001*
		Unvoiced /da/	9	0.837	0.089	9.382	0.000006*
64	L. putamen	Suck	9	1.402	0.160	8.790	0.000010*
		Unvoiced /da/	9	0.988	0.132	7.480	0.000038*
65	Midline cingulate	Suck	9	2.108	0.232	9.090	0.000008*
		Unvoiced /da/	9	1.684	0.215	7.830	0.000026*
66	L. cingulate	Suck	9	1.271	0.096	13.212	0.000000*

		Unvoiced /da/	**9**	**0.959**	**0.096**	**9.960**	**0.000004***
67	R. inf. frontal gyrus	Suck	9	1.648	0.156	10.563	0.000002*
		Unvoiced /da/	9	1.226	0.129	9.495	0.000006*
68	L. superior temporal gyrus	Suck	9	3.089	0.388	7.959	0.000023*
		Unvoiced /da/	9	2.313	0.212	10.915	0.000002*
58	L. superior temporal sulcus	Suck	9	-0.734	0.092	-7.955	0.000023*
		Unvoiced /da/	9	-0.715	0.084	-8.524	0.000013*

* Significantly different from baseline

Figure 11 a. Right insula (ROI #47)

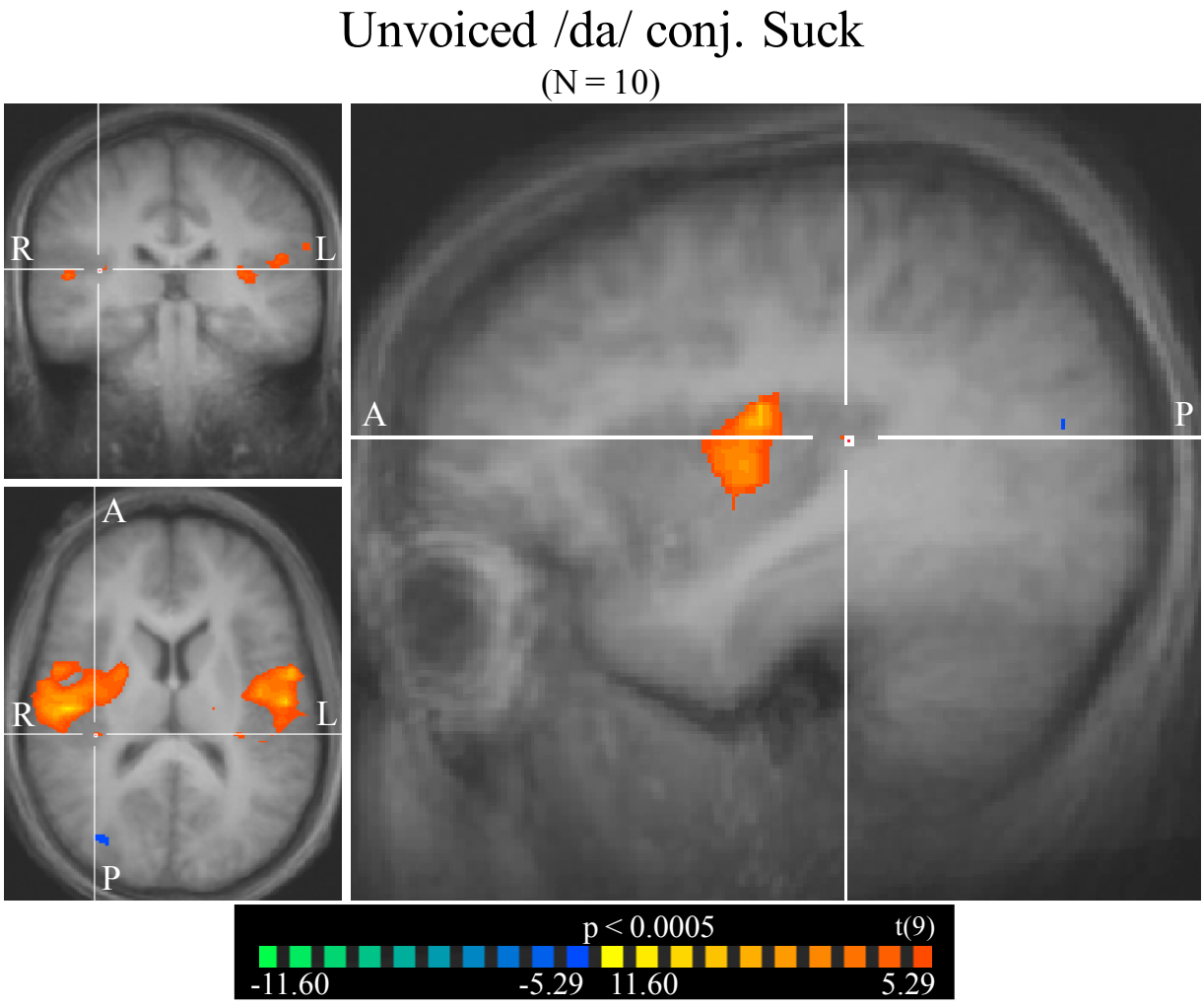

(TC pictured: 36, -28, 13)

Figure 11 b. Left insula (ROI #49)

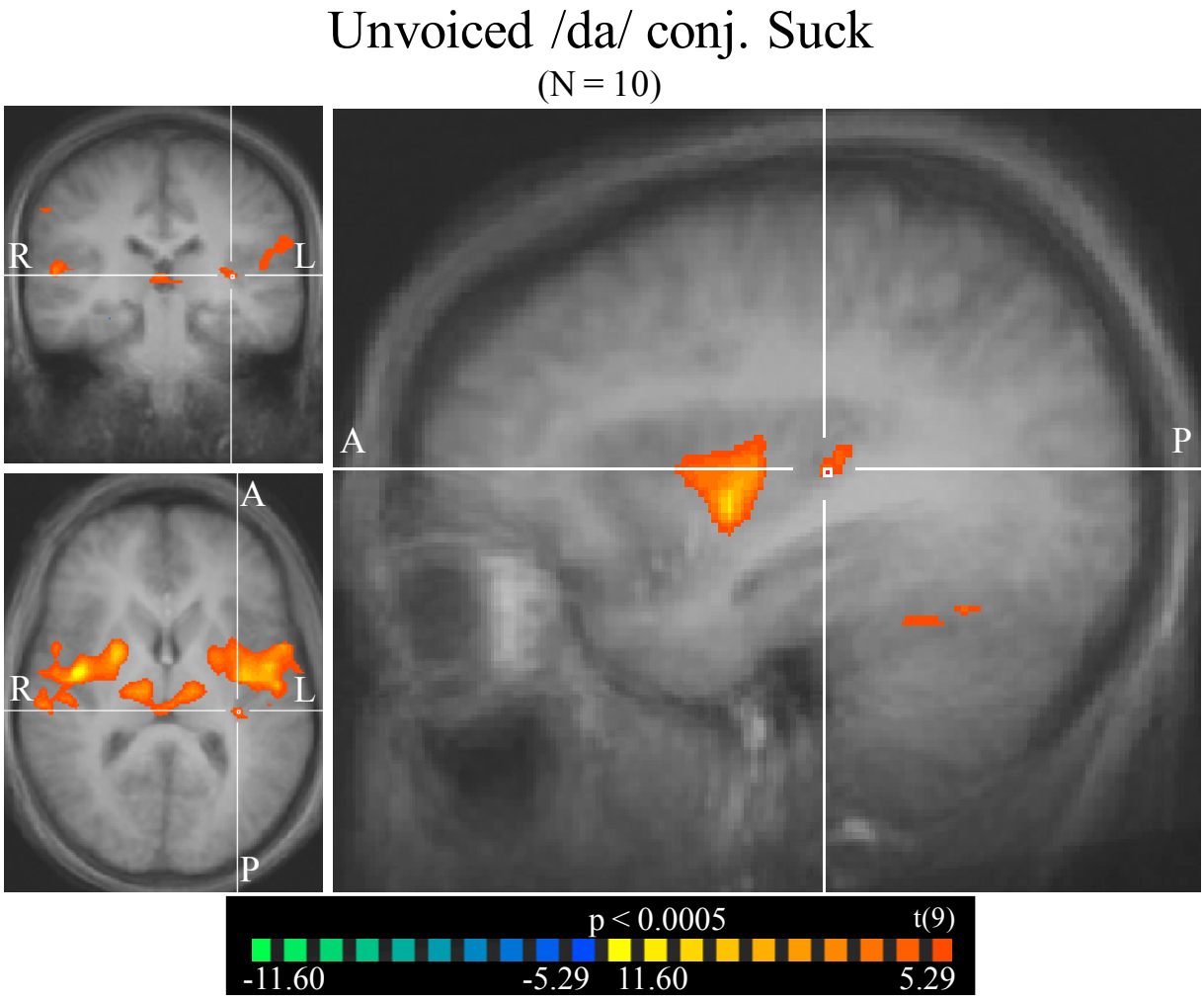

(TC pictured: -33, -25, 7)

Figure 11 c. Mean % Signal change compared to baseline

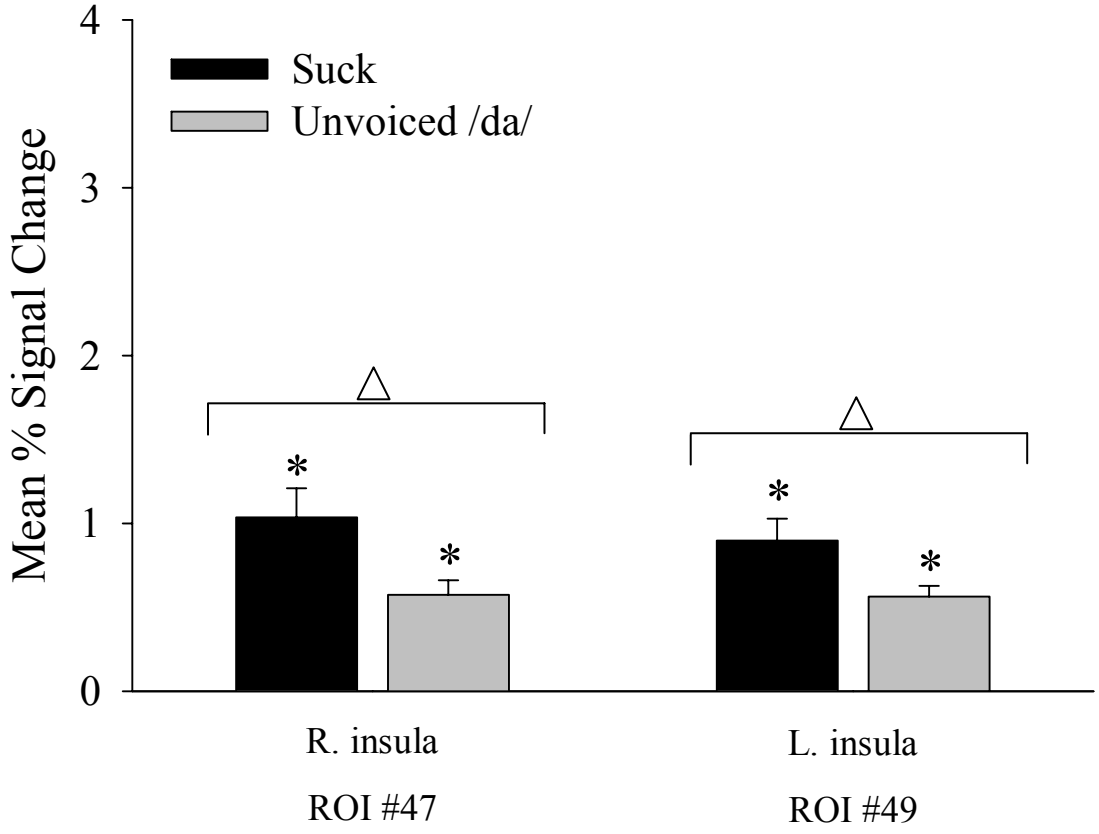

△ Significant main effect across task

* Significantly different from baseline

Figure 11 d. Right & left cerebellum, anterior lobes (ROI #51, 52)

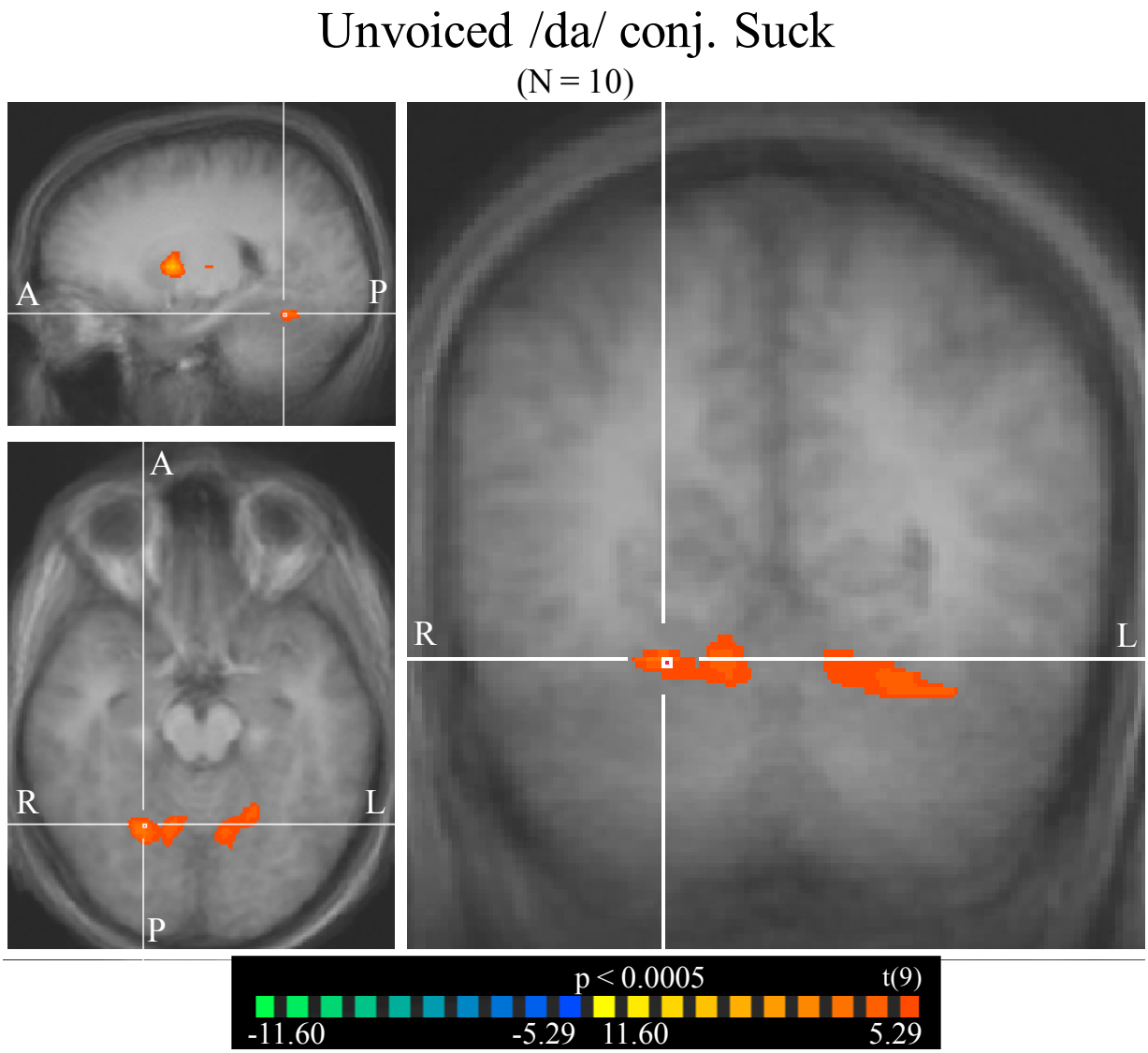

(TC pictured: 21, -55, -17)

Figure 11 e. Mean % signal change compared to baseline

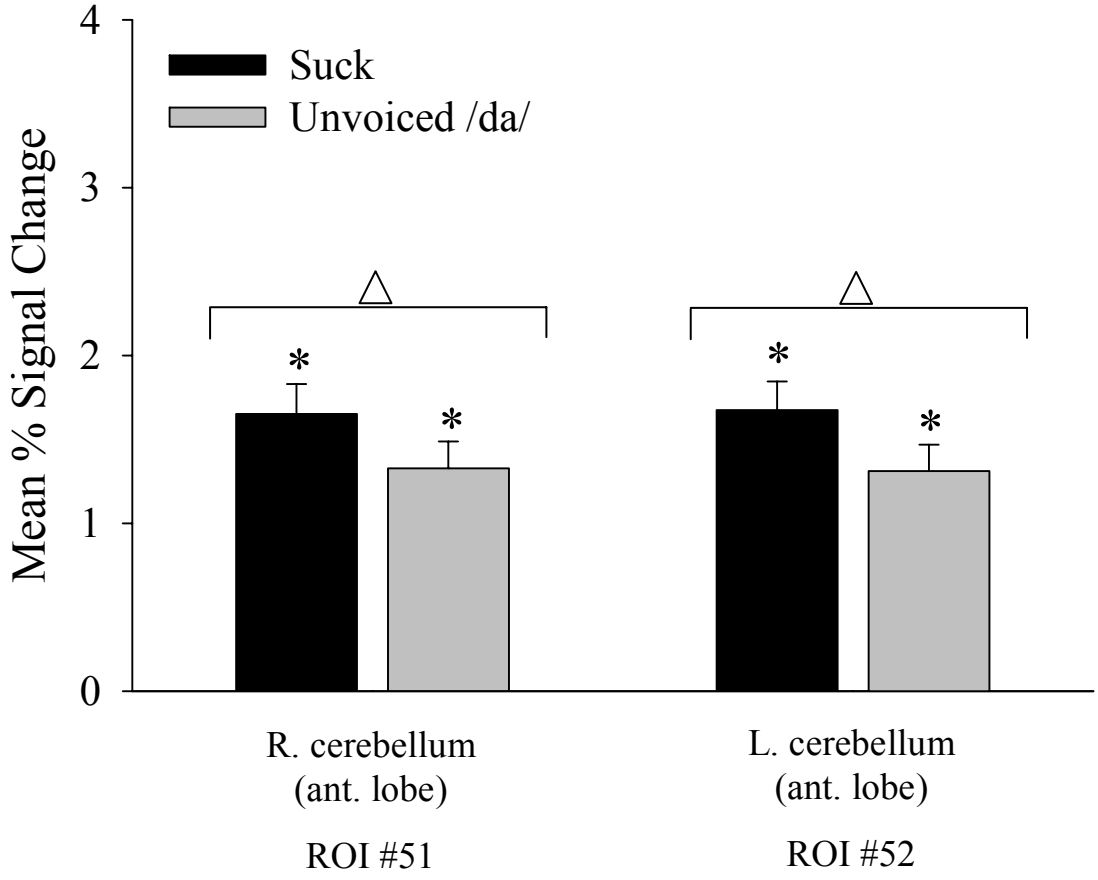

△ Significant main effect across task

* Significantly different from baseline

Table 12 a. Multi-Subject RFX GLM, conjunction of task conditions

ROI	Cluster Region	BA	# of voxels	Peak Voxel				
				x	y	z	t value	p value
46	**R. insula, transverse temporal & precentra gyri, & supramarginal cortex**	**4, 41, 13, 40**	**4069**	**42**	**-7**	**7**	**16.211**	**0.000000**
48	**L. precentral & inf. frontal gyri, insula, putamen, globus pallidus**	**4, 44, 13**	**4251**	**-48**	**-16**	**31**	**13.284**	**0.000000**
60	**R. thalamus (VL n.)**	**N/A**	**259**	**12**	**-16**	**1**	**9.549**	**0.000005**
61	**L. thalamus (VL n.)**	**N/A**	**194**	**-12**	**-16**	**1**	**10.091**	**0.000003**
62	**R. putamen**	**N/A**	**72**	**27**	**-4**	**-2**	**9.047**	**0.000008**
63	**R. putamen**	**N/A**	**494**	**24**	**2**	**7**	**10.535**	**0.000002**
64	**L. putamen**	**N/A**	**4**	**-24**	**-1**	**7**	**7.480**	**0.000038**
65	**Midline cingulate**	**24**	**18**	**0**	**-1**	**46**	**7.746**	**0.000029**
66	**L. cingulate**	**24**	**214**	**-6**	**-2**	**40**	**7.215**	**0.000050**
67	R. inf. frontal gyrus	44	57	51	2	10	9.632	0.000005
68	L. superior temporal gyrus	38	7	-60	-7	4	7.626	0.000032
58	L. superior temporal sulcus	19	5	-45	-67	22	-7.722	0.000029

Table 12 b. RFX GLM of ROIs

ROI	Region	Contrast	df	mean	se	t value	p value
46	R. insula, transverse temporal & precentral gyri & supramarginal cortex	Suck	9	1.988	0.045	44.012	0.000000*
		Unvoiced /da/	9	1.509	0.060	25.015	0.000000*
48	L. precentral & inf. frontal gyri, insula, putamen, globus pallidus	Suck	9	2.176	0.077	28.124	0.000000*
		Unvoiced /da/	9	1.695	0.096	17.631	0.000000*
60	R. thalamus (VL n.)	Suck	9	1.206	0.110	10.959	0.000002*
		Unvoiced /da/	9	0.922	0.097	9.504	0.000005*
61	L. thalamus (VL n.)	Suck	9	1.236	0.096	12.841	0.000000*
		Unvoiced /da/	9	0.962	0.105	9.194	0.000007*
62	R. putamen	Suck	9	1.527	0.125	12.174	0.000001*
		Unvoiced /da/	9	1.018	0.105	9.685	0.000005*
63	R. putamen	Suck	9	1.239	0.102	12.189	0.000001*
		Unvoiced /da/	9	0.837	0.089	9.382	0.000006*
64	L. putamen	Suck	9	1.402	0.160	8.790	0.000010*
		Unvoiced /da/	9	0.988	0.132	7.480	0.000038*
65	Midline cingulate	Suck	9	2.108	0.232	9.090	0.000008*
		Unvoiced /da/	9	1.684	0.215	7.830	0.000026*
66	L. cingulate	Suck	9	1.271	0.096	13.212	0.000000*

		Unvoiced /da/	**9**	**0.959**	**0.096**	**9.960**	**0.000004***
67	R. inf. frontal gyrus	Suck	9	1.648	0.156	10.563	0.000002*
		Unvoiced /da/	9	1.226	0.129	9.495	0.000006*
68	L. superior temporal gyrus	Suck	9	3.089	0.388	7.959	0.000023*
		Unvoiced /da/	9	2.313	0.212	10.915	0.000002*
58	L. superior temporal sulcus	Suck	9	-0.734	0.092	-7.955	0.000023*
		Unvoiced /da/	9	-0.715	0.084	-8.524	0.000013*

* Significantly different from baseline

Figure 12 a. Right & left thalamic nuclei (ROI #60, 61)

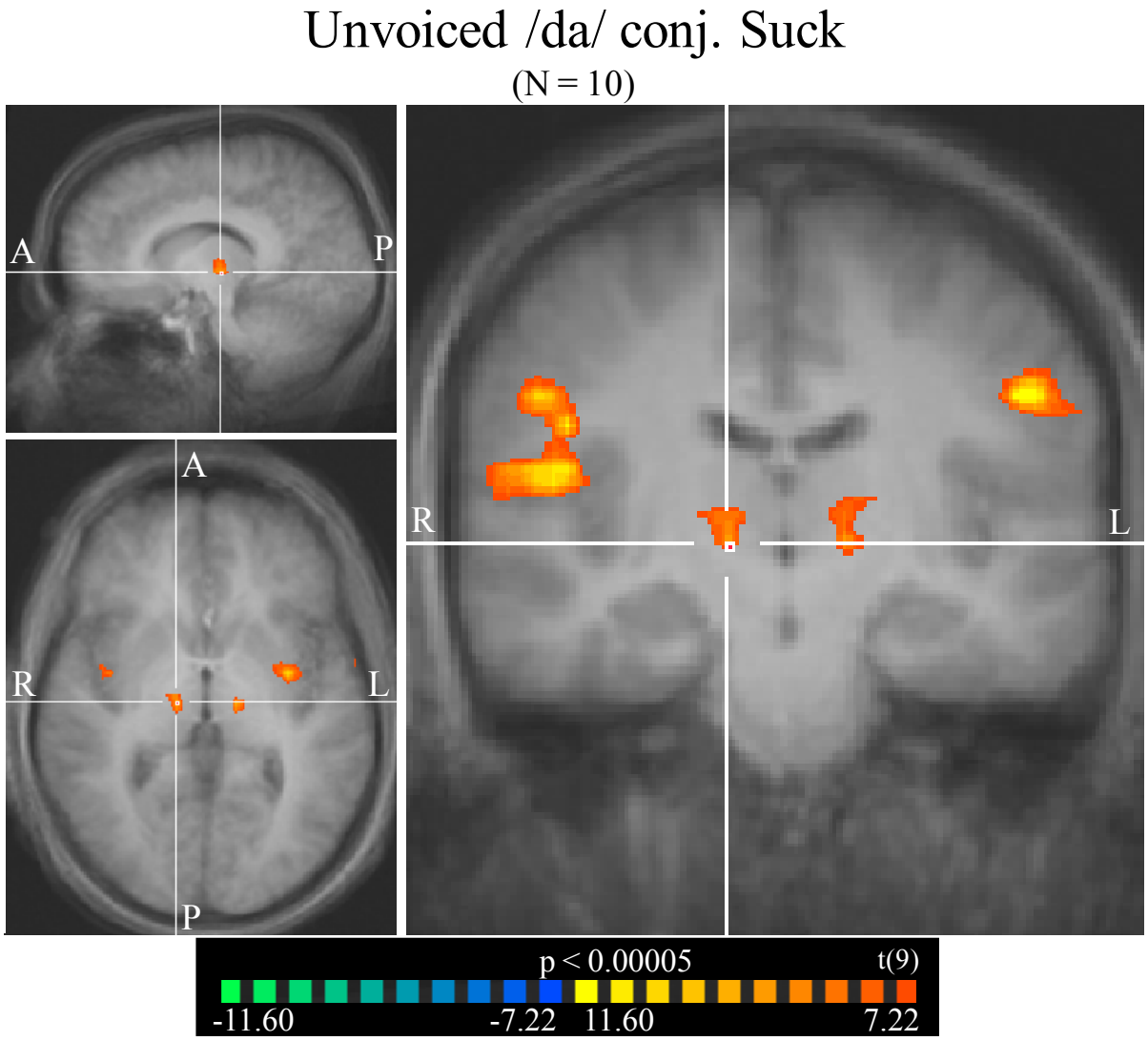

(TC pictured: 12, -16, 1)

Figure 12 b. Mean % signal change compared to baseline

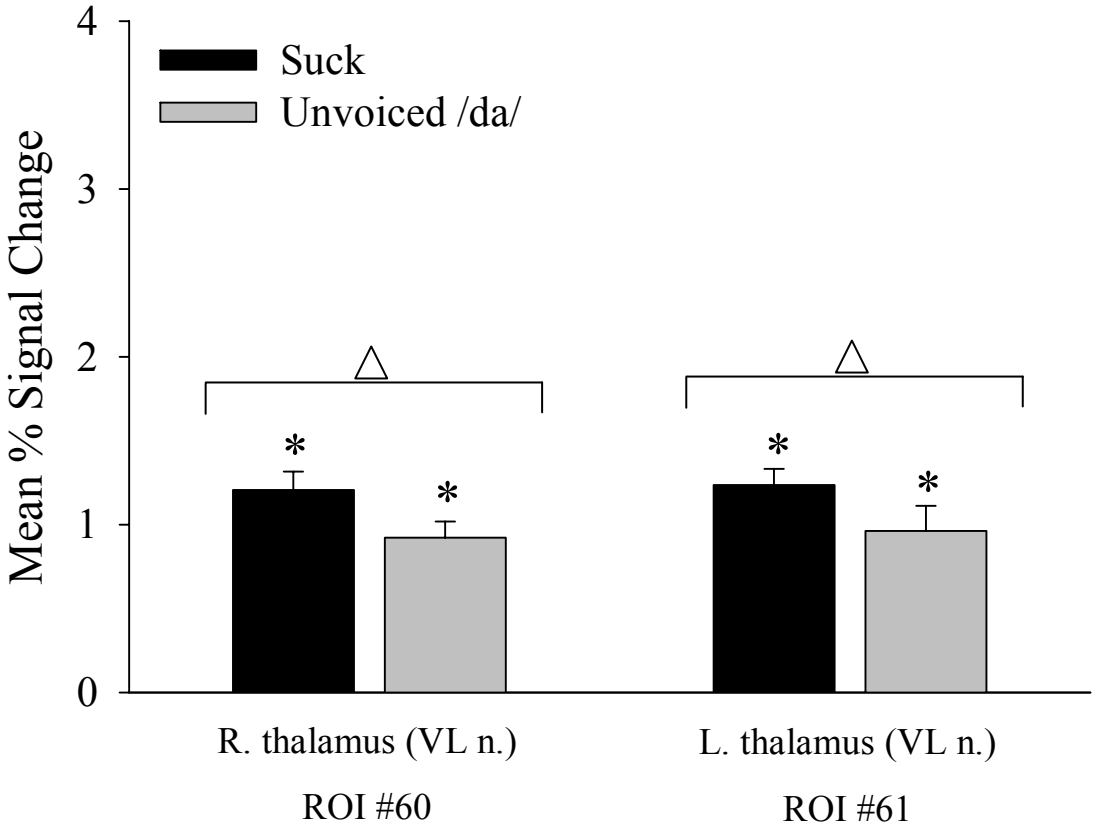

△ Significant main effect of task

* Significantly different from baseline

Figure 12 c. Right & left putamen (ROI #62, 64)

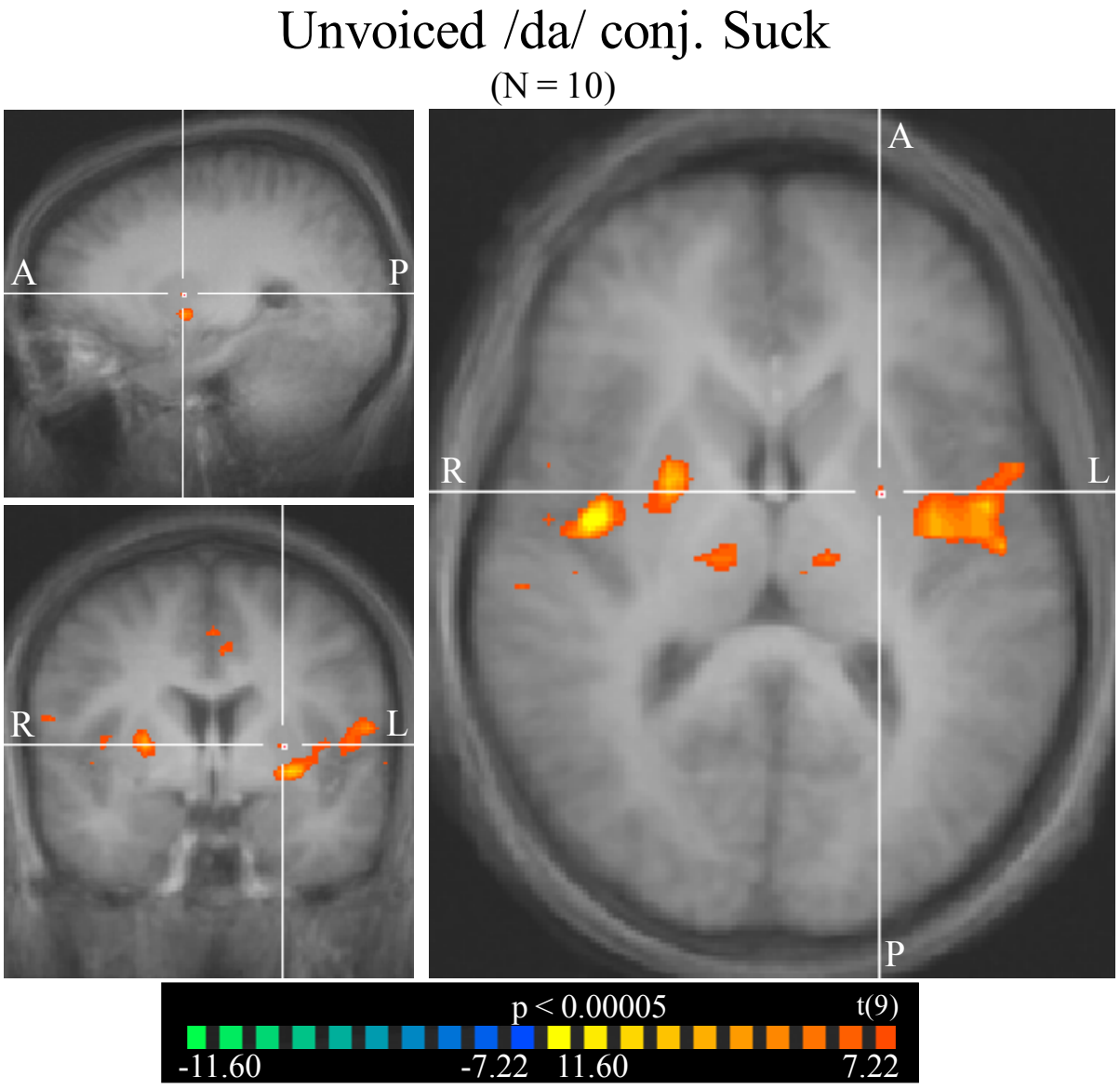

(TC pictured: -24, -1, 7)

Figure 12 d. Mean % signal change compared to baseline

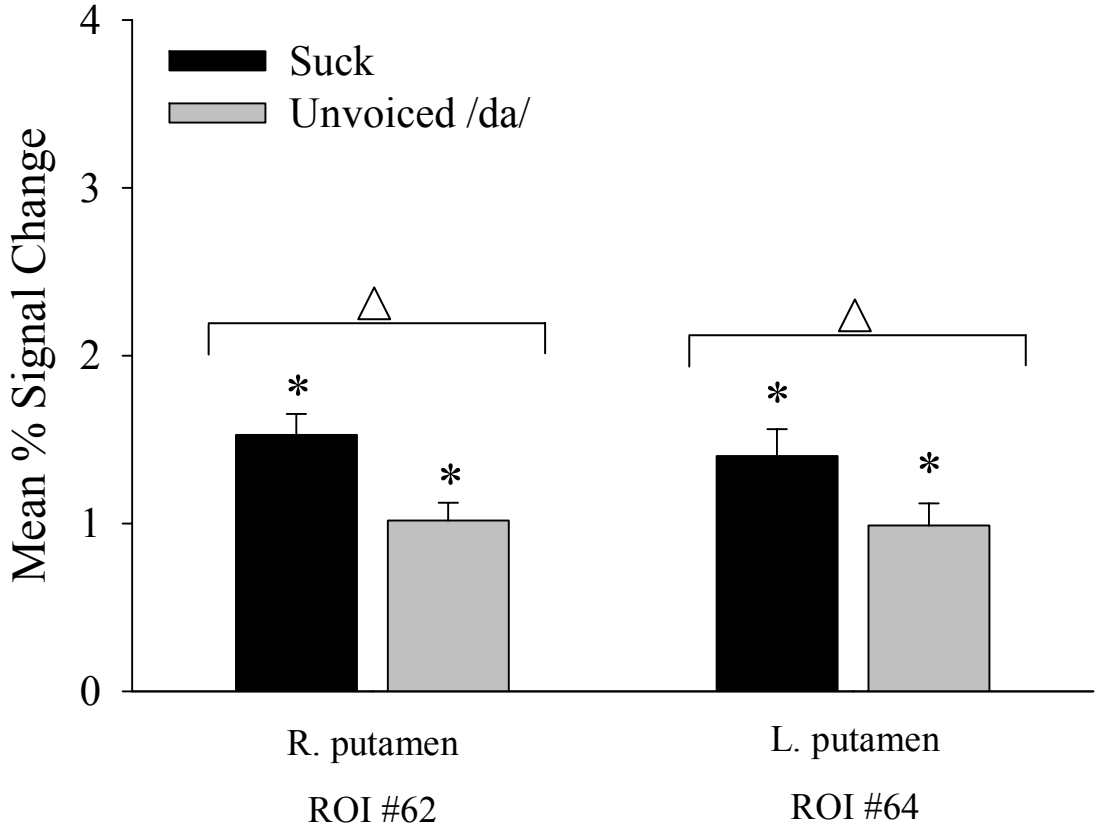

△ Significant main effect of task

* Significantly different from baseline

Part 1c: Whole Brain: RFX analysis, main effect of rate

To determine the main effect of rate, a multi-subject RFX GLM analysis including all participants, separate subject predictors, and percent signal transform was performed. To identify *a priori* ROIs actively correlated with the ororhythmic rate conditions, the contrast [3 Hz > 1 Hz] was applied and the data were thresholded at $p < 0.0005$. Table 13a (p. 91) lists the statistical details for *a priori* ROIs in bold text and post hoc ROIs in plain text. Table 13b (p. 93) lists the average magnitude of signal compared to baseline for the 1 Hz and 3 Hz rate conditions collapsed across the task condition for *a priori* ROIs in bold text and post hoc ROIs in plain text. Figures 13a-e (pp. 96-100) include bar graphs and SPM maps representing the mean percent signal change of the rate conditions compared to baseline for some of the *a priori* ROIs.

Areas found to be more active in the 3 Hz compared to 1 Hz rate conditions were: bilateral cerebellum (Figures 13a-b, pp. 96-97), superior temporal gyri; midline pons (Figures 13d-e, pp. 99-100); right transverse temporal gyrus, superior colliculus, and superior partietal gyrus; left thalamus (Figure 13c, p. 98) and basal ganglia. No activation was found in the sensorimotor cortices as a function of rate.

Table 13 a. Multi-Subject RFX GLM, main effect of rate

ROI	Cluster Region	BA	# of voxels	Peak Voxel				
				x	y	z	t value	p value
62	**R. med. cerebellum (post. lobe vermis & R/L ant. lobes)**	**N/A**	**6073**	**6**	**-61**	**-29**	**11.001**	**0.000002**
63	**R. med. cerebellum, vermis (post. lobe)**	**N/A**	**12**	**3**	**-52**	**-41**	**5.811**	**0.000256**
				3	**-52**	**-42**	**5.811**	**0.000256**
64	**R. lat. cerebellum (post. lobe)**	**N/A**	**355**	**30**	**-64**	**-38**	**7.667**	**0.000031**
65	**R. lat. cerebellum (post. lobe)**	**N/A**	**55**	**30**	**-49**	**-26**	**7.024**	**0.000062**
66	**L. lat. cerebellum (post. lobe)**	**N/A**	**67**	**-36**	**-55**	**-26**	**6.086**	**0.000182**
67	**Midline pons**	**N/A**	**12**	**-3**	**-28**	**-29**	**6.059**	**0.000188**
68	**L. thalamus (VA n.)**	**N/A**	**15**	**-9**	**-10**	**7**	**6.578**	**0.000102**
69	**L. caudate n.**	**N/A**	**8**	**-21**	**-4**	**22**	**6.246**	**0.000150**
70	**L. caudate n.**	**N/A**	**5**	**-24**	**-16**	**25**	**6.007**	**0.000201**
71	R. sup. colliculus	N/A	126	9	-28	1	6.968	0.000066
72	R. superior temporal gyrus	22	4	54	-1	1	5.616	0.000327
73	R. transverse temporal gyrus	41	224	63	-19	13	6.816	0.000078
74	R. transverse temporal gyrus	N/A	95	39	-31	13	5.884	0.000234

75	R. sup. parietal gyrus	7	38	18	-85	34	6.789	0.000080
76	L. sup. colliculus	N/A	91	-6	-34	-8	8.555	0.000013
77	L. superior temporal gyrus	42	15	-54	-37	7	5.576	0.000345
78	L. transverse temporal gyrus	22	886	-48	-7	1	9.690	0.000005
79	L. transverse temporal gyrus	22	1797	-48	-43	16	10.113	0.000003
80	L. post. transverse temporal gyrus	N/A	7	-27	-52	16	6.285	0.000143
81	L. supramarginal gyrus	40	5	-45	-25	19	5.571	0.000347
82	L. sup. parietal gyrus	7	411	-6	-85	37	9.613	0.000005
83	L. sup. parietal gyrus	7	9	-3	-70	55	5.871	0.000237
84	L. sup. parietal gyrus	7	10	-3	-82	43	6.026	0.000196
85	L. deep parietal	N/A	13	-36	-22	31	5.605	0.000332
86	R. amygdala	N/A	16	24	5	-14	6.450	0.000118
87	L. inf. frontal gyrus	44	4	-54	-4	10	5.451	0.000405
88	L. collateral sulcus	N/A	14	-21	-58	4	5.794	0.000262

Table 13 b. RFX GLM of ROIs

ROI	Region	Contrast	df	mean	se	t value	p value
62	**R. medial cerebellum (post. lobe vermis & R/L ant. lobes)**	**1 Hz**	**9**	**0.823**	**0.136**	**6.074**	**0.000185***
		3 Hz	**9**	**1.212**	**0.147**	**8.256**	**0.000017***
63	**R. med. cerebellum, vermis (post. lobe)**	**1 Hz**	**9**	**0.362**	**0.305**	**1.187**	**0.265535**
		3 Hz	**9**	**0.654**	**0.351**	**1.861**	**0.095616**
64	**R. lat. cerebellum (post. lobe)**	**1 Hz**	**9**	**0.097**	**0.158**	**0.613**	**0.554964**
		3 Hz	**9**	**0.514**	**0.189**	**2.714**	**0.023834**
65	**R. lat. cerebellum (post. lobe)**	**1 Hz**	**9**	**1.017**	**0.253**	**4.025**	**0.002994**
		3 Hz	**9**	**1.347**	**0.279**	**4.829**	**0.000935**
66	**L. lat. cerebellum (post. lobe)**	**1 Hz**	**9**	**0.801**	**0.238**	**3.364**	**0.008332**
		3 Hz	**9**	**1.171**	**0.233**	**5.036**	**0.000703**
67	**Midline pons**	**1 Hz**	**9**	**0.356**	**0.115**	**3.091**	**0.012914**
		3 Hz	**9**	**0.631**	**0.107**	**5.889**	**0.000232***
68	**L. thalamus (VA n.)**	**1 Hz**	**9**	**0.549**	**0.117**	**4.689**	**0.001138**
		3 Hz	**9**	**0.831**	**0.138**	**6.040**	**0.000193***
69	**L. caudate n.**	**1 Hz**	**9**	**0.258**	**0.119**	**2.168**	**0.058276**
		3 Hz	**9**	**0.438**	**0.123**	**3.554**	**0.006180**
70	**L. caudate n.**	**1 Hz**	**9**	**0.165**	**0.077**	**2.132**	**0.061829**
		3 Hz	**9**	**0.277**	**0.076**	**3.665**	**0.005194**
71	R. sup. colliculus	1 Hz	9	0.604	0.238	2.535	0.031960

		3 Hz	9	0.978	0.236	4.147	0.002495
72	R. superior temporal gyrs	1 Hz	9	1.401	0.236	5.947	0.000216*
		3 Hz	9	1.841	0.282	6.534	0.000107*
73	R. transverse temporal gyrus	1 Hz	9	2.552	0.462	5.528	0.000367*
		3 Hz	9	3.409	0.396	8.614	0.000012*
74	R. transverse temporal gyrus	1 Hz	9	0.459	0.143	3.213	0.010608
		3 Hz	9	0.941	0.178	5.285	0.000503
75	R. sup. parietal gyrus	1 Hz	9	-0.280	0.410	-0.684	0.511438
		3 Hz	9	0.241	0.381	0.633	0.542753
76	L. sup. colliculus	1 Hz	9	0.260	0.188	1.386	0.198998
		3 Hz	9	0.635	0.192	3.308	0.009112
77	L. superior temporal gyrus	1 Hz	9	0.152	0.227	0.671	0.519273
		3 Hz	9	0.602	0.273	2.203	0.055060
78	L. transverse temporal gyrus	1 Hz	9	1.172	0.117	9.988	0.000004*
		3 Hz	9	1.673	0.091	18.394	0.000000*
79	L. transverse temporal gyrus	1 Hz	9	0.598	0.275	2.175	0.057619
		3 Hz	9	1.178	0.307	3.838	0.003981
80	L. post. transverse temporal gyrus	1 Hz	9	0.119	0.088	1.362	0.206172
		3 Hz	9	0.250	0.095	2.641	0.026873
81	L. supramarginal gyrus	1 Hz	9	0.639	0.236	2.714	0.023855
		3 Hz	9	1.105	0.266	4.151	0.002481
82	L. sup. parietal gyrus	1 Hz	9	-0.132	0.384	-0.344	0.738412
		3 Hz	9	0.576	0.364	1.584	0.147762
83	L. sup. parietal	1 Hz	9	-0.749	0.400	-1.872	0.093938

	gyrus	3 Hz	9	0.259	0.358	0.723	0.487961
84	L. sup. parietal gyrus	1 Hz	9	-0.242	0.550	-0.439	0.670966
		3 Hz	9	0.714	0.495	1.442	0.183061
85	L. deep parietal	1 Hz	9	0.586	0.197	2.982	0.015404
		3 Hz	9	0.771	0.195	3.948	0.003367
86	R. amygdala	1 Hz	9	-0.035	0.295	-0.120	0.907164
		3 Hz	9	0.338	0.299	1.132	0.286927
87	L. inf. frontal gyrus	1 Hz	9	2.009	0.365	5.506	0.000377*
		3 Hz	9	2.290	0.391	5.860	0.000241*
88	L. collateral sulcus	1 Hz	9	0.232	0.160	1.453	0.180286
		3 Hz	9	0.589	0.166	3.541	0.006300

* Significantly different from baseline

Figure 13 a. Right medial cerebellum, vermis posterior lobe (ROI #63, 64, 66)

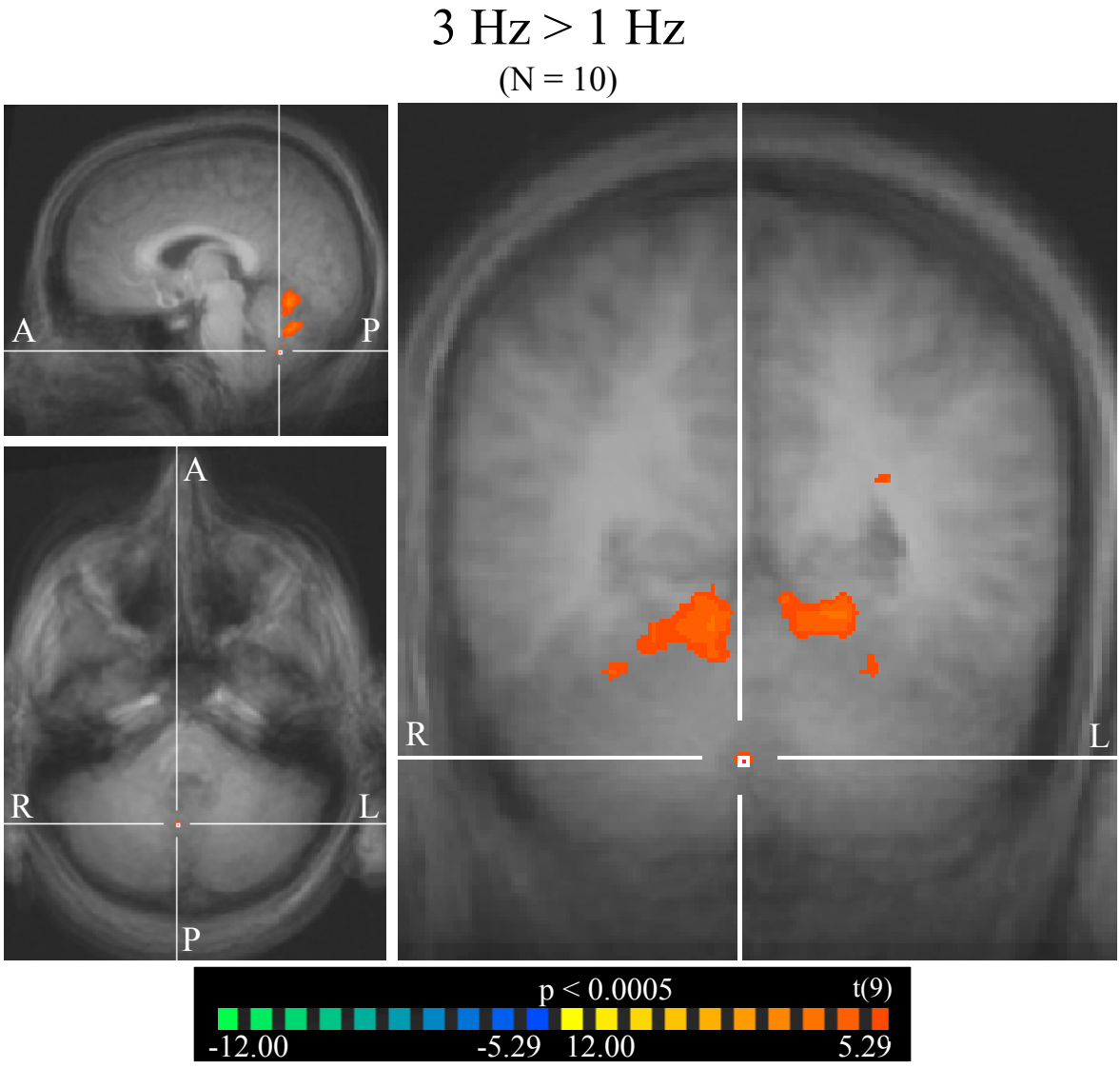

(TC pictured: 3, -52, -41)

Figure 13 b. Mean % signal change compared to baseline

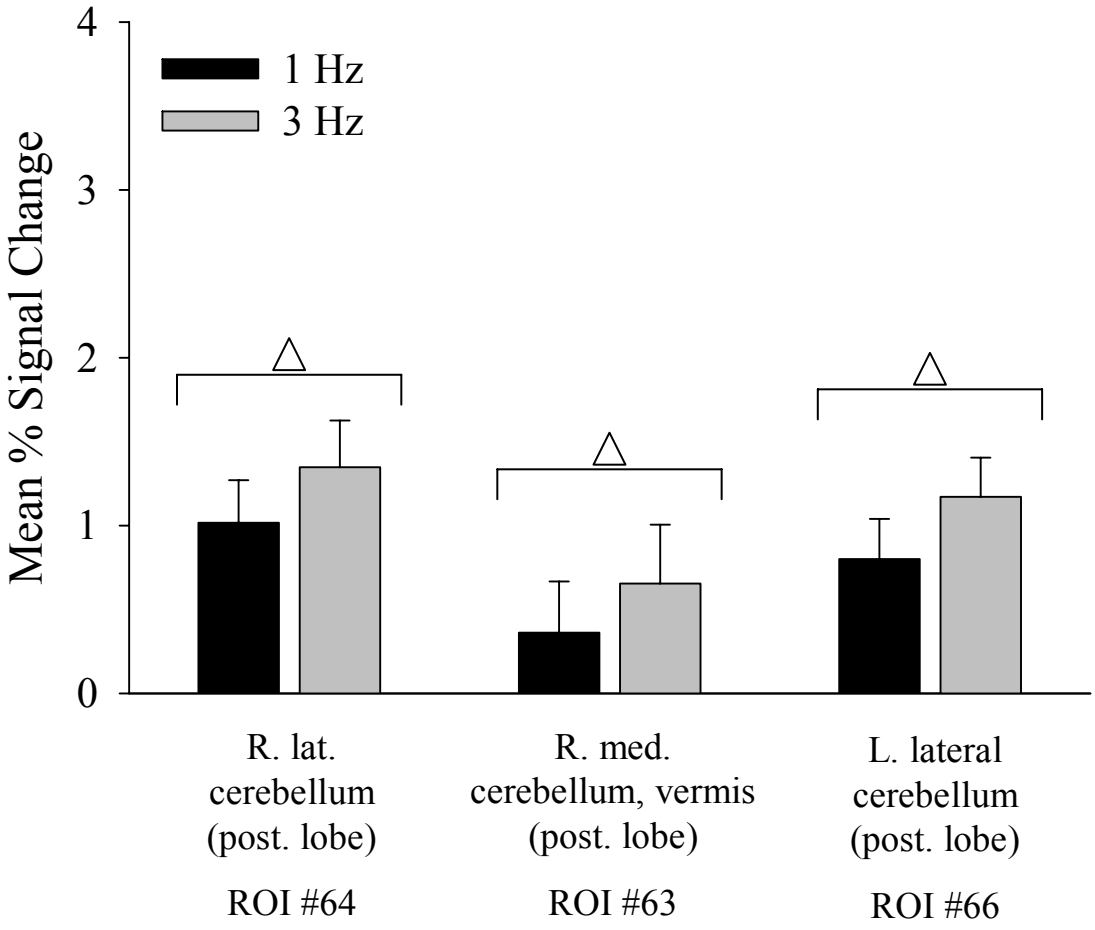

△ Significant main effect of rate

∗ Significantly different from baseline

Figure 13 c. Left thalamus, VA n. (ROI #68)

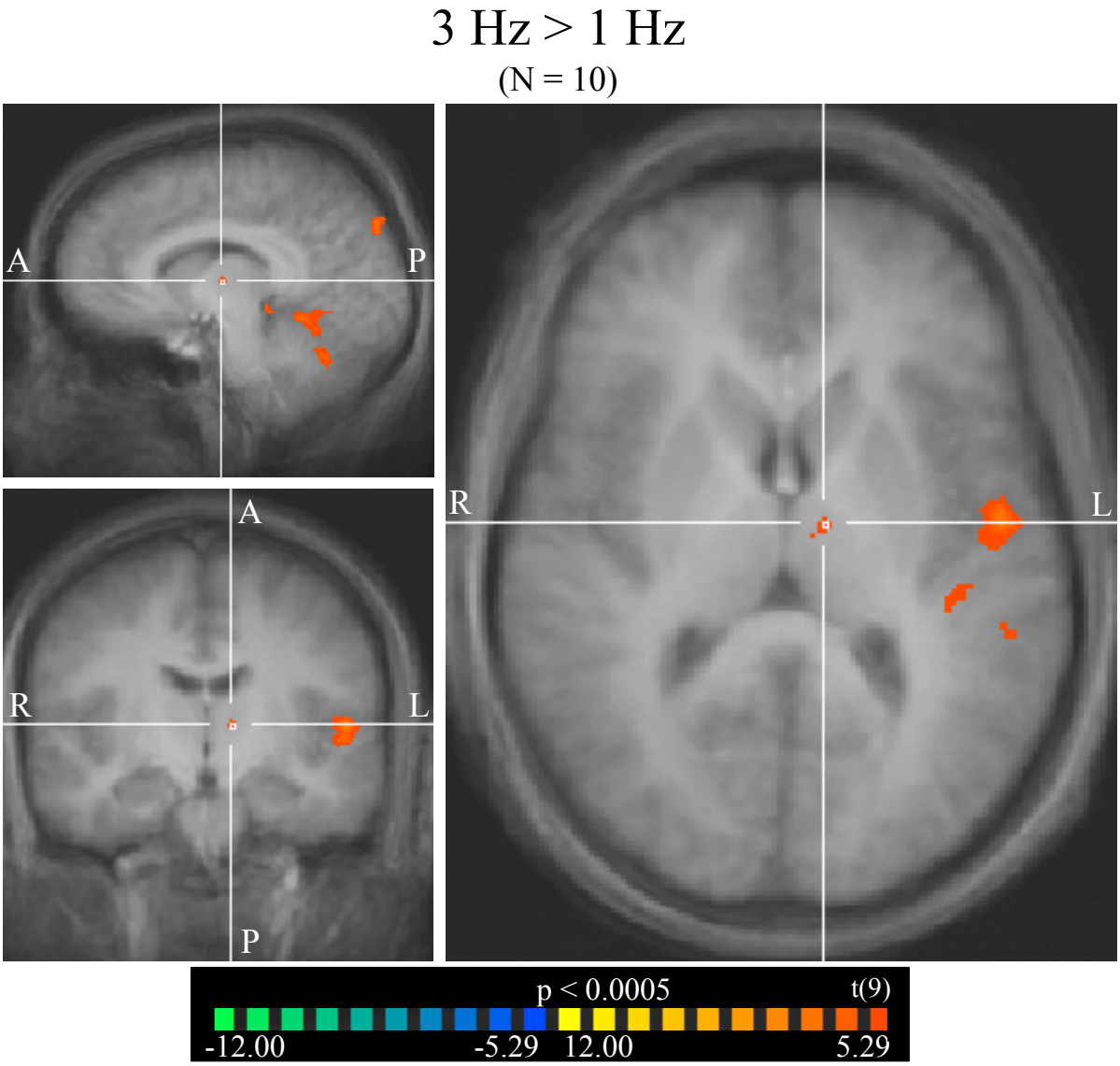

(TC pictured: -9, -10, 7)

Figure 13 d. Midline pons (ROI #67)

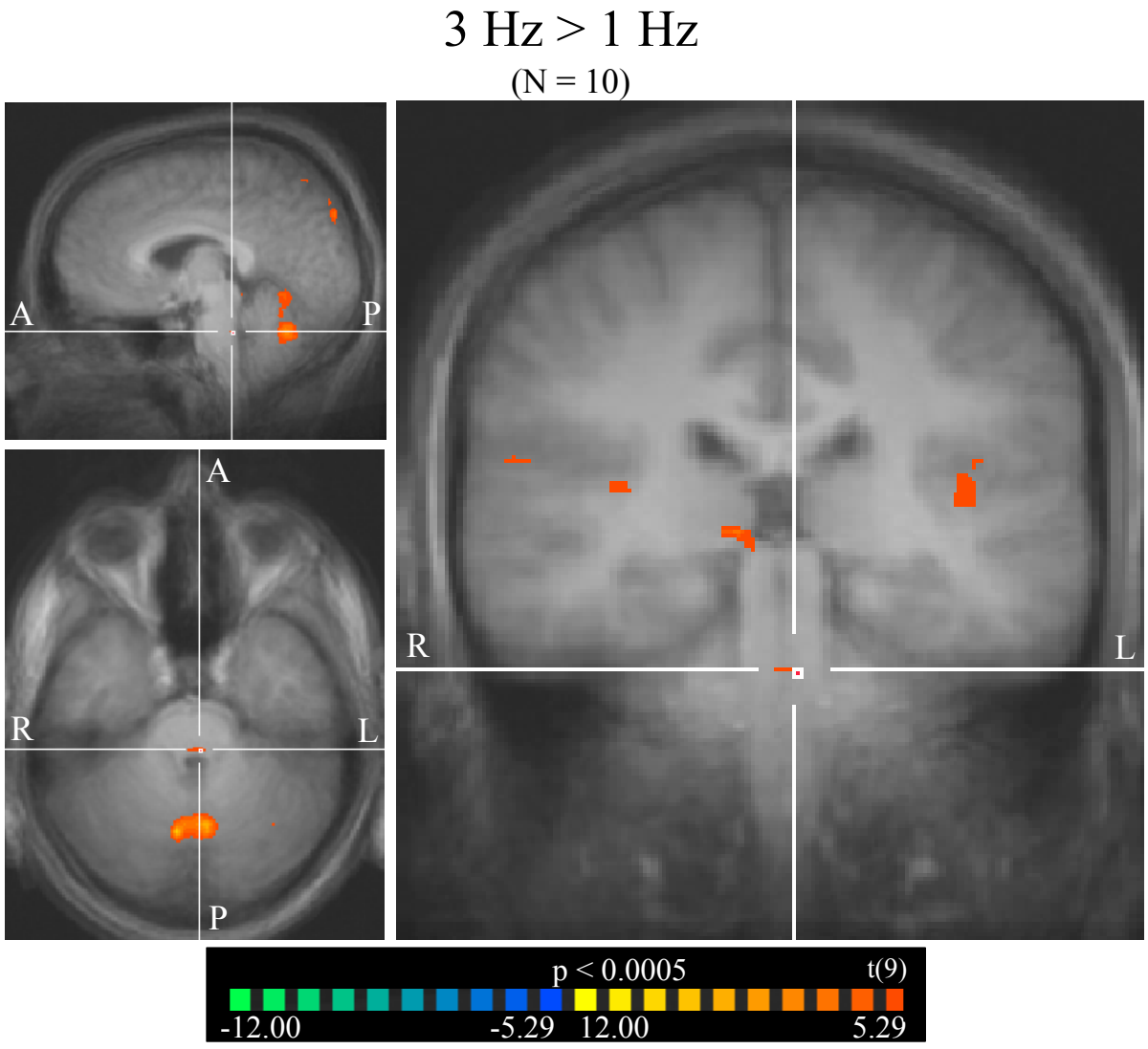

(TC pictured: -3, -28, -29)

Figure 13 e. Mean % signal change compared to baseline

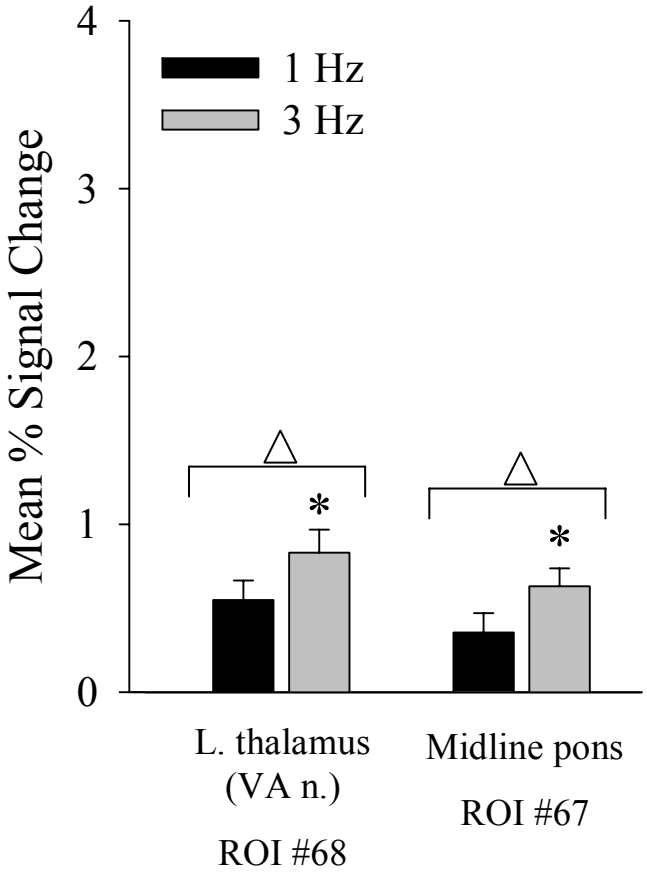

△ Significant main effect of rate

* Significantly different from baseline

Part 1d: Whole Brain: Conjunction analysis, main effect of rate

To initially assess the overlapping substrates by rate, two simple SPM map overlays (one for overlapping tasks, one for overlapping rates) were computed, thresholded at FDR < 0.01, and visually assessed for shared correlates (Figures 14a-c, pp. 102-103). To formally determine the minimally shared brain areas correlated to both rate conditions, a conjunction of contrasts 3 [1 Hz > baseline] and 4 [3 Hz > baseline] was performed and data were thresholded with $p < 0.0005$. Table 15a (p. 104) lists the statistical details for *a priori* ROIs in bold text and post hoc ROIs in plain text. Table 15b (p. 106) lists the average magnitude of signal compared to baseline for the 1 Hz and 3 Hz rate conditions collapsed across task for *a priori* ROIs in bold text and post hoc ROIs in plain text. Figures 15a-e (pp. 108-112) include bar graphs and SPM maps representing the mean percent signal change of the rate conditions compared to baseline for some of the *a priori* ROIs.

Areas found to be active in both 1 Hz and 3 Hz rate conditions were: bilateral temporal lobes, cingulate (Figures 15a-c, pp. 108-110); right-lateralized frontal and occipital lobes; left-lateralized cerebellum, pontomedullary region (Figures 15d-e, pp. 111-112), and insula. Further inspection ($p < 0.000005$) revealed distinct bilateral precentral gyri, insula, basal ganglia, and left thalamus (Tables 16a,b, Figures 16a-f, pp. 113-121).

Figure 14 a. Overlapping substrates as a function of rate (cortical)

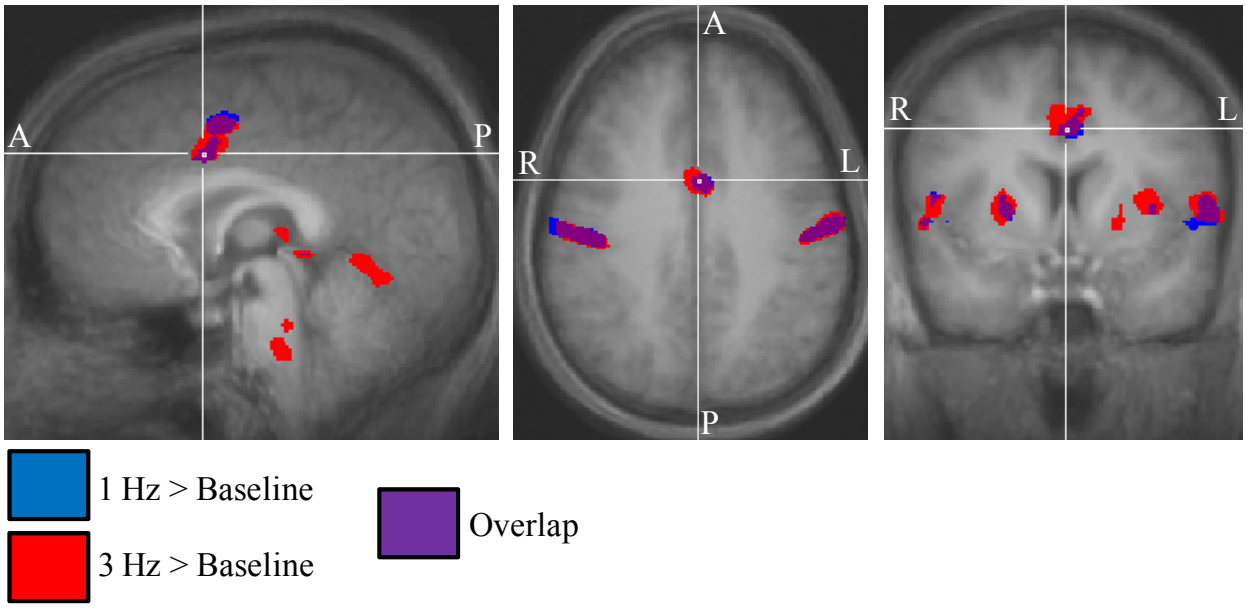

Figure 14 b. Overlapping substrates as a function of rate (brainstem)

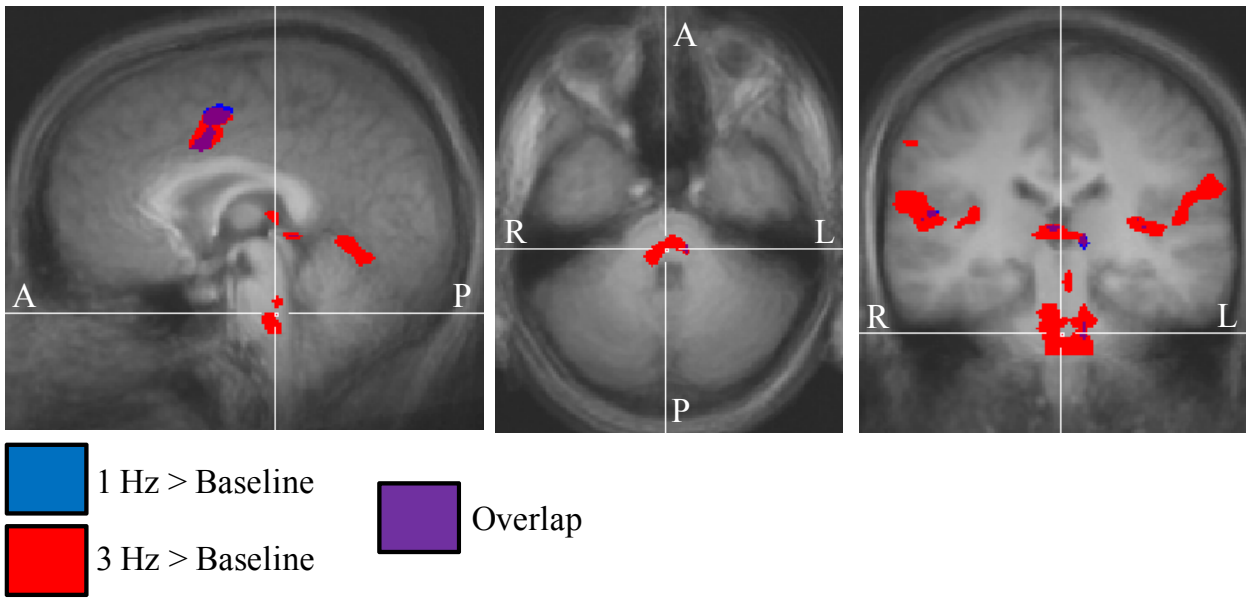

Figure 14 c. Overlapping substrates as a function of rate (subcortical)

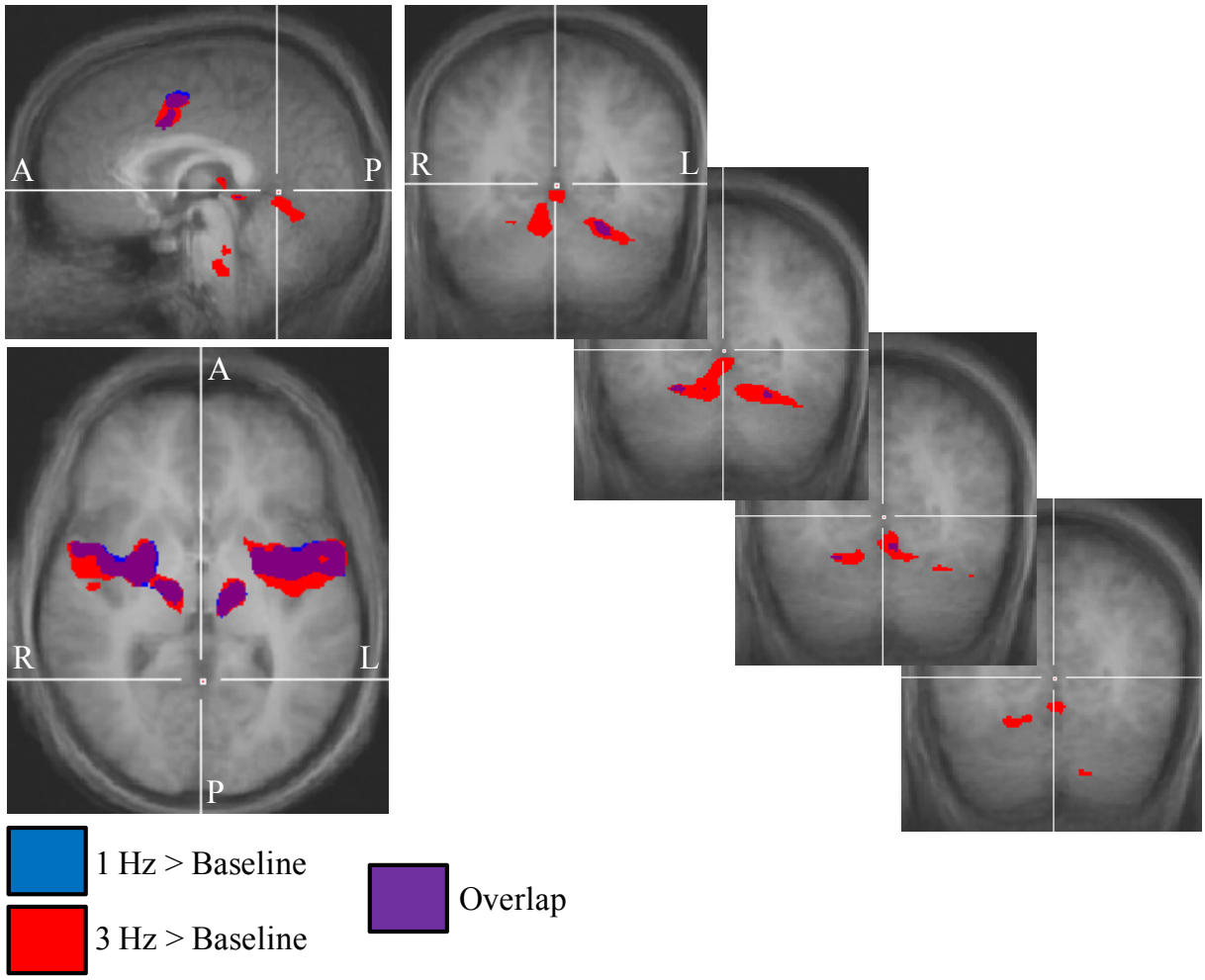

Table 15 a. Multi-Subject RFX GLM, conjunction of rate conditions

ROI	Cluster Region	BA	# of voxels	Peak Voxel				
				x	y	z	t value	p value
89	R. insula & cortical - subcortical spread	13, 4, 40, 41	20414	42	-7	7	15.262	0.000000
90	L. cortical - subcortical spread	13, 4, 40, 41, 36	17764	-48	-16	31	14.048	0.000000
91	L. insula	13	162	-33	-28	10	6.864	0.000074
92	L. pontomedullary region	N/A	5	-6	-28	-38	5.622	0.000325
93	L. pontomedullary region	N/A	87	-9	-25	-35	6.785	0.000080
94	L. thalamus (VL n.)	N/A	1682	-12	-16	1	10.550	0.000002
95	R. post. cingulate sulcus	31	194	3	-52	34	-6.549	0.000105
96	L. ant. cingulate	12	8	-6	35	4	-5.806	0.000258
97	L. cingulate	24	2131	-3	2	40	10.445	0.000002
98	R. cerebellum (ant. lobe)	N/A	538	21	-58	-17	7.405	0.000041
99	L. cerebellum (ant. lobe)	N/A	1489	-21	-49	-17	7.538	0.000035
100	L. cerebellum (post. lobe)	N/A	12	-12	-64	-41	5.535	0.000363

				-12	**-64**	**-42**	**5.535**	**0.000363**
101	Midline sup. colliculus	N/A	39	0	-34	-2	6.599	0.000099
102	R. superior frontal sulcus	8	6	21	20	46	-5.632	0.000321
103	R. middle temporal gyrus	21	12	54	-19	-14	-6.740	0.000085
104	R. middle occipital gyrus	19	28	36	-73	19	-5.946	0.000216
105	L. supramarginal gyrus	40	5	-66	-19	16	5.588	0.000386
				-67	-19	16	5.588	0.000386
106	L. post. orbital gyrus	11	198	-48	35	-2	-8.367	0.000015
107	L. superior temporal sulcus	7	278	-45	-67	22	-7.278	0.000047
108	L. middle occipital gyrus	19	291	-36	-82	22	-8.085	0.000020
109	L. transverse parietal sulcus	7	5	-6	-52	46	-5.594	0.000337
110	L. rolandic operculum	40	12	-45	-31	19	5.979	0.000208

Table 15 b. RFX GLM of ROIs

ROI	Region	Contrast	df	mean	se	t value	p value
89	R. insula & cortical - subcortical spread	1 Hz	9	1.579	0.063	25.247	0.000000*
		3 Hz	9	1.869	0.083	22.538	0.000000*
90	L. cortical - subcortical spread	1 Hz	9	1.783	0.095	18.858	0.000000*
		3 Hz	9	2.076	0.102	20.309	0.000000*
91	L. insula	1 Hz	9	0.501	0.064	7.867	0.000025*
		3 Hz	9	0.913	0.121	7.528	0.000036*
92	L. pontomedullary region	1 Hz	9	0.540	0.087	6.195	0.000160*
		3 Hz	9	0.931	0.144	6.445	0.000119*
93	L. pontomedullary region	1 Hz	9	0.431	0.057	7.607	0.000033*
		3 Hz	9	0.694	0.096	7.207	0.000050*
94	L. thalamus (VL n.)	1 Hz	9	0.823	0.071	11.529	0.000001*
		3 Hz	9	1.041	0.102	10.256	0.000003*
95	R. post. cingulate sulcus	1 Hz	9	-0.780	0.110	-7.069	0.000059*
		3 Hz	9	-0.801	0.120	-6.672	0.000091*
96	L. ant. cingulate	1 Hz	9	-0.686	0.100	-6.837	0.000076*
		3 Hz	9	-0.771	0.122	-6.306	0.000140*
97	L. cingulate	1 Hz	9	1.148	0.095	12.099	0.000001*
		3 Hz	9	1.533	0.176	8.720	0.000011*
98	R. cerebellum (ant. lobe)	1 Hz	9	1.407	0.170	8.289	0.000017*
		3 Hz	9	1.773	0.193	9.204	0.000007*
99	L. cerebellum (ant. lobe)	1 Hz	9	1.244	0.141	8.802	0.000010*
		3 Hz	9	1.605	0.152	10.587	0.000002*

100	**L. cerebellum (post. lobe)**	**1 Hz**	**9**	**1.092**	**0.197**	**5.553**	**0.000355***
		3 Hz	**9**	**1.283**	**0.205**	**6.258**	**0.000148***
101	Midline sup. colliculus	1 Hz	9	1.024	0.157	6.515	0.000110*
		3 Hz	9	1.649	0.216	7.643	0.000032*
102	R. superior frontal sulcus	1 Hz	9	-0.439	0.075	-5.882	0.000234*
		3 Hz	9	-0.491	0.087	-5.632	0.000321*
103	R. middle temporal gyrus	1 Hz	9	-0.799	0.244	-3.279	0.009552
		3 Hz	9	-1.011	0.223	-4.534	0.001418
104	R. middle occipital gyrus	1 Hz	9	-0.659	0.097	-6.782	0.000081*
		3 Hz	9	-0.565	0.086	-6.543	0.000106*
105	L. supramarginal gyrus	1 Hz	9	2.320	0.340	6.821	0.000077*
		3 Hz	9	2.523	0.606	4.166	0.002425
106	L. post. orbital gyrus	1 Hz	9	-1.521	0.153	-9.953	0.000004*
		3 Hz	9	-1.687	0.208	-8.120	0.000020*
107	L. superior temporal sulcus	1 Hz	9	-0.744	0.099	-7.532	0.000036*
		3 Hz	9	-0.716	0.092	-7.804	0.000027*
108	L. middle occipital gyrus	1 Hz	9	-0.847	0.120	-7.049	0.000060*
		3 Hz	9	-0.811	0.089	-9.146	0.000007*
109	L. transverse parietal sulcus	1 Hz	9	-0.851	0.147	-5.795	0.000261*
		3 Hz	9	-0.764	0.137	-5.597	0.000336*
110	L. rolandic operculum	1 Hz	9	0.561	0.088	6.405	0.000125*
		3 Hz	9	1.165	0.167	6.987	0.000064*

* Significantly different from baseline

Figure 15 a. Left anterior cingulate (ROI #96)

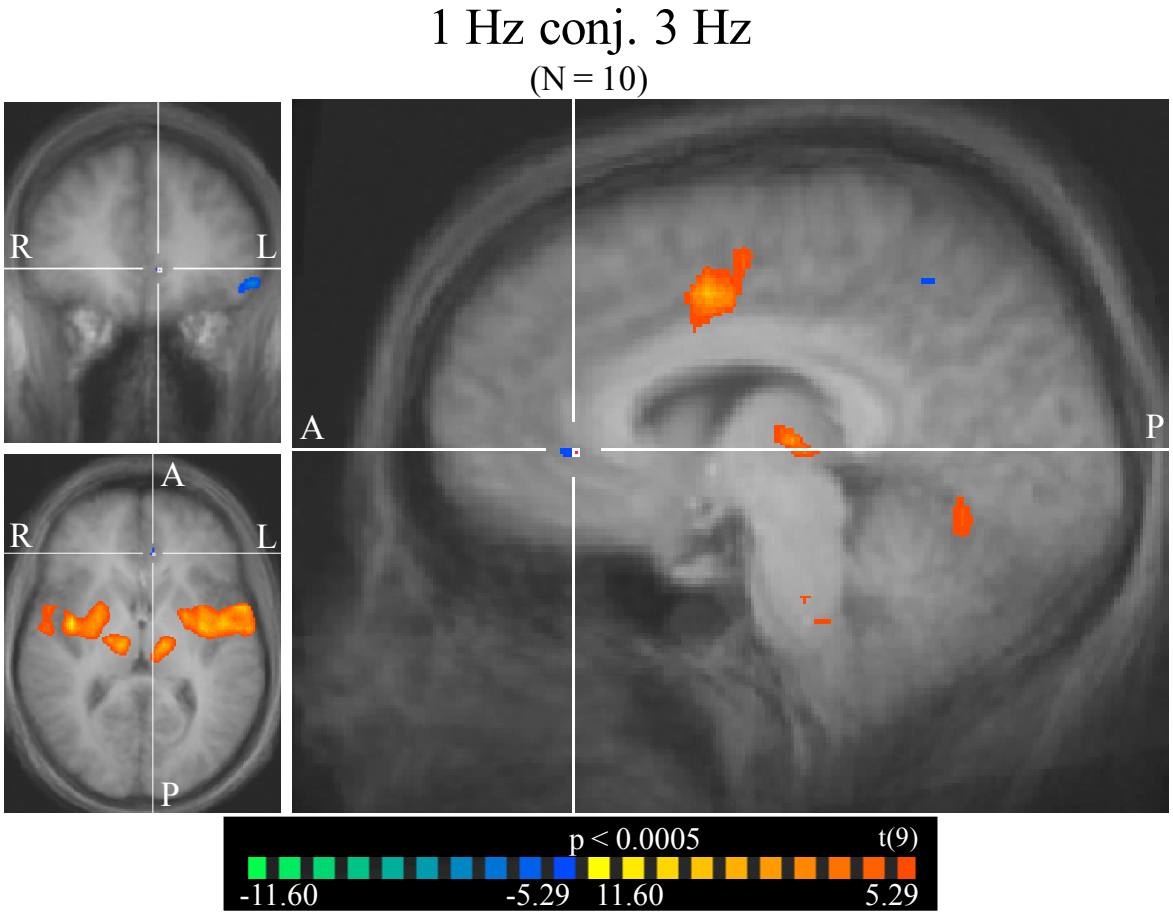

(TC pictured: -6, 35, 4)

Figure 15 b. Right posterior cingulate sulcus (ROI #95)

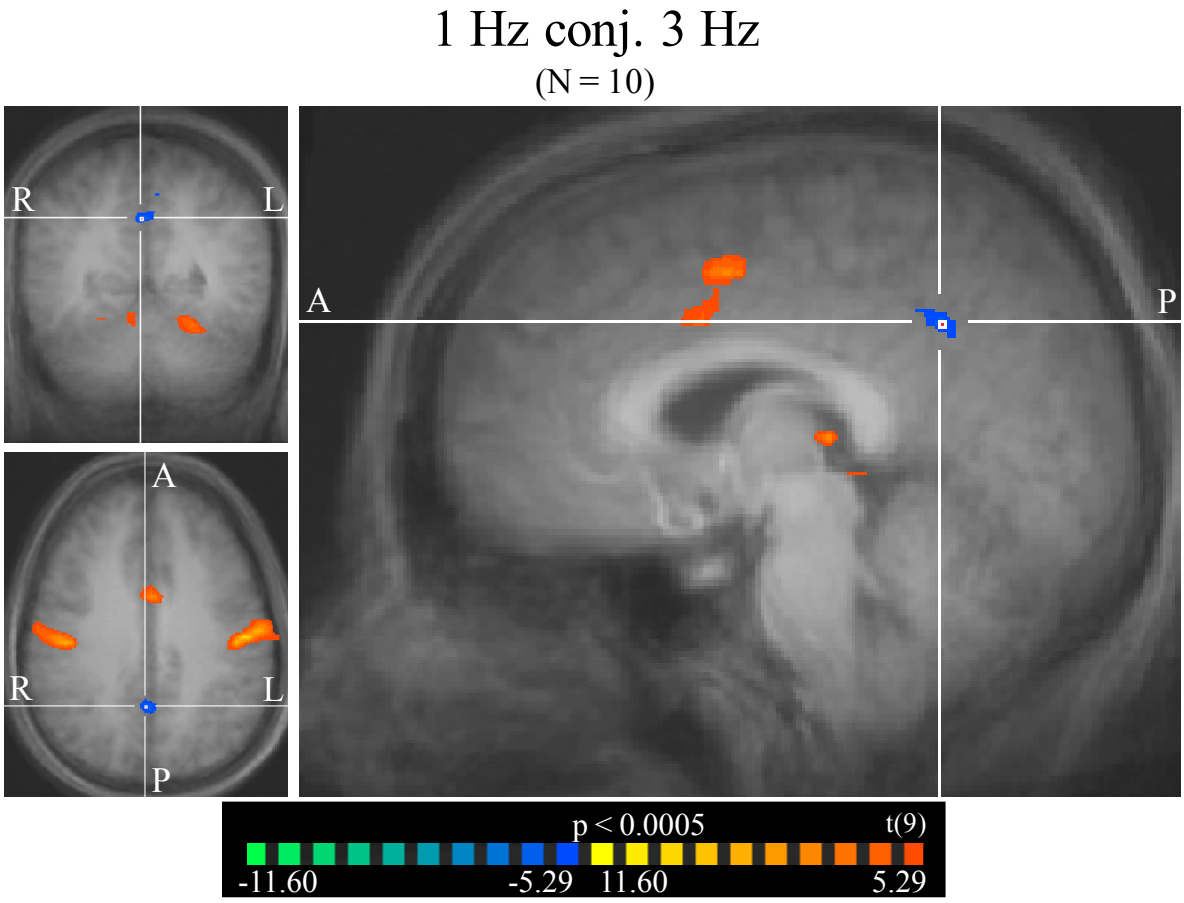

(TC pictured: 3, -52, 34)

Figure 15 c. Mean % signal change compared to baseline

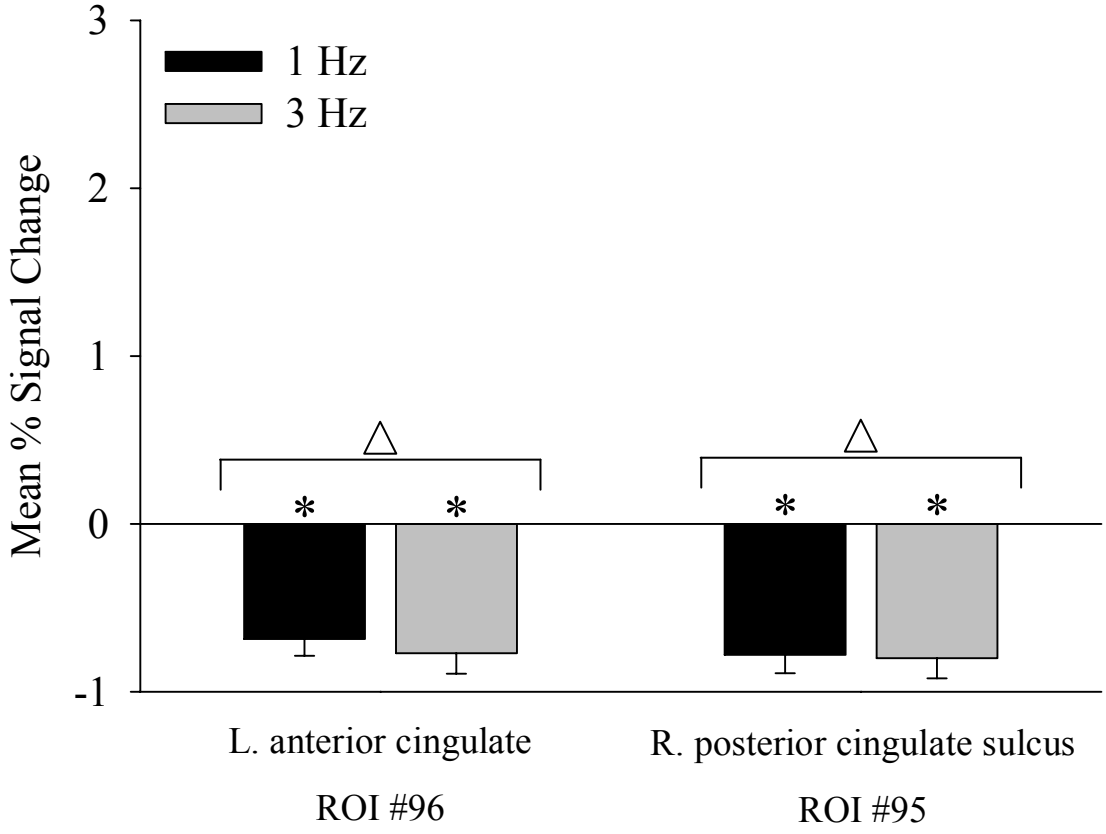

△ Significant main effect across rate

* Significantly different from baseline

Figure 15 d. Left pontomedullary regions (ROI #92, 93)

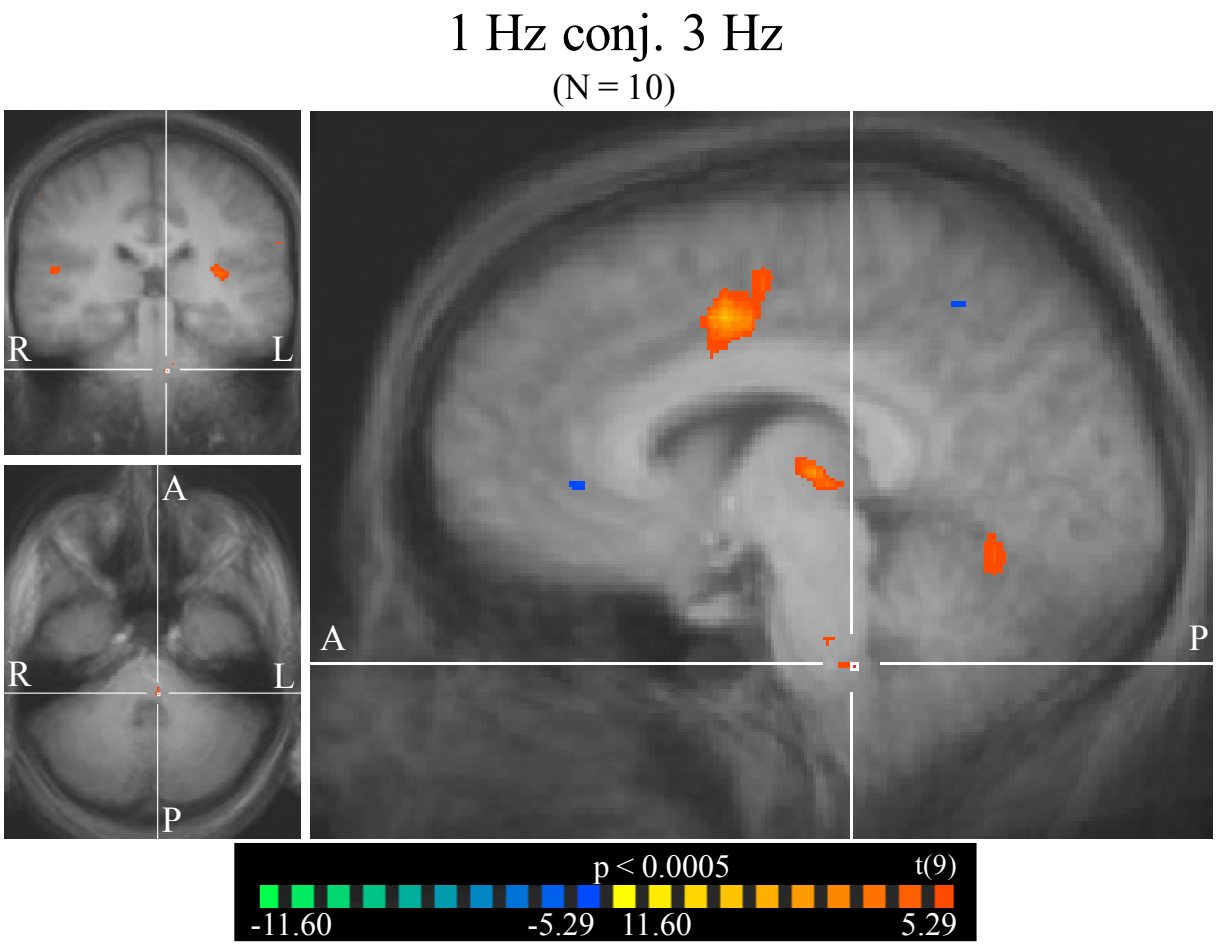

(TC: -6, -28, -38)

Figure 15 e. Mean % signal change compared to baseline

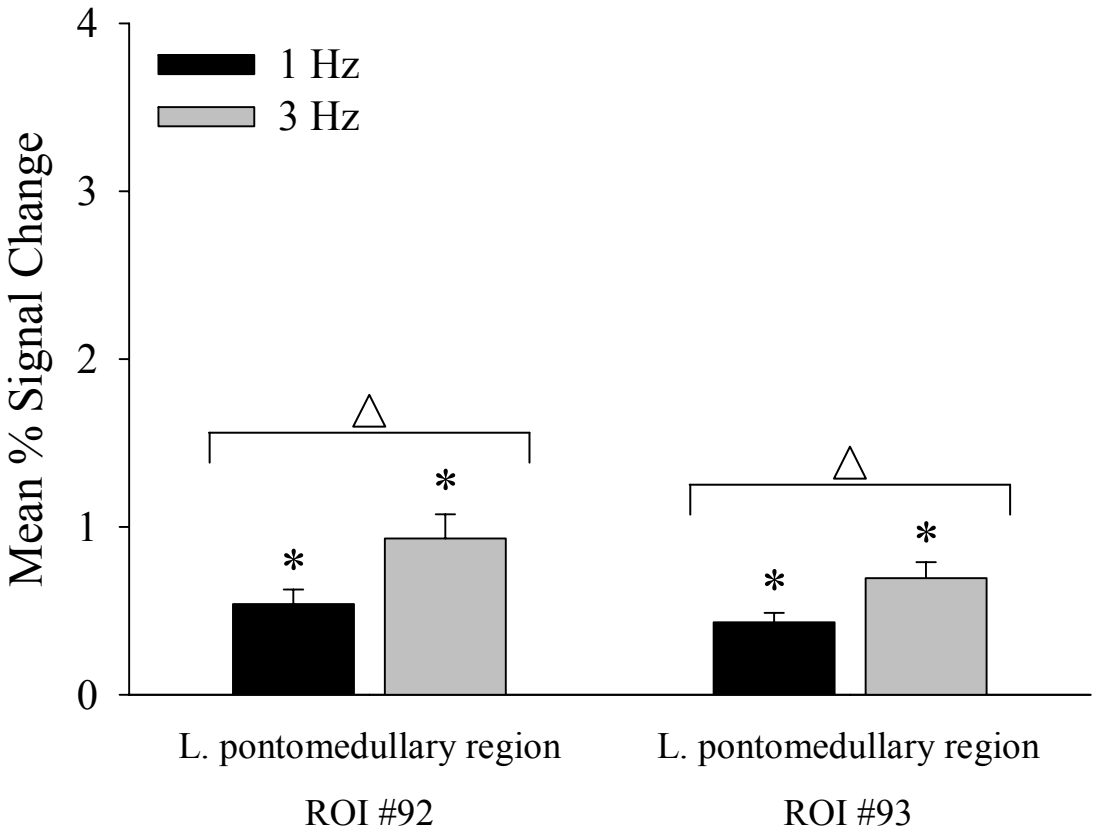

△ Significant main effect across rate

* Significantly different from baseline

Table 16 a. Multi-Subject RFX GLM, conjunction of rate conditions

ROI	Cluster Region	BA	# of voxels	Peak Voxel				
				x	y	z	t value	p value
89	**R. insula**	**13**	**170**	**42**	**-7**	**7**	**15.262**	**0.000000**
90	**L. precentral gyrus**	**4**	**129**	**-48**	**-16**	**31**	**14.048**	**0.000000**
94	**L. thalamus (VL n.)**	**N/A**	**21**	**-12**	**-16**	**1**	**10.550**	**0.000002**
111	**R. precentral gyrus**	**4**	**21**	**51**	**-16**	**31**	**11.495**	**0.000001**
112	**R. central sulcus**	**N/A**	**4**	**43**	**-19**	**37**	**10.365**	**0.000003**
113	**R. putamen**	**N/A**	**67**	**27**	**-4**	**-2**	**13.306**	**0.000000**
114	**L. insula**	**13**	**53**	**-39**	**-7**	**10**	**10.693**	**0.000002**
115	**L. putamen**	**N/A**	**59**	**-33**	**-4**	**1**	**10.667**	**0.000002**
116	R. rolandic operculum	40	218	57	-10	16	12.542	0.000001
117	L. rolandic operculum	40	42	-45	-4	7	10.469	0.000002
118	L. rolandic operculum	40	128	-51	-13	13	11.857	0.000001
119	L. inf. front. gyrus	44	48	-57	-7	19	10.595	0.000002
120	L. inf. front. gyrus	44	4	-57	5	4	10.153	0.000003
121	L. inf. front. gyrus	44	4	-54	5	7	10.104	0.000003
122	L. inf. front. gyrus	44	9	-54	2	10	10.461	0.000002

Table 16 b. RFX GLM of ROIs

ROI	Region	Contrast	df	mean	se	t value	p value
89	**R. insula**	**1 Hz**	**9**	**1.076**	**0.057**	**19.022**	**0.000000***
		3 Hz	**9**	**1.219**	**0.077**	**15.785**	**0.000000***
90	**L. precentral gyrus**	**1 Hz**	**9**	**3.170**	**0.207**	**15.330**	**0.000000***
		3 Hz	**9**	**3.514**	**0.209**	**16.814**	**0.000000***
94	**L. thalamus (VL n.)**	**1 Hz**	**9**	**0.923**	**0.069**	**13.363**	**0.000000***
		3 Hz	**9**	**1.091**	**0.095**	**11.535**	**0.000001***
111	**R. precentral gyrus**	**1 Hz**	**9**	**2.757**	**0.218**	**12.638**	**0.000000***
		3 Hz	**9**	**3.029**	**0.243**	**12.485**	**0.000001***
112	**R. central sulcus**	**1 Hz**	**9**	**1.722**	**0.144**	**11.989**	**0.000001***
		3 Hz	**9**	**2.059**	**0.199**	**10.365**	**0.000003***
113	**R. putamen**	**1 Hz**	**9**	**1.252**	**0.090**	**13.900**	**0.000000***
		3 Hz	**9**	**1.471**	**0.103**	**14.254**	**0.000000***
114	**L. insula**	**1 Hz**	**9**	**1.531**	**0.138**	**11.062**	**0.000002***
		3 Hz	**9**	**1.676**	**0.149**	**11.212**	**0.000001***
115	**L. putamen**	**1 Hz**	**9**	**0.930**	**0.079**	**11.766**	**0.000001***
		3 Hz	**9**	**1.096**	**0.063**	**17.362**	**0.000000***
116	R. rolandic operculum	1 Hz	9	1.643	0.068	24.251	0.000000*
		3 Hz	9	1.921	0.098	19.689	0.000000*
117	L. rolandic operculum	1 Hz	9	1.451	0.108	13.454	0.000000*
		3 Hz	9	1.865	0.122	15.260	0.000000*
118	L. rolandic operculum	1 Hz	9	1.600	0.142	11.247	0.000001*
		3 Hz	9	1.875	0.155	12.065	0.000001*

119	L. inf. front. gyrus	1 Hz	9	1.742	0.146	11.934	0.000001*
		3 Hz	9	2.017	0.131	15.360	0.000000*
120	L. inf. front. gyrus	1 Hz	9	1.854	0.171	10.819	0.000002*
		3 Hz	9	2.282	0.220	10.384	0.000003*
121	L. inf. front. gyrus	1 Hz	9	2.215	0.187	11.871	0.000001*
		3 Hz	9	2.794	0.266	10.515	0.000002*
122	L. inf. front. gyrus	1 Hz	9	2.960	0.201	14.738	0.000000*
		3 Hz	9	3.341	0.210	15.894	0.000000*

* Significantly different from baseline

Figure 16 a. Left precentral gyrus (ROI #90)

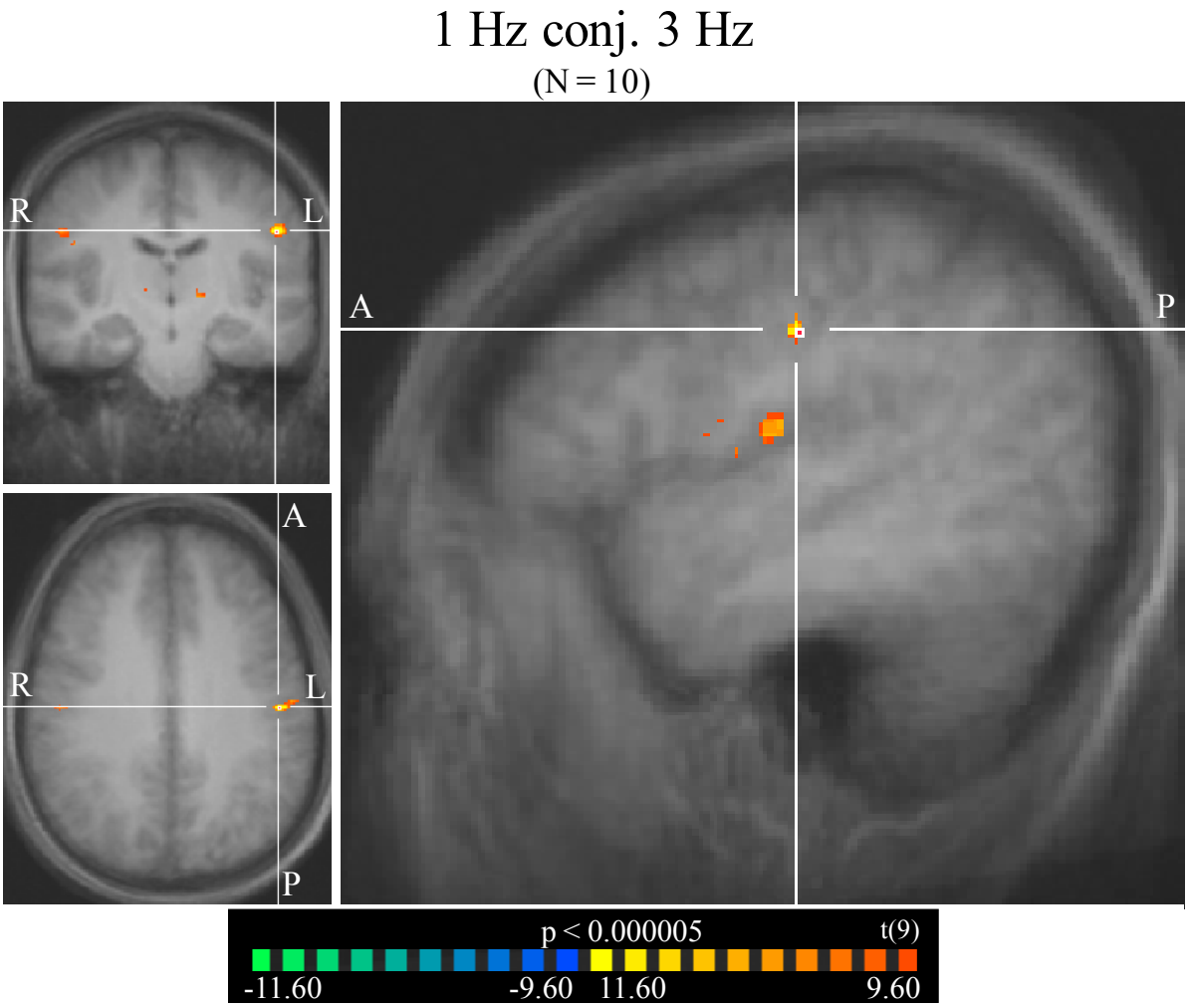

(TC pictured: -48, -16, 31)

Figure 16 b. Mean % signal change compared to baseline

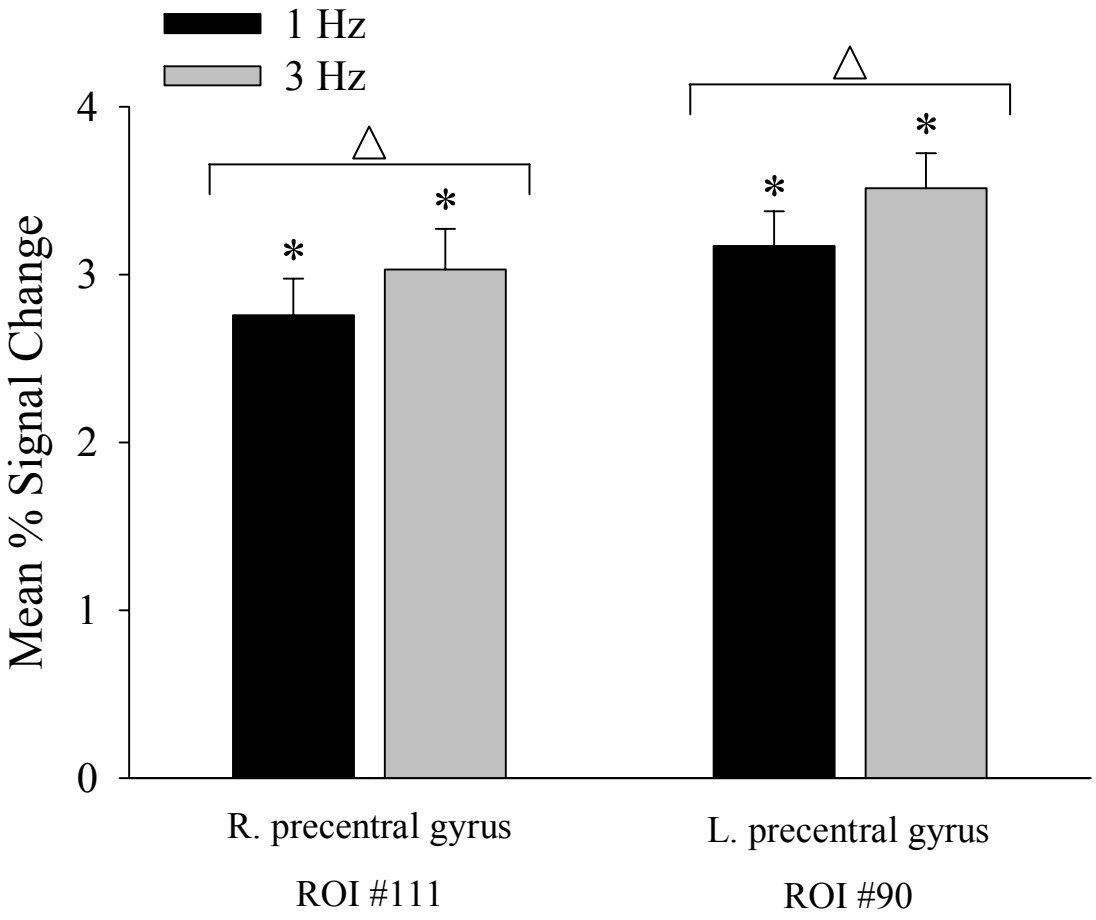

△ Significant main effect across rate

* Significantly different from baseline

Figure 16 c. Right insula (ROI #89)

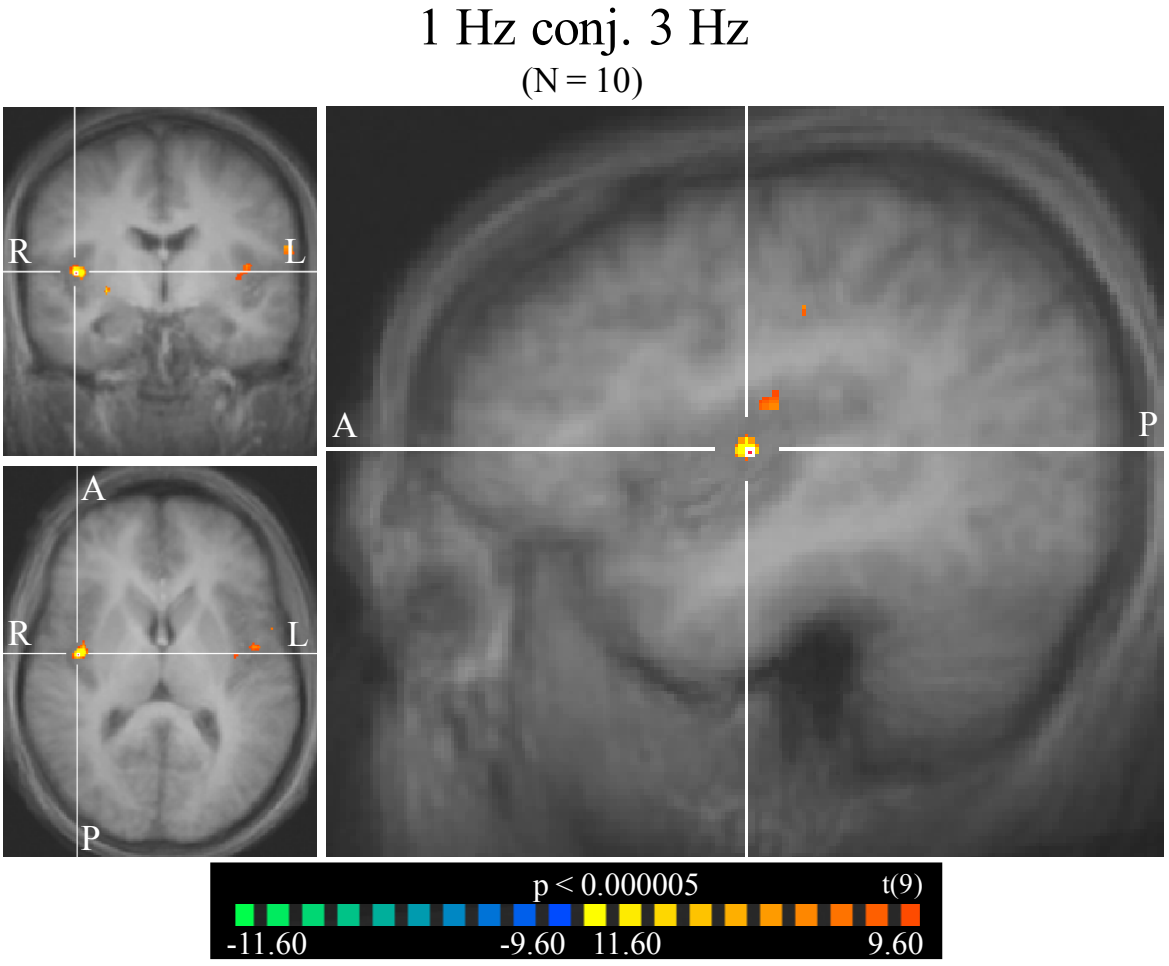

(TC pictured: 42, -7, 7)

Figure 16 d. Mean % signal change compared to baseline

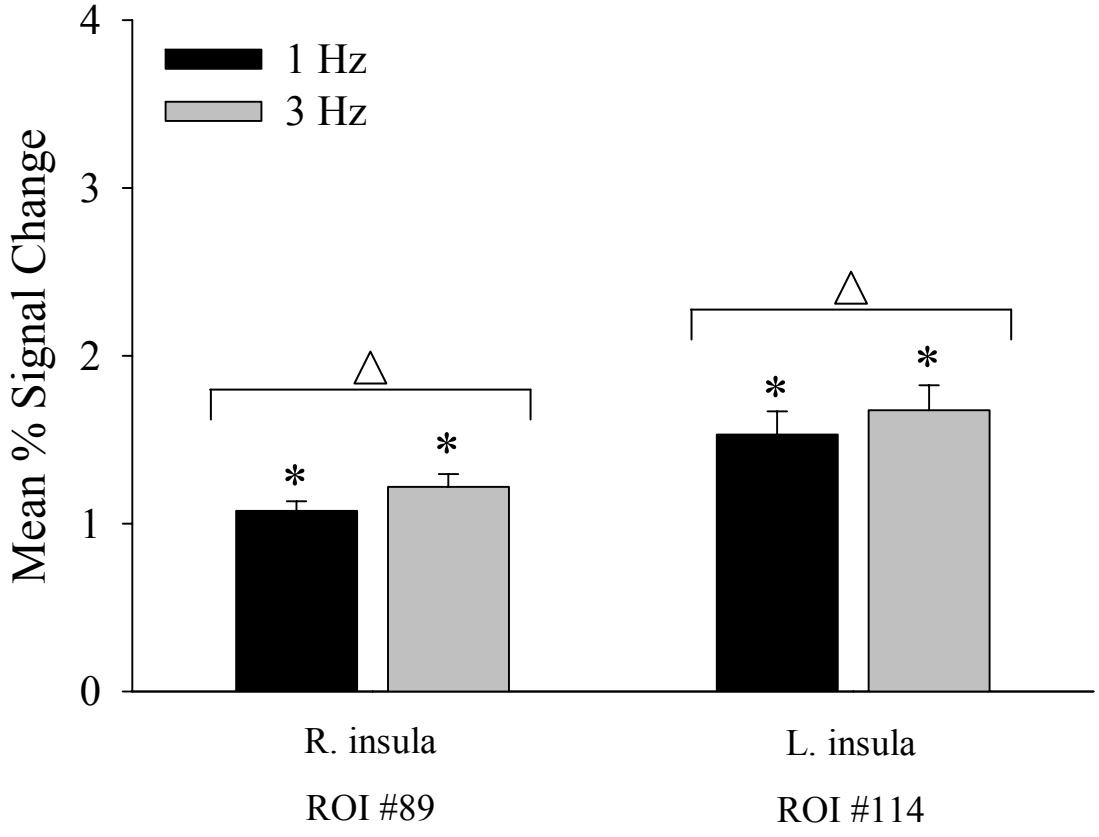

△ Significant main effect across rate

* Significantly different from baseline

Figure 16 e. Right & left putamen (ROI #113, 115)

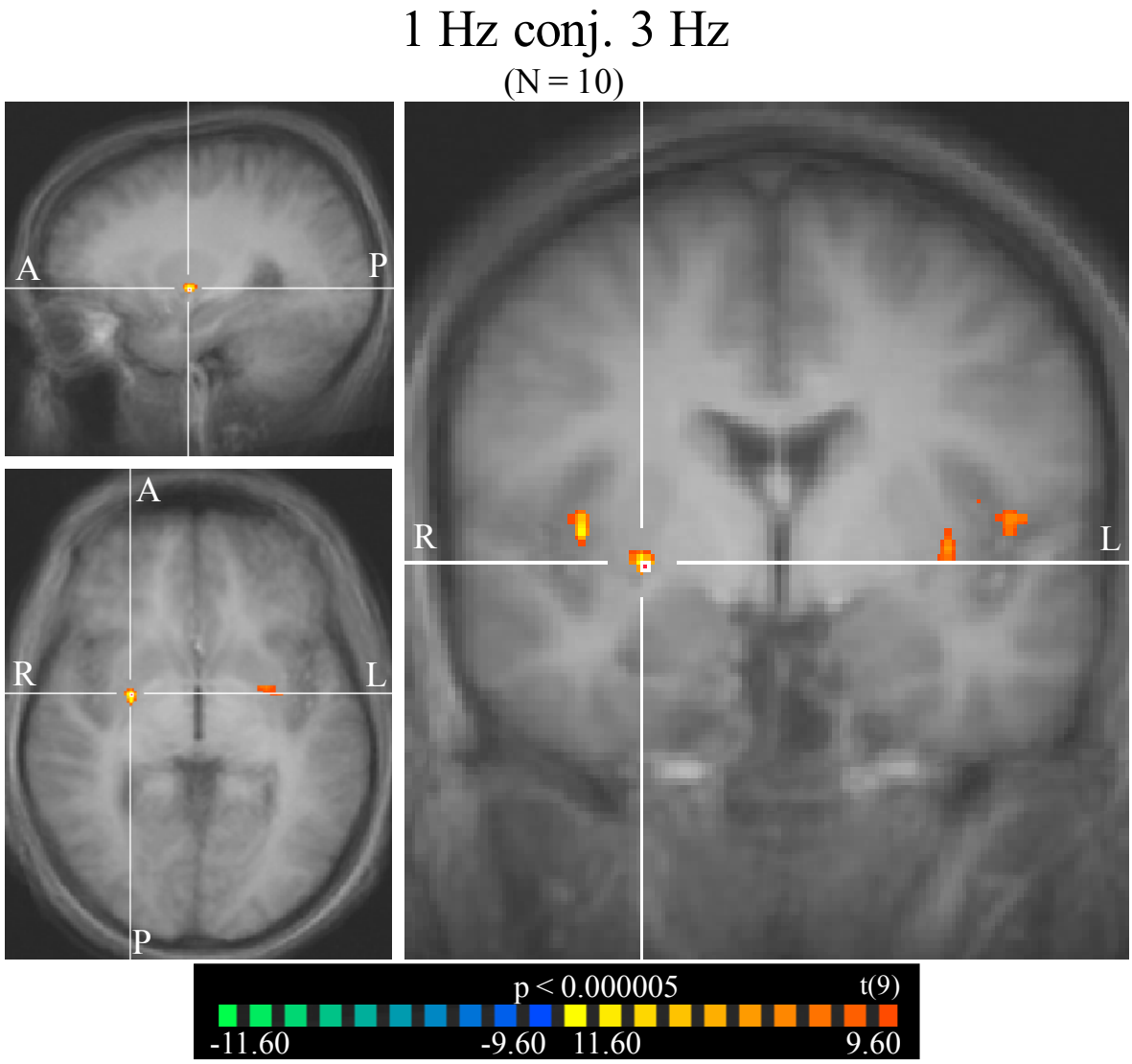

(TC pictured: 27, -4, -2)

Figure 16 f. Mean % signal change compared to baseline

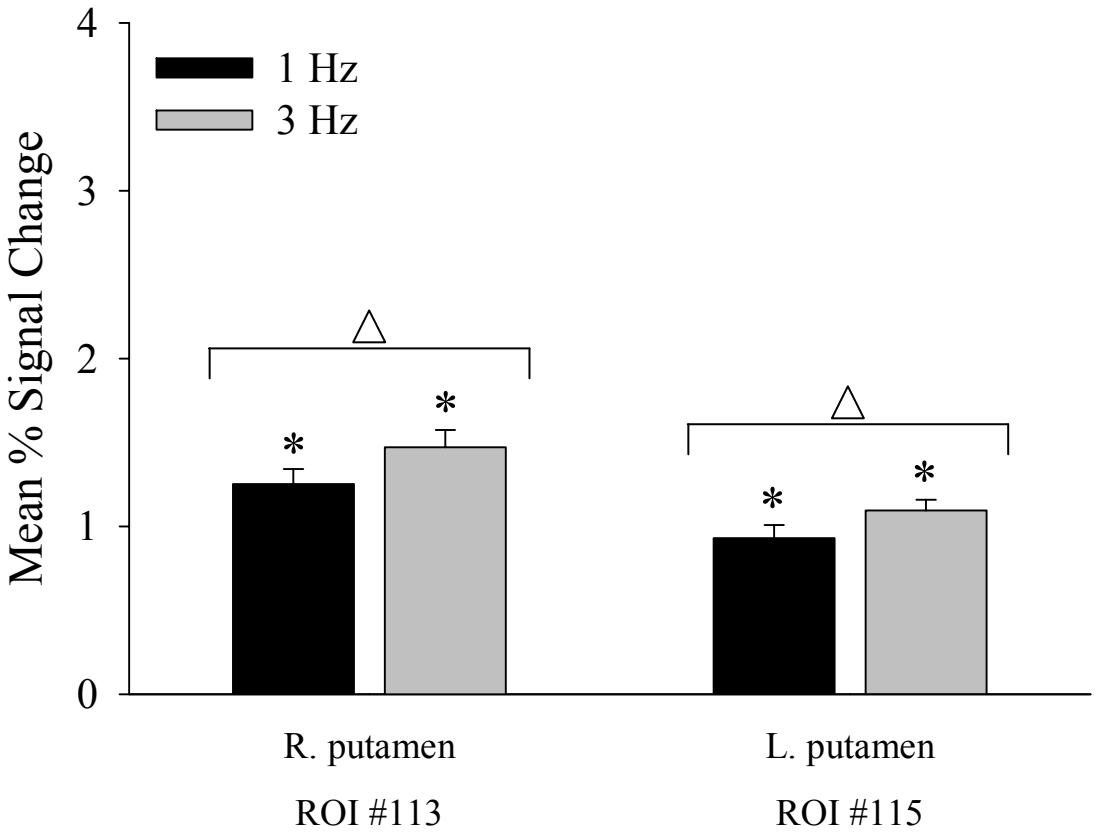

△ Significant main effect across rate

* Significantly different from baseline

Part 2: Brainstem Mask Analysis

Part 2a: Brainstem Mask: FFX analysis, main effect of task

To determine the main effect of task within the masked brainstem region, a single-study FFX GLM analysis collapsed across all participants, implementing a percent signal transformation was performed. To identify *a priori* ROIs actively correlated with the ororhythmic task conditions, the contrast [Suck > Unvoiced /da/] was applied and the data were thresholded at $p < 0.0001$. Table 17a (p. 123) lists the statistical details for *a priori* ROIs in bold text and post hoc ROIs in plain text. Table 17b (p. 123) lists the average magnitude of signal compared to baseline for the Suck and Unvoiced /da/ task conditions collapsed across the rate condition for *a priori* ROIs in bold text and post hoc ROIs in plain text. Figures 17a-b (pp. 124-125) include a bar graph representing the mean percent signal change of the task conditions compared to baseline for the *a priori* ROI.

Areas found to be more active in the Suck compared to Unvoiced /da/ task conditions were: left pons (Figures 17a-b, pp 124-125); and right pons/midbrain.

Table 17 a. Single-study FFX GLM, main effect of task

ROI	Cluster Region	BA	# of voxels	Peak Voxel				
				x	y	z	t value	p value
123	**L. pons**	**N/A**	**58**	**137**	**144**	**148**	**4.276**	**0.000020**
124	R. pons/midbrain	N/A	615	122	141	142	4.878	0.000001

Table 17 b. FFX GLM of ROIs

ROI	Region	Contrast	df	mean	se	t value	p value
123	**L. pons**	**Suck**	**2404**	**1.085**	**0.116**	**9.361**	**0.000000***
		Unvoiced /da/	**2404**	**0.526**	**0.116**	**4.549**	**0.000006***
124	R. pons/midbrain	Suck	2404	1.370	0.237	5.785	0.000000*
		Unvoiced /da/	2404	0.162	0.236	0.686	0.493016

* Significantly different from baseline

Figure 17 a. ROI #123 – Left pons

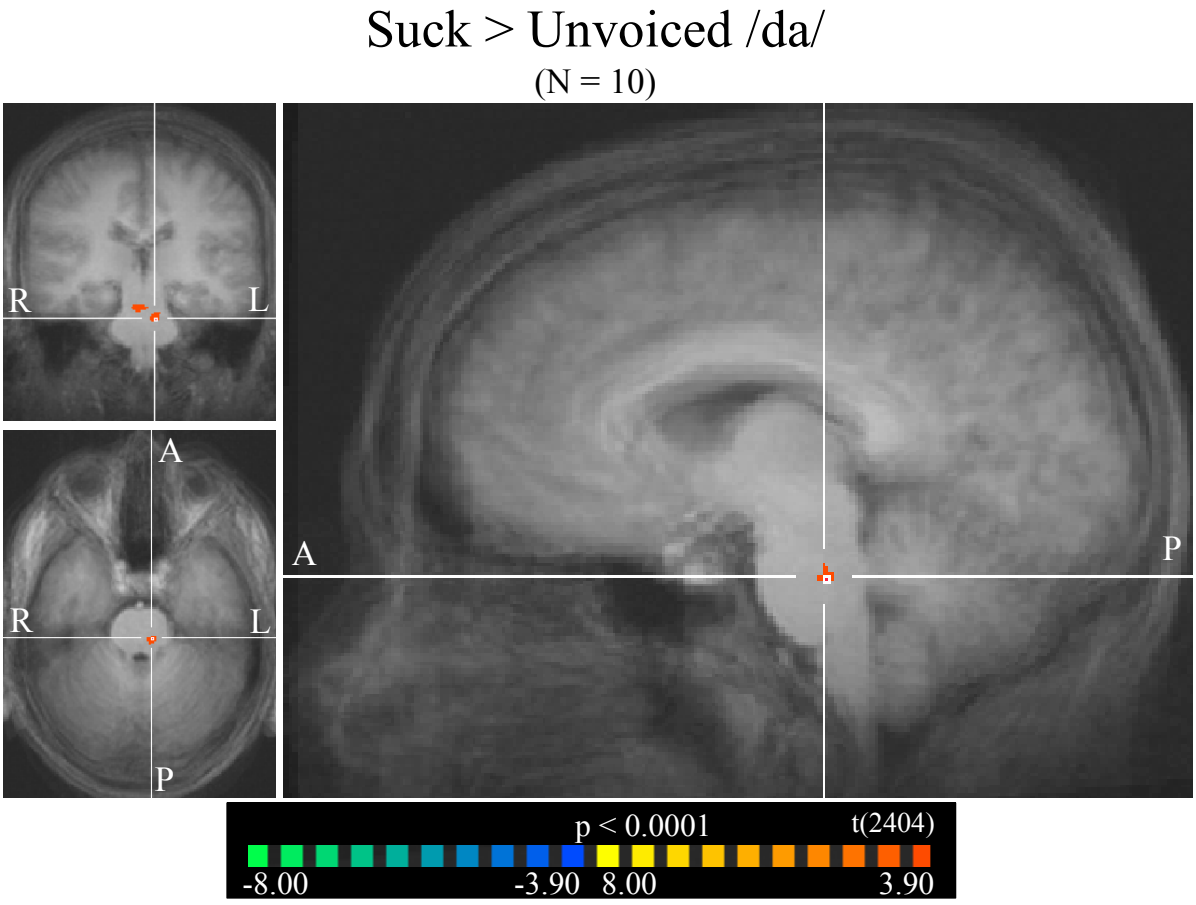

(Coordinate pictured: 135, 144, 148)

Figure 17 b. % signal change compared to baseline

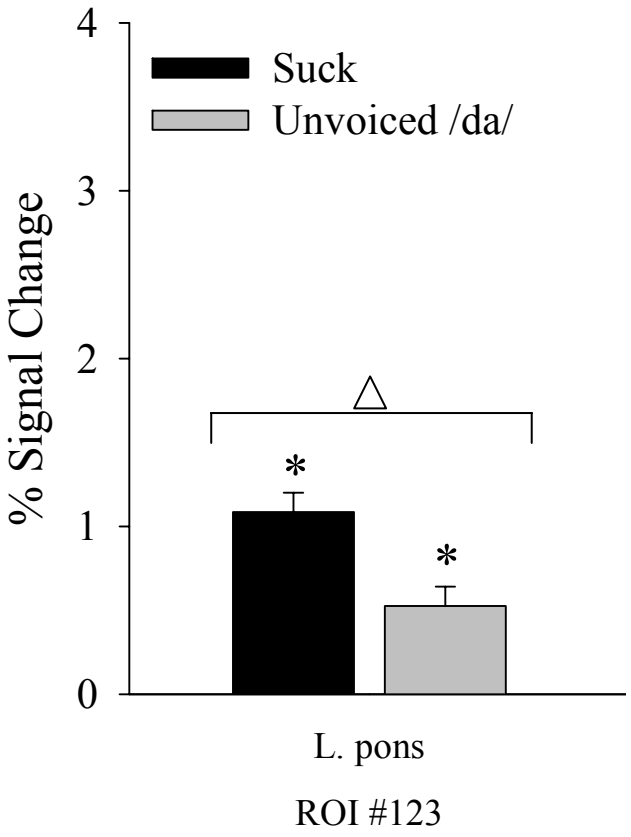

△ Significant main effect of task

* Significantly different from baseline

Part 2b: Brainstem Mask: Conjunction analysis, main effect of task

To initially assess the overlapping substrates by task, two simple SPM map overlays (one for overlapping tasks, one for overlapping rates) were computed, thresholded at p(Bonf) < 0.00001, and visually assessed for shared correlates within the masked brainstem area (Figure 18a, p. 127). To formally determine the minimally shared brain areas correlated to both Unvoiced /da/ and Suck task conditions, a conjunction of contrasts 1 [Unvoiced /da/ > baseline] and 2 [Suck > baseline] was performed and data were thresholded with $p < 0.001$. Table 19a (p. 128) lists the statistical details for *a priori* ROIs in bold text (no post hoc ROIs were indicated). Table 19b (p. 128) lists the average magnitude of signal compared to baseline for the Suck and Unvoiced /da/ task conditions collapsed across rate for the *a priori* ROIs in bold text. Figures 19a-b (pp. 129-130) include a bar graph and SPM map representing the mean percent signal change of the task conditions compared to baseline for one of the *a priori* ROIs.

Areas found to be active in both Unvoiced /da/ and Suck task conditions were located bilaterally in the medulla (Figures 19a-b, pp. 129-130).

Figure 18 a. Overlapping substrates as a function of task (brainstem mask)

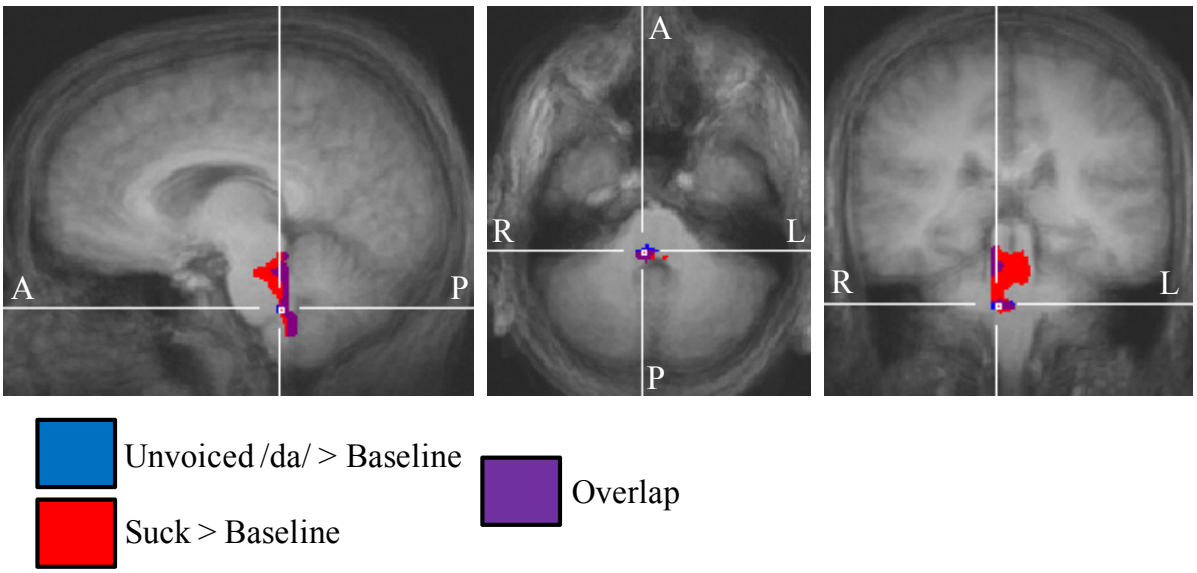

Table 19 a. Multi-Subject RFX GLM, conjunction of task conditions

ROI	Cluster Region	BA	# of voxels	Peak Voxel				
				x	y	z	t value	p value
125	R. dorsal medulla	N/A	54	126	156	160	5.190	0.000571
				125	157	160	5.190	0.000571
				125	156	160	5.190	0.000571
				125	156	159	5.190	0.000571
				124	156	160	5.190	0.000571
126	L. dorsal medulla	N/A	20	134	150	166	5.218	0.000550

Table 19 b. RFX GLM of ROIs

ROI	Region	Contrast	df	mean	se	t value	p value
125	R. dorsal medulla	Suck	9	0.797	0.131	6.086	0.000182*
		Unvoiced /da/	9	0.697	0.126	5.545	0.000359*
126	L. dorsal medulla	Suck	9	0.769	0.117	6.569	0.000103*
		Unvoiced /da/	9	0.623	0.105	5.918	0.000224*

* Significantly different from baseline

Figure 19 a. Right dorsal medulla (ROI #125)

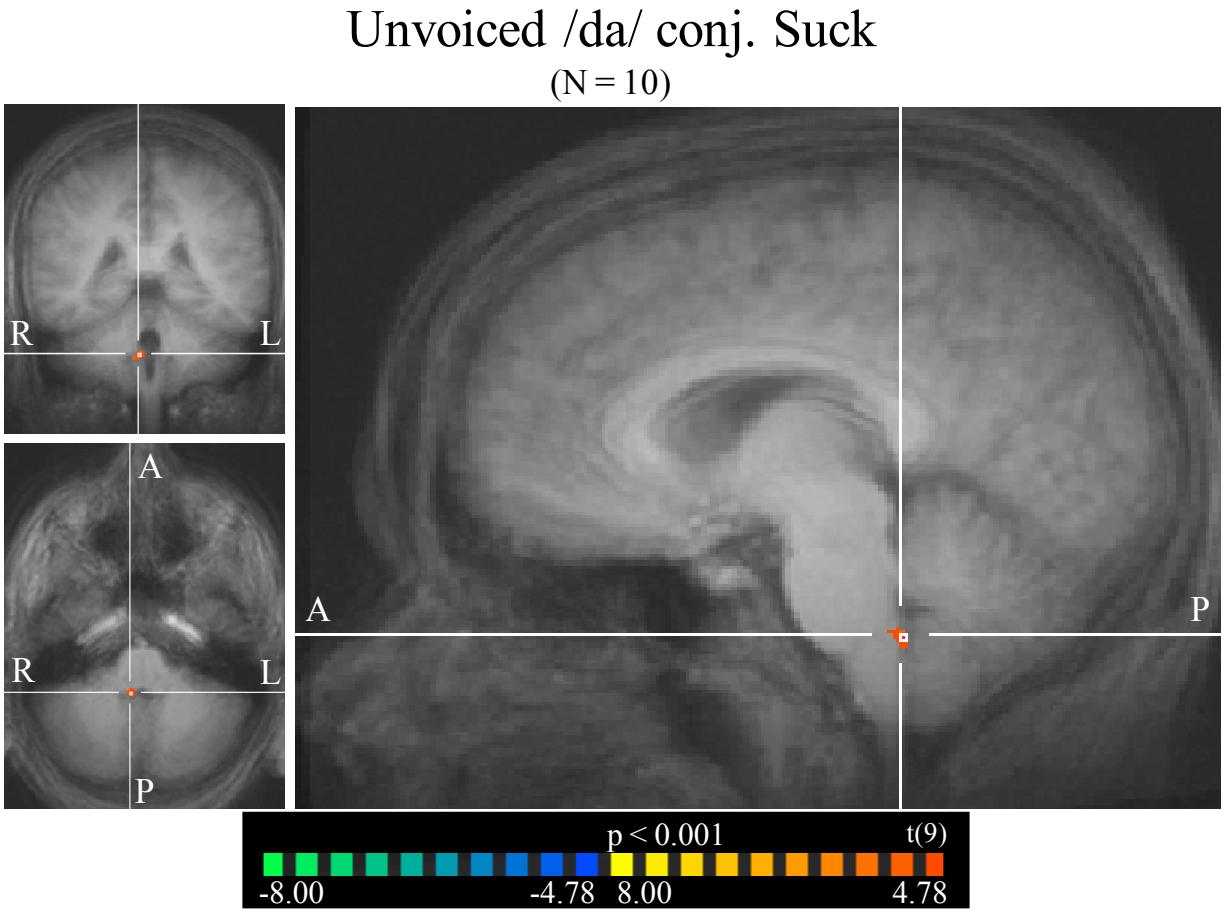

(Coordinate pictured: 126, 156, 160)

Figure 19 b. Mean % signal change compared to baseline

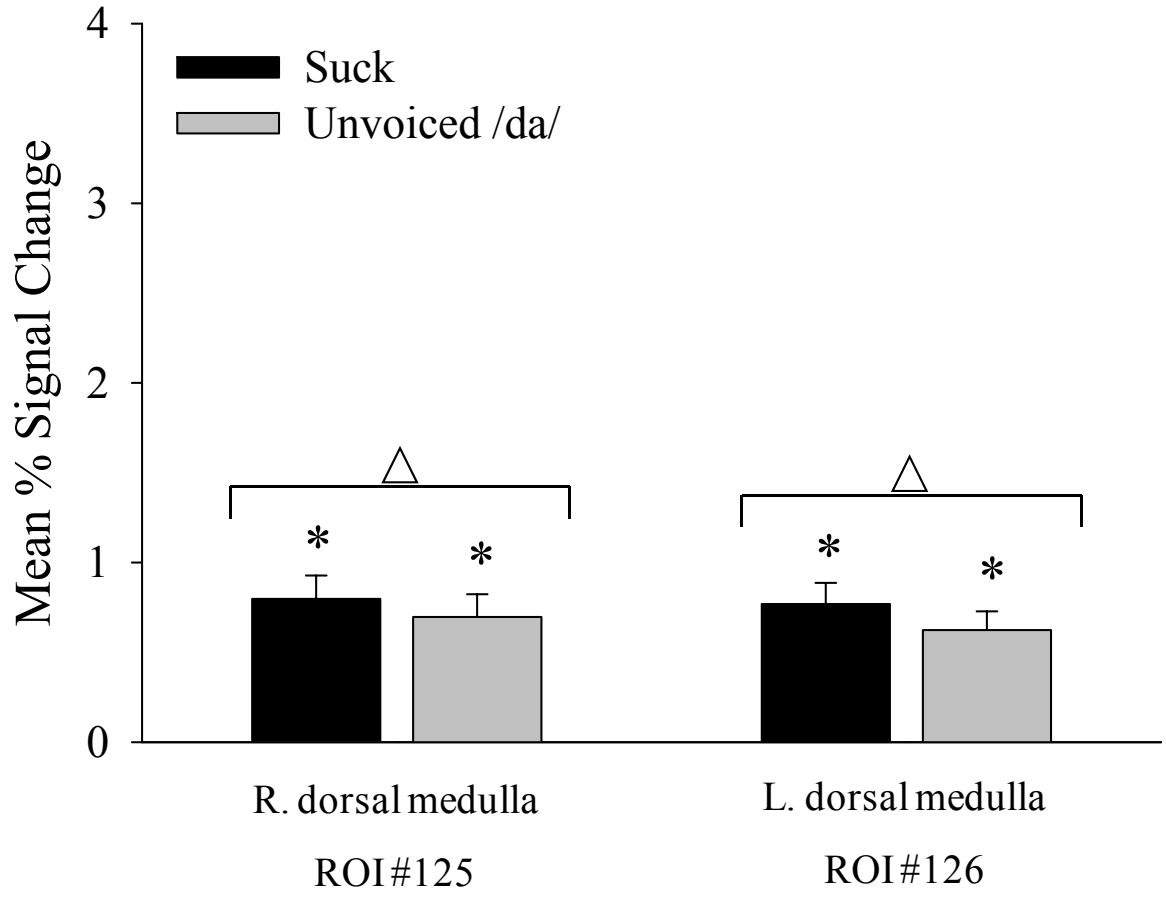

△ Significant main effect across tasks

* Significantly different from baseline

Part 2c: Brainstem Mask: FFX analysis, main effect of rate

To determine the main effect of rate within the masked brainstem region, a single-study FFX GLM analysis collapsed across all participants, implementing a percent signal transformation, was performed. To identify *a priori* ROIs actively correlated with the ororhythmic rate conditions, the contrast [3 Hz > 1 Hz] was applied and the data were thresholded at $p < 0.0001$. Table 20a (p. 132) lists the statistical details for the *a priori* ROI in bold text (no post hoc ROIs were indicated). Table 20b (p. 132) lists the average magnitude of signal compared to baseline for the 3 Hz and 1 Hz rate conditions collapsed across task for the *a priori* ROI in bold text. Figures 20a-b (pp. 133-134) include an SPM map and bar graph representing the mean percent signal change of the rate conditions compared to baseline for the *a priori* ROI.

Areas found to be more active in the 3 Hz compared to 1 Hz rate conditions were located in the right-lateralized pons (Figures 20a-b, pp. 133-134).

Table 20 a. Single-Study FFX GLM, main effect of rate

ROI	Cluster Region	BA	# of voxels	Peak Voxel				
				x	y	z	t value	p value
127	R. pons	N/A	76	125	150	151	4.366	0.000013

Table 20 b. FFX GLM of ROIs

ROI	Region	Contrast	df	value	se	t value	p value
127	R. pons	1 Hz	2404	0.293	0.085	3.461	0.000548*
		3 Hz	2404	0.672	0.085	7.945	0.000000*

* Significantly different from baseline

Figure 20 a. Right pons (ROI #127)

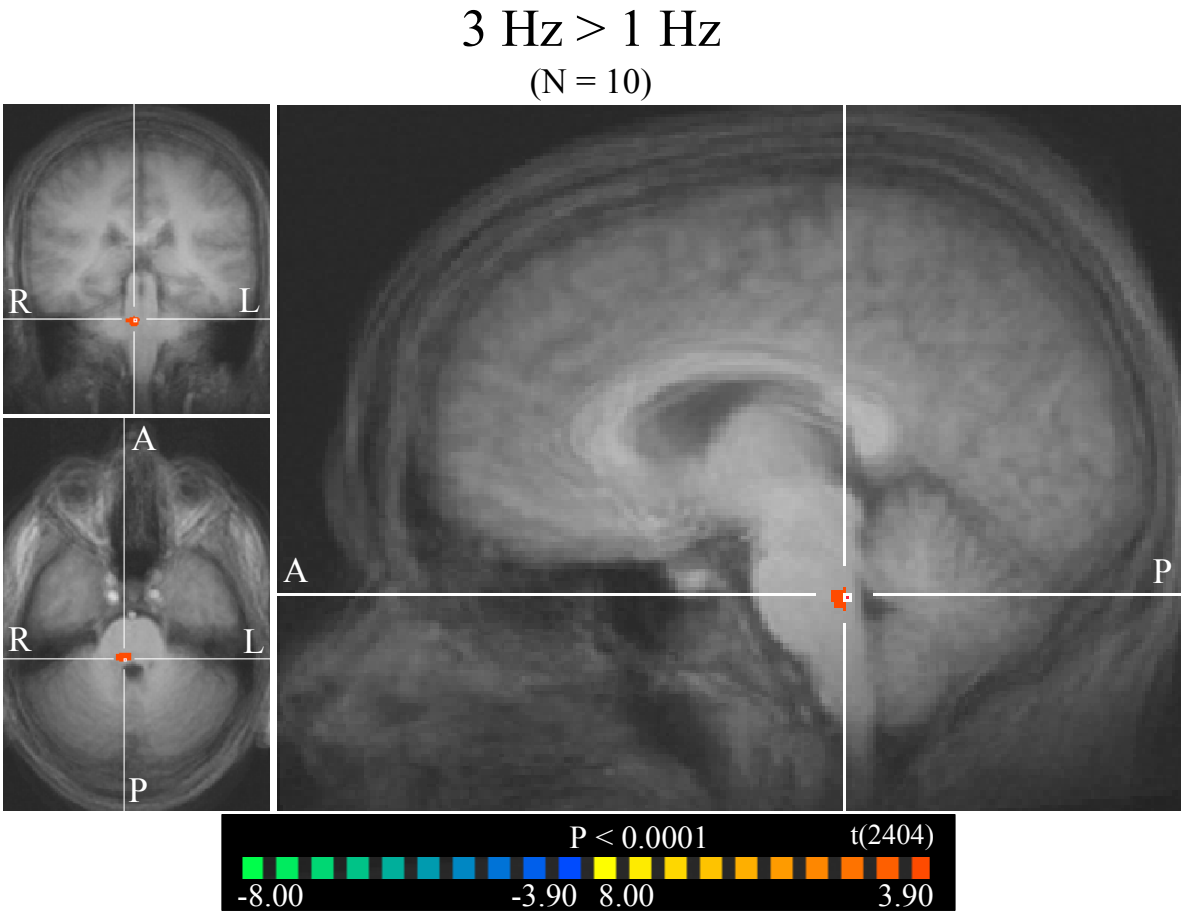

(Coordinate pictured: 125, 150, 151)

Figure 20 b. Mean % signal change compared to baseline

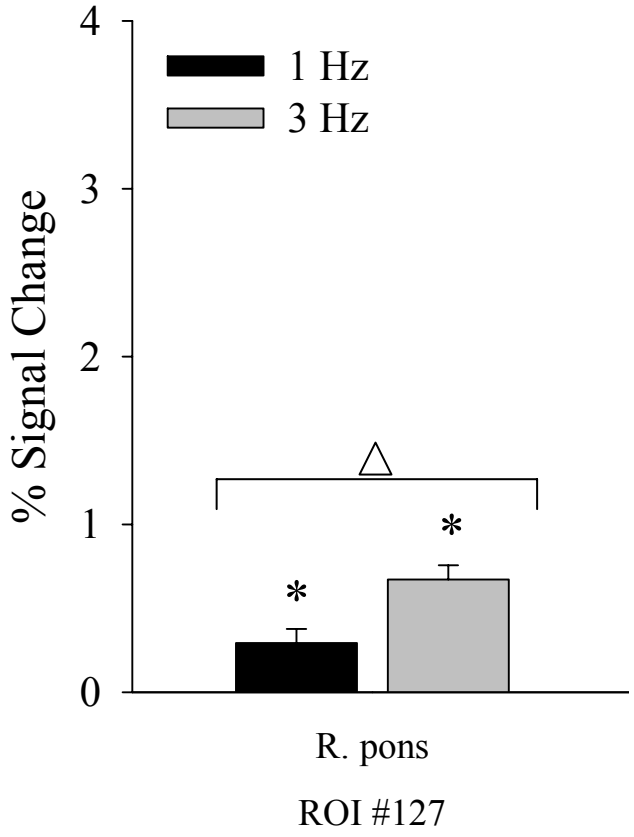

△ Significant main effect of rate

* Significantly different from baseline

Part 2d: Brainstem Mask: Conjunction analysis, main effect of rate

To initially assess the overlapping substrates by rate, two simple SPM map overlays (one for overlapping tasks, one for overlapping rates) were computed, thresholded at p(Bonf) < 0.00001, and visually assessed for shared correlates within the masked brainstem area (Figure 21a, p. 136). To formally determine the minimally shared brain areas correlated to both 1 Hz and 3 Hz rate conditions, a conjunction of contrasts 3 [1 Hz > baseline] and 4 [3 Hz > baseline] was performed and data were thresholded with $p < 0.001$. Table 22a (p. 137) lists the statistical details for *a priori* ROIs in bold text (no post hoc ROIs were indicated). Table 22b (p.137) lists the average magnitude of signal compared to baseline for the 1 Hz and 3 Hz rate conditions collapsed across task for *a priori* ROIs in bold text. Figures 22a-b (pp. 138-139) include an SPM map and bar graph representing the mean percent signal change of the rate conditions compared to baseline for the *a priori* ROI.

Areas found to be active in both 1 Hz and 3 Hz rate conditions were located in the right-lateralized dorsal pons and left-lateralized medulla.

Figure 21 a. Overlapping substrates as a function of rate (brainstem mask)

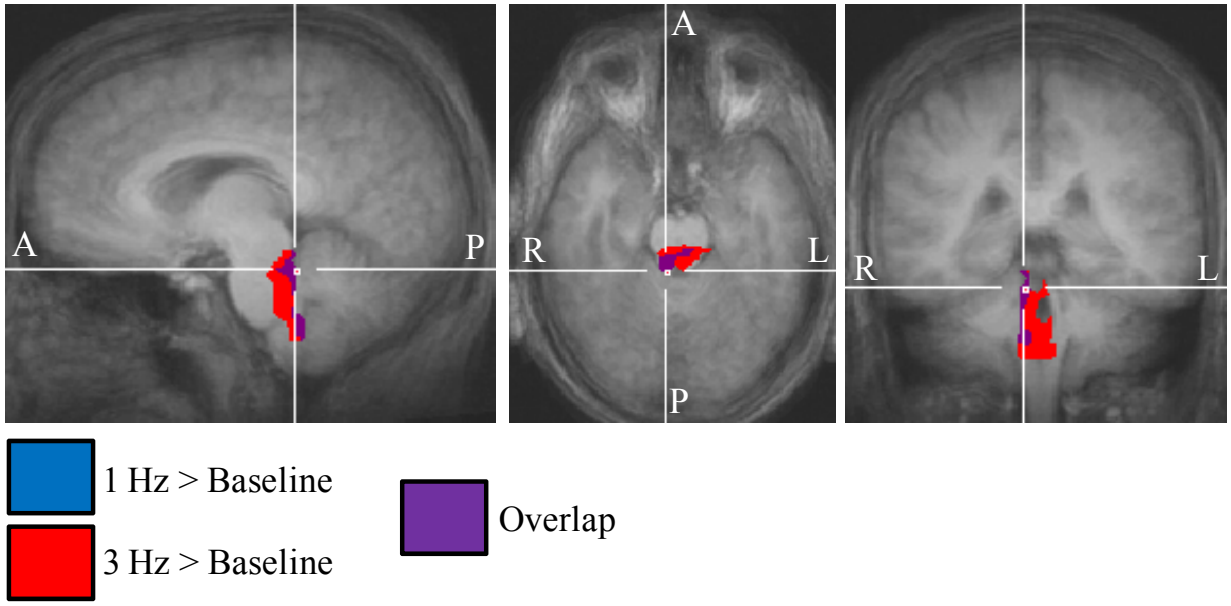

Table 22 a. Multi-Subject RFX GLM, conjunction of rate conditions

ROI	Region	BA	# of voxels	Peak Voxel				
				x	y	z	t value	p value
127	R. dorsal pons	N/A	8	121	153	154	4.960	0.000781
				122	153	154	4.960	0.000781
				122	154	154	4.960	0.000781
128	L. medulla	N/A	133	134	150	160	5.684	0.000300

Table 22 b. RFX GLM of ROIs

ROI	Region	Contrast	df	mean	se	t value	p value
127	R. dorsal pons	1 Hz	9	0.465	0.094	4.960	0.000781*
		3 Hz	9	0.781	0.129	6.072	0.000185*
128	L. medulla	1 Hz	9	0.487	0.064	7.552	0.000035*
		3 Hz	9	0.785	0.115	6.848	0.000075*

* Significantly different from baseline

Figure 22 a. Right dorsal pons (ROI #127)

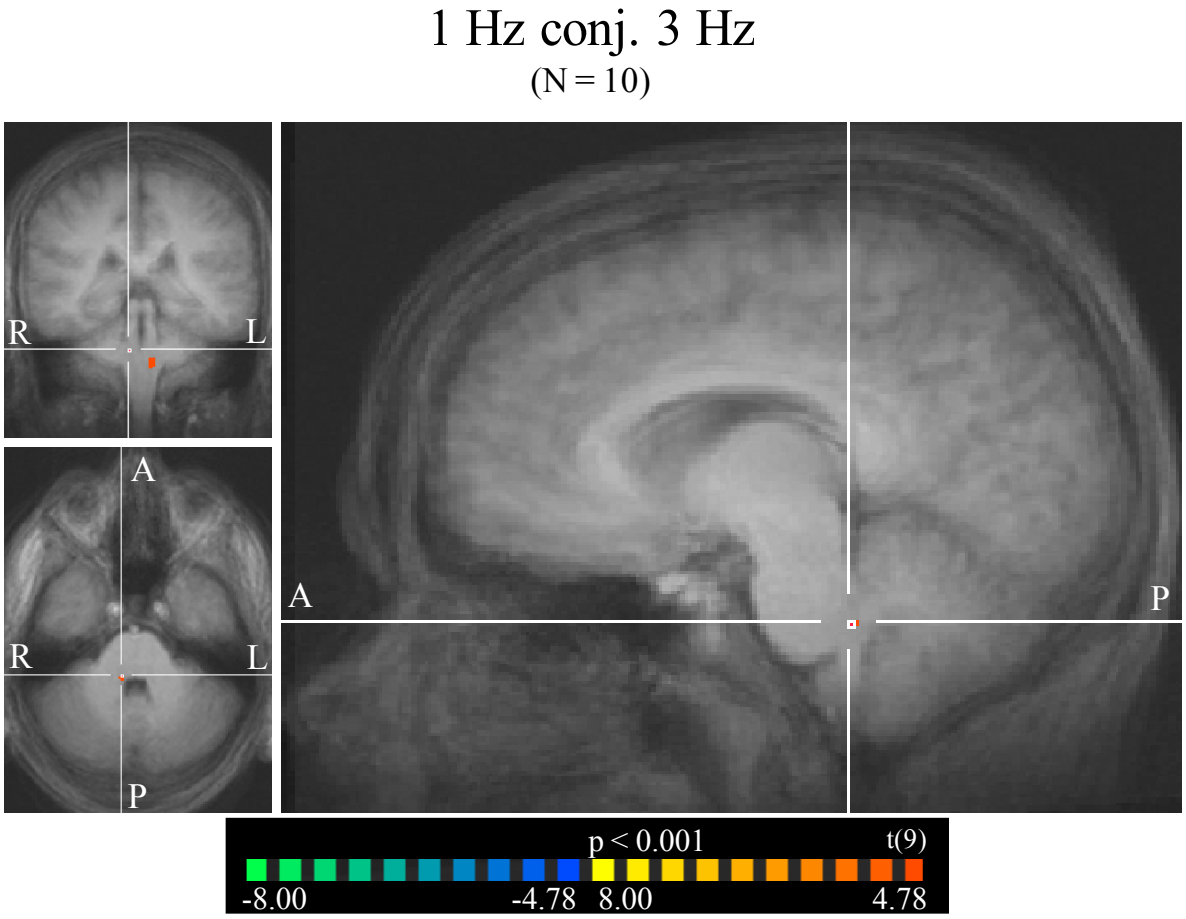

(Coordinate pictured: 122, 152, 154)

Figure 22 b. Mean % signal change compared to baseline

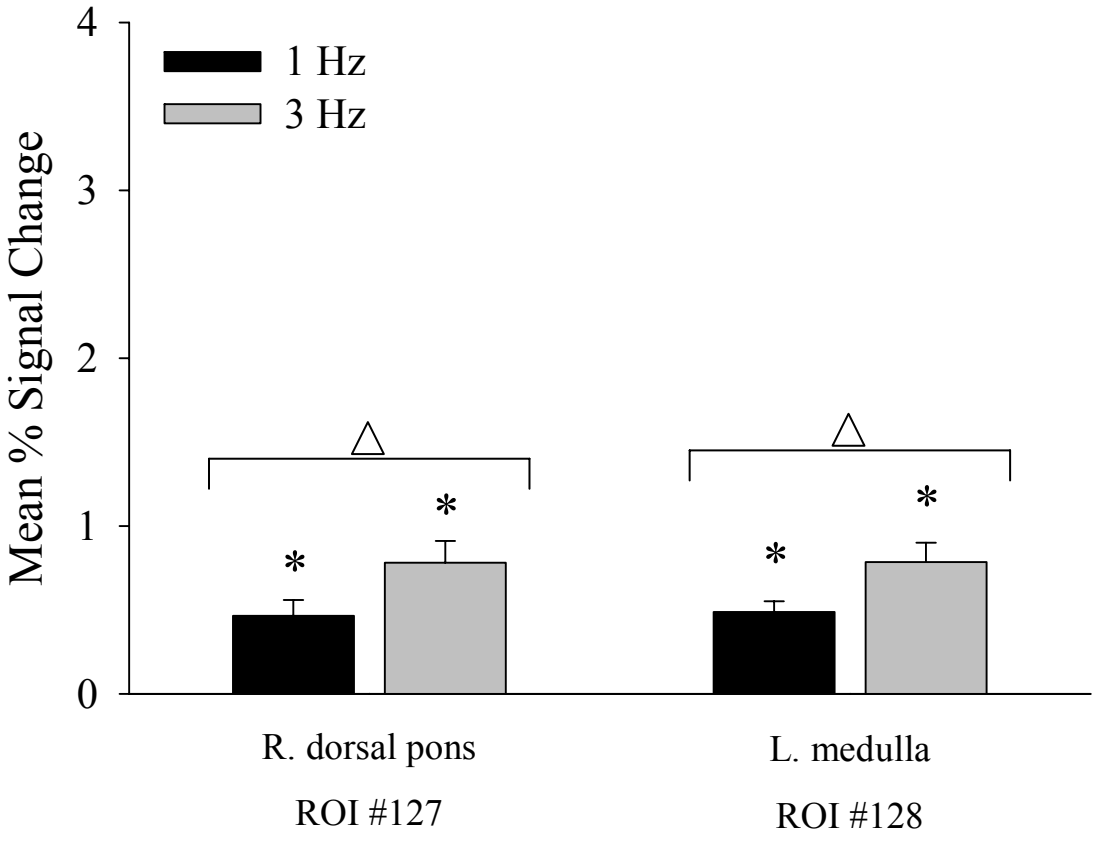

△ Significant main effect across rates

* Significantly different from baseline

CHAPTER 4: DISCUSSION

Overview of Current Study

Our goal was to characterize the location, magnitude, and spatial extent of the BOLD response actively correlated with specific speech (unvoiced /da/) and nonspeech (suck) ororhythmic behaviors performed by healthy adults. Both tasks were considered to be highly learned and were chosen from a large repertoire of speech and nonspeech behaviors studied in humans across the lifespan and relative to health or disease. The tasks were designed to minimize confounding variables of auditory feedback, somatosensory feedback associated with vocalization, or largely differing oromotor articulations. An unvoiced speech task minimized laryngeal engagement present during vocalization and absent during isolated nonspeech behaviors such as mastication and suck. The monosyllabic articulation of /da/ was biomechanically similar to the articulation related to suck.

The findings from the present investigation that the brain activity correlated to suck and unvoiced /da/ ororhythmic behaviors performed at 1 or 3 Hz was manifest by extensively overlapping cortical, subcortical, and brainstem regions was not unexpected. The following discussion attempts to cast the findings from the present investigation within the context of the extant literature, technical considerations, and potential future applications.

Main effect of task

Our findings of shared functional correlates for the ororhythmic suck and unvoiced /da/ behaviors were consistent with descriptions of shared functional areas subserving speech and nonspeech tasks described in other studies such as bilateral face area of the sensorimotor cortices and thalamic nuclei (Bonilha et al., 2006; Lotze, Seggewies, Erb, Grodd, & Birbaumer, 2000; Salmelin & Sams, 2002).

Whole-brain group level analyses indicated additional areas manifesting significantly correlated activity as a function of task included: bilateral basal ganglia (left putamen, right globus pallidus) and insula; right cerebellar cortex (anterior lobe), deep nucleus, and vermis. These areas demonstrated significantly higher BOLD mean percent signal change (compared to baseline) correlated with the suck task compared to the unvoiced /da/ task. Conjunction analysis indicated shared brain areas significantly correlated to both task conditions included bilateral sensorimotor cortex, basal ganglia (putamen), insula, thalamus, anterior lobe of the cerebellum, and left cingulate.

The masked brainstem group level analyses indicated areas in the pons (trigeminal motor nucleus) and midbrain (red nucleus) were significantly correlated with task. These areas demonstrated significantly higher BOLD mean percent signal change (compared to baseline) correlated with the suck task compared to the unvoiced /da/ task. Conjunction analysis indicated shared brain areas significantly correlated to both task conditions in the medulla.

Main effect of rate

Our findings of shared functional correlates for the 1 Hz and 3 Hz ororhythmic performance rates are not entirely consistent with descriptions of bilateral cortical and subcortical functional areas subserving variable rates of ororhythmic behaviors described in other studies such as bilateral sensorimotor cortex, supplementary motor area, basal ganglia, or thalamus (Riecker, Kassubek, Groschel, Grodd, & Ackermann, 2006; Riecker et al., 2002).

Whole-brain group level analyses in the present study indicated areas manifesting significantly correlated activity as a function of rate include: bilateral anteromedial and posteriolateral lobes of the cerebellum; right anteriomedial and posteromedial cerebellum; left thalamus and caudate; and midline pons. These areas demonstrated significantly higher BOLD mean percent signal change (compared to baseline) correlated with the 3 Hz rate compared to the 1 Hz rate. Conjunction analysis indicated shared brain areas significantly correlated to both rate conditions included: bilateral motor cortex, cingulate, insula, anterior lobe cerebellum; left thalamus, posterior cerebellar lobe, and pontomedullary region.

The masked brainstem group level analyses indicated an area of the pons with significantly correlated activity as a function of rate. This area demonstrated significantly higher BOLD mean percent signal change (compared to baseline) in response to the 3 Hz rate compared to the 1 Hz rate. Conjunction analysis indicated shared brain areas significantly correlated to both rate conditions in the pons and medulla.

Central Encoding of Ororhythmic Behaviors

Brainstem contributions to ororhythmic behaviors

The mechanism by which the brainstem regulates bilateral synchronization of trigeminal motor pattern generation underlying sucking rhythm has been thoroughly investigated with mammalian *in vitro* preparations and is likely to involve: (1) trigeminal interneurons located around and within the trigeminal motor nucleus which synapse onto contralateral neurons, and (2) midline-crossing dendrites of rhythm generating neurons (Barlow et al., 2010; Chandler & Tal, 1986; Janczewski & Karczewski, 1984; Koizumi, Nomura, Yokota, Enomoto, Tamanishi, et al., 2009; Kolta, Westberg, & Lund, 2000; Li, Takada, Kaneko, & Mizuno, 1996). Our current findings combined with the existing evidence for brainstem ororhythmic pattern generating circuitry from *in vitro* preparations for suck (Koizumi et al., 2009), and *in vivo* imaging of nonspeech (Komisaruk et al., 2002) and vocalized speech (Simonyan, Ludlow, & Vortmeyer, 2009), make a case for a critical role of brainstem circuitry in rhythm generation for ongoing ororhythmic behaviors such as suck, mastication, and speech (Barlow & Estep, 2006; Barlow et al., 2010; Lund & Kolta, 2006a). More specifically, our findings provide functional evidence for shared ororhythmic task (i.e., suck and unvoiced /da/) correlates localized to the dorsal medulla (pp. 126-130), and shared ororhythmic rate (i.e., 1 Hz and 3 Hz) correlates localized to the dorsal pons and pontomedullary junction (pp. 135-139).

Sensorimotor mechanisms

Signals propagated among remote brain regions are amplified and dampened to meet the ever changing internal and external demands unique to an organism's perception and interaction within an environment. Multiple feedback systems including general performance monitoring and sensory processing are assumed to be simultaneously functioning during ongoing motor control in order to detect and correct speech production errors (Christoffels, Formisano, & Schiller, 2007; Ganushchak & Schiller, 2006; Hartsuiker & Kolk, 2001; Holroyd & Coles, 2002; Masaki et al., 2001; Schiller, 2005). Self-monitoring during ongoing speech is hypothesized to be a centrally controlled process (Levelt, 1989) where auditory and somatosensory feedback engage interacting neural networks that continuously evaluate the spatiotemporal patterning of speech (e.g., pitch, intensity, rate) and appropriately update the speech-motor plan (Burnett, Freedland, Larson & Hain, 1998; Jones & Munhall, 2000; Schiller, 2005).

The insula has been hypothesized to be a multimodal network node allowing continuous adjustment of an articulatory plan by integrating auditory, proprioceptive, and eventually emotional demands into a finely tuned spatiotemporal innervation pattern of vocal tract musculature for producing syllable sequences (Ackermann & Riecker, 2004; Christoffels et al., 2007; Dronkers, 1996; Hickok, 2001; Hirano, Kojima, Naito, Honjo, Kamoto, et al., 1997; Indefrey & Levelt, 2004; Kuriki, Mori, & Hirata, 1999; Nestor, Graham, Fryer, Williams, Patterson, et al., 2003; Riecker et al., 2000; Wise et al., 1999). The insula is reciprocally connected to the anterior cingulate cortex (ACC) and projects unilaterally to motor areas. The ACC plays a significant role in oromotor control and has been suggested to be engaged in processes of error processing, goal-directed behavior, and response selection and initiation

related to word production (Barch, Braver, Sabb, & Noll, 2000; Carter, Braver, Barch, Botvinick, Noll, et al., 1998; Gerhring & Knight, 2000; Kiehl, Liddle, & Hopfinger, 2000; Shuster & Lemieux, 2005), and ongoing speech monitoring (Botvinik, Braver, Barch, Carter, & Cohen, 2001; Christoffels et al., 2007).

The insula has also been suggested to be a substrate for the integration of lower level aspects of the speech motor plan with a more abstract representation of speech sounds used in sequence planning (Bohland & Guenther, 2006) whether it be encoding variable (Murphy et al., 1997; Riecker et al., 2000; Soros et al., 2006) or repetitive (Riecker et al., 2005) speech sequences. Our findings of a significant main effect of task in bilateral (left-lateralized) insula, and bilateral shared significant correlates across task (left-lateralized) and rate (right-lateralized) provide support for the left insula as monitoring task-specific feedback, whereas the right insula may process rate-specific feedback. These findings provide functional neuroimaging support for the notion of multiple feedback systems operating simultaneously as a function of ororhythmic task and rate.

The cerebellum is consistently associated with articulation during overt speech in functional imaging studies and assumed to play a role in the fine adjustment of oromotor activity (Hirano et al., 1997; Wise et al., 1999). Superior cerebellar regions are particularly involved in the feedforward control and anticipatory co-articulation in speech production (Guenther et al., 2006; Bohland & Guenther, 2006) and during nonspeech movements (Grodd, Hulsmann, Lotze, Wildgruber, & Erb, 2001). The superior cerebellum is heavily implicated in adaptive timing mechanisms in ongoing control of the articulators through crossed thalamo-cortical projections to the motor cortex and/or direct connections with the periphery.

Our findings provide support for: (1) a task-specific role of the deep cerebellar nuclei, (2) a task- and rate- specific role of the vermis, (3) bilateral anterior cerebellar lobes contributing across task and rate variables, and (4) a rate-specific control by bilateral posterolateral lobes.

Oromotor sequence selection and coordination

The coordination of motor sequences is subserved by multiple channels of basal ganglia-thalamocortical (BGTC) connections, and the connections of their related nuclei. Subloops of the BGTC are created from prefrontal and motor area modules. Each subdivision of the motor areas receives a mixed and weighted transthalamic input from both the cerebellum and basal ganglia (Nakano, 2000). Basal ganglia also project to many areas in the midbrain (e.g., red nucleus, and superior colliculus) and brainstem (e.g., medial medullary reticular formation), which contain premotor interneurons that are involved in various types of ororhythmic behaviors (Chandler & Tal, 1986; Nakamura, Muramatsu, & Yoshida, 1990; Nozaki et al., 1986, 1993). Convergence of the loops occurs at the level of the basal ganglia nuclei as well as the brainstem pedunculopontine nucleus which is an area that contains premotor multisynaptic neurons that coordinate activity of masticatory, facial, and lingual muscles (Fay & Norgren, 1997a,b,c).

Cortical inputs carrying sensorimotor, cognitive, and dopaminergic inputs carrying reward-related information 'train' the basal ganglia to optimize their output to the thalamus. In this way, basal ganglia output to the thalamus manifests an advanced ability to organize behavior by including motor skill mechanisms in which new movements patterns can be created through practice and learning. It has been suggested that the basal ganglia play an essential function in the control of reward-seeking behavior by organizing and sequencing multiple body movements

(Boecker, Dagher, Ceballos-Baumann, Passingham, Samuel, et al., 1998; Hikosaka, 2007; Paradiso, Cunic, Saint-Cyr, Hoque, Lozano, et al., 2004) and vocal tract articulatory targets (Bohland & Guenther, 2006; Brown, Martinez, Hodges, Fox, & Parsons, 2004; Middleton & Strick, 2000; Pickett, Kunihom, Protopapas, Friedman, & Liedberman., 1998). Following orienting movements such as saccadic eye movement and head turning, mouth movements including biting, licking, sucking, chewing, and vocalization complete reward-seeking behavior as a basic means of ingestion, expressing emotions, and communication (Gil-da-Costa, Braun, Lopes, Hause, Carson, et al., 2004; Poremba, Malloy, Sauders, Carson, Herscovitch, et al., 2004), which require context-dependent selections.

The basal ganglia mechanisms utilizing their GABAergic outputs to the periaqueductal gray and reticular formation brainstem areas may play important roles in vocal pattern generators and nonspeech behavioral selections (Hage & Jurgens, 2006; Hikoska, 2007; Kirzinger & Jurgens, 1991; Von Krosigk & Smith, 1991; Zhang, Davis, Bandler, & Carrive, 1994). Although the spatiotemporal patterns of individual movements are largely innate and fixed, the basal ganglia play an essential role in selecting appropriate movements and arrange them in an appropriate, contextually dependent, sequence (Mink, 1996; Nambu, Tokuno, & Takada, 2002).

The current investigation revealed bilateral basal ganglia (putamen) activity to vary as a function of task, and also contain areas shared across tasks and across rates. Thalamic correlates were generally bilateral with a right-lateralized main effect of task and areas of shared across tasks, and a left-lateralized main effect of rate and areas shared across rates. Our findings of bilateral basal ganglia and thalamic activity are in agreement with other studies of the main

effect of task. Somewhat unique to our findings are the lateralized tendencies of thalamic correlates as a function of task and rate.

Lateralization effects

Bilateral activation of the sensorimotor cortices during speech production has been reported in many neuroimaging studies (Herholz, Thiel, Wienhard, Pietrzyk, von Stockhausen, et al., 1996; Muller, Rothermel, Behen, Muzik, Mangner, et al., 1997; Salmelin, Hari, Lounsamaa, & Sams, 1994) with systematic lateralization found in the left inferior frontal cortex that comprises the classical Broca area. Other areas of lateralized activation correlated to speech production include: left-lateralized areas of the frontal opercular region, anterior insula; right-lateralized inferior cerebellum, caudate, and base of the pons (Bohland & Guenther, 2006; Murphy et al., 1997). Investigations of increasing linguistic content of lip and tongue movements (e.g., comparison of verbal versus nonverbal correlates) reveal a more focal motor cortex involvement and left-hemisphere lateralization of face area (Salmelin & Sams, 2002). When the linguistic content of the task is minimized by instructing participants to perform 'automatic' language production (e.g., repeating a meaningless sentence, Murphy et al., 1997; repeating heard nouns, Wise et al., 1999), it was demonstrated that the articulatory plan was formulated in the left lateral premotor cortex and the left anterior insula, not in Broca area (Wise et al., 1999).

Our findings of significant bilateral activation of the primary sensory areas roughly localized to the homunculus representation of the lips, jaw, and tongue anatomical locations of the components of the speech motor system are in agreement with findings from other studies of

syllabic speech and nonspeech behaviors (Bohland & Guenther, 2006; Guenther et al., 2006; Lotze et al., 2000). These results support the notion that the primary motor and somatosensory cortices are bilaterally engaged in the online control of the articulators and registration of orosensory feedback. Our findings reveal the following areas as more highly correlated with the suck task compared to the unvoiced /da/ task: unilateral left precentral gyrus and right cerebellum activations; bilateral insular activation that was left-lateralized in spread and magnitude, and basal ganglia and thalamic activations that were right-lateralized in spread and magnitude. Our conjunction analyses revealed areas actively correlated with both suck and unvoiced /da/ tasks located in unilateral left cingulate; and bilateral, left lateralized in spread and magnitude (cerebellum anterior lobe), right lateralized in spread and magnitude (putamen and thalamus).

Studies of cortical and subcortical correlates of speech motor control demonstrate different relations between the frequency of syllable repetitions and the BOLD signal at the level of the cortical structures (positive linear rate/response function), the right striatum (negative linear relationship), and the right cerebellum and left thalamus (positive linear rate/response function with threshold at 3 Hz) and the left inferior frontal gyrus, left anterior insula, and the tectum (nonlinear rate/response functions) (Ackermann, Ricker, Mathiak, Erb, Grodd, et al., 2001; Wildgruber, Ackermann, & Grodd, 2001). Riecker and colleagues (2005) hypothesized a threshold effect possible because other studies using slower stimulus rates failed to demonstrate functional lateralization (Riecker et al., 2005). Our findings of unilateral left thalamus and caudate; bilateral activation that was right-lateralized in spread and magnitude (cerebellum, posterior lobe) being more highly correlated with the 3 Hz rate provide support for further study

of regional threshold effects. Our conjunction analyses revealed areas actively correlated with both 1 Hz and 3 Hz rates located in unilateral left cingulate, pontomedullary region, thalamus, and cerebellum/posterior lobe; bilateral, left lateralized in spread and magnitude for precentral gyrus and cerebellum anterior lobe, right lateralized in spread and magnitude for insula and putamen.

Extended Hypotheses

Within the motor control literature studies have suggested that rhythmic (continuous oscillatory) movement circuits are included within the network that encodes single discrete (gestural) movements. The limb motor control literature supports the notion of less cerebral activity associated with rhythmic movements compared to gestural movements based on the former being computationally simpler to carry out. Areas likely involved in cortical pattern generation for rhythmic movement include SMA, pre-SMA, caudal and rostral cingulate zones, and cerebellum. Gestural movements typically incorporate different and/or more complex acceleration and deceleration profiles of the discrete movements. For example, in a study of wrist flexion-extension tasks, the entire functional rhythmic movement circuit was included in the more distributed network of brain areas encoding gestural movements (Schaal et al., 2004). It is yet to be determined whether rhythmic orofacial motor primitives are part of a distributed circuit that incorporates cerebral areas for higher-level cognitive planning, or if motor loops coexist separately to encode rhythmic and discrete movements.

Correlates of unvoiced syllabic speech are further engaged by suck.

The automaticity of centrally patterned behaviors such as suck, mastication, and vocalization draws on motor circuits located in the brainstem PAG, whereas additional prefrontal and parietal areas are recruited for higher-level mechanisms related to the cognitive control of speech (Lund & Kolta, 2006a; Schaal et al., 2004). Over-learned articulatory programs such as that hypothesized for commonly used syllables are hypothesized to be held within the premotor

cortex as prespecified motor routines (Levelt, 2001). Compared to an on-line assembly of single phonemes or isolated orofacial/laryngeal movements, the storage of preprogrammed motor routines would considerably reduce the higher-order computational demands for speech production (Ackermann & Riecker, 2004).

The DIVA model of speech production (Guenther et al., 2006) offers one computational account for how voiced phonemic tokens are produced utilizing auditory and/or orosensory feedback and feedforward systems. The Speech Sound Map component of the DIVA model predicts BA 44 and neighboring premotor areas participate in sequencing well-learned 'speech chunks' and further suggests there should be additional activity when multiple chunks are produced (Guenther, 2006). In agreement with this hypothesis are observations from functional neuroimaging studies investigating correlates of multi-syllabic versus mono-syllabic words. Regions of complexity-correlated activations have been observed in BA 44, premotor regions, inferior parietal lobe, and inferior frontal gyrus. Together, these findings support the notion that (1) subsyllabic information is involved with encoding speech sequences, and (2) utterances are assembled and not simply executed from a single motor memory (Bohland & Guenther, 2006; Guenther, 2006; Shuster & Lemieux, 2005).

The current study expands this knowledge base and has identified a significant main effect of task within discrete areas of activation localized to the midbrain (red nucleus) and the pons (trigeminal motor nucleus, reticular formation) that are more actively correlated with the suck task compared to the unvoiced /da/ task. These findings support the notion of the suck and unvoiced syllabic /da/ tasks being centrally patterned within shared brainstem areas, however with a higher neural demand posed on brainstem circuitry by the suck task compared to the

unvoiced /da/ task. This preliminary work provides the first functional neuroimaging evidence for shared brainstem substrate localized to the red nucleus and trigeminal motor nucleus for encoding both unvoiced speech and nonspeech suck ororhythmic tasks. Compared to the unvoiced speech task, the suck task further engages the shared brainstem substrate.

Spontaneously increased activation of sensory areas during ororhythmic behavior.

Spontaneous activation, or activation in the absence of any external stimulus, cannot be attributed to specific inputs or outputs. Extreme caution is advised when interpreting fMRI data because very little is currently known about the neural processes underlying widespread fluctuations of the fMRI signals. Further investigation of the neural and vascular system under what are as close as possible to null stimulation conditions should be considered before interpreting activation patterns in studies of spontaneous activity (Logothetis, Murayama, Augath, Steffen, Werner, et al., 2009). Activation of auditory cortex in humans and other species can be affected by inputs from other sensory modalities (Hunter, Eickhoff, Miller, Farrow, Wilkinson, et al., 2006; Kraemer, Macrae, Green, & Kelley, 2005; Schroeder & Foxe, 2005; Voisin, Bidet-Caulet, Bertrand, & Fonlupt, 2006). Areas of coactivation that might increase activity in the auditory system include the anterior cingualte cortex and structures in the frontal lobes (Halpern & Zatorre, 1999; Hoshiyama, Gunji, & Kakigi, 2001; Hunter et al., 2006; McGuire, Silbersweig, Murray, David, Frackowiak, et al., 1996; Voisin et al., 2006). These findings support the notion of the expectation of a stimulus modulates activity in sensory areas. Such priming or preparation for an expected sensory stimulus by top-down attentional mechanisms has been demonstrated to modulate activity in visual cortical areas (Chawla, Rees,

& Friston, 1999; Kastner & Ungerleider, 2000) and may be a common property of sensory cortex.

The current study utilized unvoiced ororhythmic behaviors to investigate the encoding of orofacial articulatory aspects of speech and nonspeech tasks. Although we did not record any audio signal during the experimental tasks, we assume participants were performing the suck and speech behaviors silently as instructed during the initial practice session. After study completion, each participant confirmed they did not say /da/ out loud. Bilateral temporal lobe correlates manifesting a main effect of task (and rate) in the current study showed higher activation during the suck task (3 Hz rate) compared to the unvoiced /da/ task (and 1 Hz rate). Bilateral temporal areas of activation were also found to be shared across task and across rate. Because it is unknown whether any auditory experience was associated with the current unvoiced speech and suck tasks of the current study we are unable to unequivocally define a cause for the increased activity in auditory cortex.

Since speech is usually associated with an auditory consequence, one possible explanation of temporal lobe activity indicated in the current study could be activation of mirror neurons. Regional activations in human frontal, parietal, and temporal areas respond specifically to action independent of whether the action is executed or passively observed (Decety & Grezes, 1999). Functional MRI adaptation paradigms exploring oromotor repetition suppression are needed to better understand the role of the mirror neuron system in orofacial control for speech and nonspeech gestures. Findings of the current study support the notion of a multimodal representation, independent of effector, for goal directed orofacial behavior (e.g., suck, mastication, syllabic speech gestures) encompassed by a network of mirror neurons functionally

connected across inferior parietal lobule, superior temporal gyrus, and inferior frontal gyrus (Chong, Cunnington, Williams, Kanwisher, & Mattingley, 2008; Galati, Committeri, Spitoni, Aprile, Di Russo, et al., 2008).

Investigating how baseline activity in sensory areas of the cortex including somatosensory, visual, and auditory, is modulated by task stimuli that is either self-generated or perceived from the environment provides a valuable way of probing functional connectivity and contributions to conscious experience without having to use an external stimulus, or in patient populations with deficit sensory capabilities (i.e., attenuated responses in stroke or conditions of over-stimulation). Cortical activity under such conditions is hypothesized to at least overlap with substrate responsible for processing real stimuli. Such studies will advance our understanding of where specific stimulus information is encoded and stored in sensory cortex as well as how top-down processes initiate activity within lower-level sensory areas including thalamic and brainstem nuclei.

Distributed networks overlap for the encoding of ororhythmic behaviors.

Functional neuroimaging studies have agreed upon a limited number of cerebral regions essential to articulation. A putative 'minimal speech production network' (i.e., minimal language processing) is likely to include bilateral activations in the sensorimotor cortex (Riecker et al., 2000) and cerebellum with right-sided activation in the thalamus/caudate nucleus (Murphy et al., 1997). In agreement with the DIVA model, added task complexity results in further engagement of the 'minimal speech production network' and recruit additional areas of activity outside the minimal network that are known to be involved in sequencing non-speech motor acts

such the anterior insula/frontal operculum, SMA, basal ganglia, anterior thalamus, and cerebellum (Dresel et al., 2005; Soros et al., 2006). Complexity-related increases in regional activation for more complex stimuli have been attributed to not only the greater demand on the motor control and phonologic processing systems (Bohlnad & Guenther, 2006; Soros et al., 2006), but also increased monitoring of potential response errors (Fu et al., 2002).

Very few investigations of a putative 'minimal nonspeech production network' that could encode articulations essential to adult human mastication have been published, and to our knowledge, zero functional imaging studies have been published regarding functional correlates of suck in the healthy adult. Current literature focuses on either cortical or subcortical regions without providing direction for cerebral connectivity hypotheses. The feasibility of fMRI to visualize cortical, subcortical, and specific lower brainstem sensory and motor nuclei during production of orofacial movements has been demonstrated by Komisaruk and colleagues (2002) who found significant activity within the cortex and thalamus correlated with orofacial behavior encoding, in addition to brainstem hypoglossal, facial, and trigeminal main sensory nuclei correlated to tongue movement, face/lip movement, and stimulation of the malar area, respectively. Beyond this, whole-brain investigations of cortical, subcortical, and brainstem correlates of articulations essential furthering our understanding of speech and nonspeech ororhythmic behaviors are lacking.

Distributed neural control of precisely timed movements has been well established in functional imaging studies of syllabic speech (Bengtsson, Ehrsson, Forssberg, & Ullen, 2005), and nonspeech (Maillard, Ishii, Bushara, Waldvogel, Schulman, et al., 2000; Sakamoto, Nakata, Honda, & Kakigi, 2009) behaviors. The spatiotemporal sequencing of syllables into larger

words or phrases is suggested to be subserved by corticobulbar pathways, several areas of the frontal lobe, cortico-subcortical loops between the cerebellum and basal ganglia for encoding the online temporal aspects of speech (Ackermann, Mathiak, & Ivry, 2004; Levelt, 1989; Liberman, 1996). Functional neuroimaging studies have supported this by demonstrating the cerebral control of speech rate is correlated with increased hemodynamic activation of sensorimotor cortex, SMA, anterior insula, and especially the cerebellum at rates above 3 Hz (Ackermann, 2008; Riecker et al., 2005). Other functional neuroimaging studies of speech motor control have shown bilateral superior cerebellum (in addition to SMA, left hemisphere premotor and insular cortex) to contribute to prearticulatory processes of speech motor control (Riecker et al. 2005; Wildgruber et al., 2001), whereas bilateral inferior cerebellar areas (in addition to sensorimotor cortex and basal ganglia) are thought to contribute to repetitive syllable execution (Ackermann, 2008).

Although the current study was limited to two rates (1 Hz or 3 Hz), interesting activation profiles were observed for the cerebellum when contrasting the rates with baseline. When observing the simple overlay of rate contrasts (i.e., [1 Hz vs. baseline] and [3 Hz vs. baseline]), the vermis and bilateral anterior lobes (slight right-lateralization) appear to be largely engaged at the higher rate. This area of activation entirely overlaps the comparatively small areas of activation correlated with the slower rate. An additional area of activity was revealed in the left-posterior lobe of the cerebellum correlated with the higher rate. Additionally, our findings of cerebral and brainstem activations correlated with the two rates suggest similar loops could be functional during the temporal encoding of prearticulatory processes of both unvoiced syllabic speech and suck ororhythmic behaviors.

Technical Limitations & Considerations

Healthy subject population

Investigating the neural basis of motor speech control in normal individuals using fMRI reveals clear information, whereas information from patient populations can sometimes be difficult to establish the boundaries between intact and disrupted brain tissue in individuals recovering from stroke or with progressive neurodegeneration.

Effect size

Percent signal change transformation was used to normalize the data to make sure that the differences between the mean signals between runs do not mask the smaller differences of interest between the conditions. Quantitative scaling into percent signal change is helpful to detect and eliminate bad results with abnormal extreme values. While cognitive effects give signal changes on the order of 1% (and larger in visual and auditory cortices), signal variations of over 10% may arise from motion and other artifacts in the data. Thus, a quantitative check on measured effect size can be used to screen abnormally large values likely caused by artifacts in the data. Three scale factors are involved in percent signal change: (1) peak value in the design matrix, (2) normalization by a baseline value, and (3) the sum of the positive terms in the contrast vector. Percent signal change is often calculated using a baseline of the mean of the time series on a voxel. Percent signal change is calculated by dividing the time series signal by the baseline (which is whole brain average).

Contrasts in the GLM are comparisons of one effect size to another. In our analysis, each effect was estimated in percent signal change. It should be noted that these quantitative results do not directly interpret neural excitations. The scaling does not extend back to neural excitation, because neither the BOLD effect (neural excitation to change in local dHB blood levels), or scanner effects (dHB change to recorded signal change) are well-defined. Thus, this analysis of percent signal change is only in the mathematical estimation domain, not the biology or physics domains.

Spatiotemporal resolution

Activity of the brainstem reticular formation and periaqueductal gray are not problematic to *in vivo* mapping of sensory and motor nuclei. We anticipated orofacial sensory receptors to generate feedback in response to our speech and nonspeech oromotor tasks that can be anatomically (Paxinos & Huang, 1995) and functionally differentiated at our voxel resolution of 3.75 x 3.75 x 3.00 mm^3. Other fMRI reports have demonstrated successful identification of brainstem sensory or motor nuclei (Bense, Janusch, Vucurevic, Bauermann, Schlindwein, et al., 2006; Corfield et al., 1999; Dresel et al., 2005; Komisaruk et al., 2002; Langers, van Dijk, & Backes, 2005; Mainero, Zhang, Kumar, Rosen, & Sorensen, 2007; McKay, Adams, Frackowiak, & Corfield, 2008; Sigalovsky & Melcher, 2006; Zhang, Geng, Zhang, Li, & Zhang, 2006).

Although our voxel size is comparable to other fMRI investigations of brainstem nuclei, we are limited in statistical power and the interpretation of results due to the application of an 8 mm spatial filter at the time of data acquisition. This filtering combined with the relatively small size of orofacial cranial nuclei such as the hypoglossal nucleus (~ 1 x 12 x 1 mm^3), facial and

trigeminal motor nuclei (~ 2 x 3 x 3 mm^3) (Paxinos & Huang, 1995) are likely to result in only one activated voxel correlated with ororhythmic behaviors. Our additional criteria for a region to be considered active (≤ 4 contiguous voxels) was applied to limit false-positives.

Due to the current study's lack of a jittered timing interval within its scanning sequence, it is not possible to identify individual temporal stages of preceding internal processes correlated to the tasks. This limitation of the current study can be resolved by implementing a jitter interval into the sequence to achieve sub-TR resolution. However, this approach comes at the expense of reduced experimental power as the number of trials used to estimate a signal-averaged HRF is reduced by a factor of sub-TR jitter. Further experiments implementing a jitter interval on a higher performance MR scanner will help resolve these issues.

Determining appropriate interval length

The entire block duration of the current study was 10 seconds. This was chosen based on block durations used in other sparse sampling or clustered volume fMRI acquisitions followed by random effects analyses of the correlates of speech and nonspeech orofacial movements: 8 seconds (Fu et al., 2002), 11 seconds (Dresel et al., 2005), 14 seconds (Bohland & Guenther, 2006), 15 seconds (Ozdemir, Norton, & Schlaug, 2006).

A possible limitation of fMRI studies that use a clustered volume or sparse sampling acquisition is the temporal separation between the onset of task and the onset of image acquisition which may be associated with some signal loss of the BOLD response. The temporal separation between task onset and volume acquisition in the current study was 4 seconds and is comparable to other studies: 2.5 seconds (Bohland & Guenther, 2006), 2.9 seconds (Fu et al.,

2002), 3.5 seconds (Ozdemir et al., 2006), 4.0 seconds (Soros et al., 2006), 4.95 seconds (Dresel et al., 2005).

Artifacts during overt articulation

Head motion may covary with articulation related to speech or nonspeech oromotor behaviors (Munhall, 2001). Completely inhibiting head motion is difficult. When the head does move, even slightly, activations from a given cortical location can be spread across different voxels at different time points. This effectively decreases the activation signal-to-noise ratio and distorts anatomical localization.

Keeping in mind that background noise should be considered to have a modulatory effect on overt speech production and to better approximate usual speaking conditions, many investigators have interleaved a 'silent period' between the acquisition of brain images. The scanner is transiently silent during the silent period while the subject is performing a task. One (i.e., sparse sampling) or several (clustered volume) acquisitions are then recorded by the scanner (Eden et al., 1999; Hall et al., 1999). Sparse sampling or clustered volume acquisition sequences capitalize on the delay of the HDR peak, which is about 3 to 5 seconds from stimulus onset for a single event (Glover, 1999). With this method, single tasks are performed while the scanner was transiently silent, approximating usual speaking conditions (Eden et al., 1999; Hall et al., 1999). The HDR function peaks at about 5 seconds (Friston, Jezzard, & Turner, 1994). Neuronal activity induces some auto-regulated signal that causes transient increases in rCBF. The resulting flow increases dilate the venous balloon increasing its volume and diluting venous

blood to decrease deoxyhemoglobin and follows the rCBF response with about a seconds delay (Friston, Mechelli, Turner, & Price, 2000).

The background scanner noise presents a continuous acoustic noise generated during conventional acquisition sequences that may introduce confounding effects on activation (Birn et al., 1998). Subject generated auditory feedback is a component of articulatory control that is difficult to assess during conventional acquisition sequences. Auditory activation (e.g., temporal lobe activity correlated with task or rate) found in the current study is unlikely to be caused by scanner noise because the BOLD HDR function peaks about 5 seconds after the onset of the auditory stimulus (Hulvershorn, Bloy, Gualtieri, Redmann, Leigh, et al., 2005). Our 5 second delay time following time following the acquisition (prior to task onset), supports the notion that activation of the transverse temporal gyrus (Heschl's gyrus) and of adjacent cortical areas is likely not due to the auditory processing of the participant's response.

fMRI assumptions & limitations

Assumptions are (1) BOLD signal is linear, (2) BOLD signal is stationary over time, and (3) noise is Gaussian and stationary over time. All of these assumptions are false. BOLD is nonlinear with inter-event intervals of less than 6 seconds. This nonlinearity can potentially interact with trial design to bias results. Thus we used 10 second intervals to ensure the complete evolution of the HDR. We used a sparse acquisition sequence with 10 second intervals to facilitate measurement of overt oromotor responses by allowing articulation to occur during brief periods of silence, reducing associated motion and susceptibility artifacts.

The concept of pure insertion, where subtraction of task versus baseline will reveal the one neural process that is different between two conditions, is an over-simplification of functional data analysis (Friston, Price, Fletcher, Moore, Frackowiak, et al., 1996). To avoid this assumption of pure insertion and consider that processes may interact in complex ways besides an additive linear fashion, we varied the task and rate of the ororhythmic performance to identify possible linear changes in activity, and performed a conjunction analysis where multiple subtractions of the different conditions to seek commonality in activation differences between paired tasks or paired rates (Price & Friston, 1997). A positive conjunction test implies that the region is commonly activated across the tasks.

In classical imaging statistics, one declares a voxel to be activated if its statistic exceeds some threshold. This statistic reflects the likelihood of the effect being truly present. The effect is inferred as present in a probabilistic sense and the effect is absent in some proportion of activated voxels. This relationship can be characterized by in terms of conditional probabilities, namely the specificity $1 - \alpha$ and sensitivity β and their complements false-positive and negative rates. The threshold is chosen to ensure the false-positive rate is small. Voxel-wise time series analysis results in thousands of multiple comparisons and an inflated type I (alpha) error in a family of related tests (i.e., all voxels of the dataset). The t-values of our *a priori* ROIs (listed in Table 3, p. 51) were often not high enough to "survive" Bonferroni nor FDR correction. For exploratory reasons, the statistical threshold was decreased resulting in 'uncorrected' statistical maps that are neither corrected with respect to the FDR nor Bonferroni techniques. The cutoff for reporting areas of activation is $p \leq 0.0005$, uncorrected for multiple comparisons. At this

level of significance it is expected that at least 0.05 % of voxels that are shown as significantly active are actually false positives.

Further improvements to MRI technology, experimental protocols, statistical analyses, and insightful modeling approaches will allow researchers to formulate more detailed hypotheses regarding central control. However, hypotheses formulated on the basis of fMRI experiments are unlikely to be analytically tested with fMRI itself in terms of neural mechanisms because when considering only hemodynamics, the actual state of an area and its participation in behavior is rather ambiguous (Logothetis, 2008). Multimodal research approaches supplementing functional imaging with electrophysiology and computational models provide a more comprehensive approach to interpreting the spatiotemporal BOLD signal, but also revealing the actual neuronal events that underlie the examined cognitive process. This requires a continuous interplay between human neuroimaging and animal studies at all levels of neurophysiological investigation (Bartels, Logothetis, & Moutoussis, 2008).

Future Applications

The ororhythmic behaviors investigated in the present investigation provide a reasonable starting point for future work at the systems neuroscience level for connectivity studies to address the integration and interaction among brain areas for task and rate. Whereas we addressed the task- and rate- specific correlates of specific speech and nonspeech ororhythmic tasks, future studies may address (1) task- and/or rate- specific connectivity, (2) other kinematic variables such as velocity or force of speech and/or nonspeech (e.g., mastication) task production, (3) replicate these results with larger sample sizes ($n > 10$) to increase statistical power to more appropriately test functional hypotheses and guide construction of a more comprehensive model of speech production.

Conclusion

This study is the first to show that specific speech (unvoiced syllabic /da/) and nonspeech (suck) ororhythmic behaviors are encoded by functionally overlapping cortical (bilateral sensoirmotor cortices, cingulate, insulae), subcortical (bilateral thalamus, basal ganglia, anterior cerebellar lobes), and brainstem (medulla) correlates. These results further support the notion of a distributed network of brain areas participating in the ongoing production of the speech task being generated by a subset of areas that also participate in the nonspeech behavior of suck in the healthy adult. Because there was a significant effect of ororhythmic rate (1 Hz or 3 Hz), we suggest that increased activation within the neural substrate for both tasks is correlated with either increased task complexity and/or potential error monitoring.

The minimal network revealed by the current study essential to encoding rate specific (1 Hz and 3 Hz) oromotor (suck and unvoiced /da/) tasks includes: cortical (bilateral precentral gyri, insula, cingulate), subcortical (bilateral basal ganglia, left cerebellum and thalamus), and brainstem (right dorsal pons, left medulla and pontomedullary regions) correlates. These findings are in agreement with other functional neuroimaging studies that describe a basic speech production network activated by producing simple syllable sequences to extend beyond the central sulcus to include medial premotor areas, frontal operculum, anterior insula, anterior thalamus, and cerebellum.

BIBLIOGRAPHY

Ackermann, H. (2008). Cerebellar contributions to speech production and speech perception: psycholinguistic and neurobiological perspectives. *Trends in Neurosciences, 31*, 265-272.

Ackermann, H., Mathiak, K., & Ivry, R.B. (2004). Temporal organization of "internal speech" as a basis for cerebellar modulation of cognitive functions. *Behavioral and Cognitive Neuroscience Reviews, 3*, 14-22.

Ackermann, H., Hertrich, I., & Hehr, T. (1995). Oral diadochokinesis in neurological dysarthrias. *Folia Phoniatrica Logopaedica, 47*, 15-23.

Ackermann, H., & Riecker, A. (2004). The contribution of the insula to motor aspects of speech production: a review and a hypothesis. *Brain and Language, 89*, 320-328.

Ackermann, H., Grönem, B.F., Hoch, G., & Schönle, P.W. (1993). Speech freezing in Parkinson's disease: a kinematic analysis of orofacial movements by means of electromagnetic articulography. *Folia Phoniatrica Logopaedica,45*, 84-89.

Ackermann, H., Riecker, A., Mathiak, K., Erb, M., Grodd, W., & Wildgruber, D. (2001). Rate-dependent activation of a prefrontal-insular-cerebellar network during passive listening to trains of click stimuli: an fMRI study. *NeuroReport, 12*, 4087-4092.

Ackermann, H., Mathiak, K., & Ricker, A. (2007). The contribution of the cerebellum to speech production and speech perception: clinical and functional imaging data. *Cerebellum, 6*, 202-213.

Alario, F-X., Chainay, H., Lehericy, S., & Cohen, L. (2006). The role of the supplementary motor area (SMA) in word production. *Brain Research, 1076*, 129-143.

Alexander, M.P., Naeser, M.A., & Palumbo, C. (1990). Broca's area aphasias: aphasia after lesions including the frontal operculum. *Neurology, 40*, 353-362.

Ballard, K. J., Robin, D. A., & Folkins, J. W. (2003). An integrative model of speech motor control: A response to Ziegler. *Aphasiology, 17,* 37–48.

Barch, D.M., Braver, T.S., Sabb, F.W., & Noll, D.C. (2000). Anterior cingulate and the monitoring of response conflict: evidence from an fMRI study of overt verb generation. *Journal of Cognitive Neuroscience, 12*, 298-309.

Barlow, S.M., & Estep, M. (2006). Central pattern generation and the motor infrastructure for suck, respiration, and speech. *Journal of Communication Disorders, 39*, 366-380.

Barlow, S.M., Lund, J.P., Estep, M., & Kolta, A. (2010). Central pattern generators for orofacial movements and speech. In S.M. Brudzynski (Ed.), *Handbook of Mammalian Vocalization. An Integrative Neuroscience Approach* (pp. 351-370). Oxford: Academic Press.

Bartels, A., Logothetis, N.K., & Moutoussis, K. (2008). fMRI and its interpretations: an illustration on directional selectivity in area V5/MT. *Trends in Neurosciences, 31*, 444-453.

Bengtsson, S.L., Ehrsson, H.H., Forssberg, H., & Ullen, F. (2005). Effector-independent voluntary timing: Behavioral and neuroimaging evidence. *European Journal of Neuroscience, 22*, 3255-3265.

Bense, S., Janusch, B., Vucurevic, G., Bauermann, T., Schlindwein, P., Brandt, T., et al. (2006). Brainstem and cerebellar fMRI-activation during horizontal and vertical optokinetic stimulation. *Experimental Brain Research, 174*, 312-323.

Birn, R.M., Bandettini, P.A., Cox, R.W., Jesmanowicz, A., & Shaker, R. (1998). Magnetic field changes in the human brain due to swallowing or speaking. *Magnetic Resonance in Medicine, 40*, 55-60.

Birn, R.M., Bandettini, P.A., Cox, R.W., & Shaker, R. (1999). Event-related fMRI of tasks involving brief motion. *Human Brain Mapping, 7*, 106-114.

Birn, R.M., Cox, R.W., & Bandettini, P.A. (2004). Experimental designs and processing strategies for fMRI studies involving overt verbal responses. *NeuroImage, 23*, 1046-1058.

Boecker, H., Dagher, A., Ceballos-Baumann, A.O., Passingham, R.E., Samuel, M., Friston, K.J., et al. (1998). Role of the human rostral supplementary motor area and the basal ganglia in motor sequence control: investigations with H2 15O PET. *Journal of Neurophysiology, 79*, 1070-1080.

Bohland, J.W., & Guenther, F.H. (2006). An fMRI investigation of syllable sequence production. *NeuroImage, 32*, 821-841.

Bonilha, L., Moser, D., Rorden, C., Baylis, G.C., & Fridriksson, J. (2006). Speech apraxia without oral apraxia: can normal brain function explain the physiopathology? *NeuroReport, 17*, 1027-1031.

Botvinik, M.M., Braver, D.M., Barch, C.S., Carter, J.D., & Cohen, J.D. (2001). Conflict monitoring and cognitive control. *Psychological Review, 108*, 624-652.

Brown, S., Martinez, M.J., Hodges, D.A., Fox, P.T., & Parsons, L.M. (2004). The song system of the human brain. *Brain Research. Cognitive Brain Research, 20*, 363-375.

Buchel, C., & Friston, K. (2001). Interactions among neuronal systems assessed with functional neuroimaging. *Revue Neurologique, 157*, 807-815.

Burnett, T.A., Freedland, M.B., Larson, C.R., & Hain, T.C. (1998). Voice F0 responses to manipulations in pitch feedback. *The Journal of the Acoustical Society of America, 103*, 3153-3161.

Caligiuri, M.P. (1987). Labial kinematics during speech in patients with Parkinsonian rigidity. *Brain, 110*, 1033-1044.

Carter, C.S., Braver, T.S., Barch, D.M., Botvinick, M.M., Noll, D., & Cohen, J.D. (1998). Anterior cingulated cortex, error detection, and online monitoring of performance. *Science, 280*, 747-749.

Chandler, S.H., & Tal, M. (1986). The effects of brain stem transections on the neuronal networks responsible for rhythmical jaw muscle activity in the guinea pig. *The Journal of Neuroscience, 6*, 1831-1842.

Chawla, D., Rees, G., & Friston, K.J. (1999). The physiological basis of attentioanl modulation in extrastriate visual areas. *Nature Neuroscience, 2*, 671-676.

Chong, T.J., Cunnington, R., Williams, M.A., Kanwisher, N., & Mattingley. (2008). fMRI adaptation reveals mirror neurons in human inferior parietal cortex. *Current Biology, 18*, 1576-1580.

Christoffels, I.K., Formisano, E., & Schiller, N.O. (2007). Neural correlates of verbal feedback processing: An fMRI study employing overt speech. *Human Brain Mapping, 28*, 868-879.

Ciucci, M.R., Barkmeier-Kraemer, J.M., & Sherman, S.J. (2008). Subthalamic nucleus deep brain stimulation improves deglutition in Parkinson's disease. *Movement Disorders, 23*, 676-683.

Clark, H.M. (2003). Neuromuscular treatments for speech and swallowing: a tutorial. *American Journal of Speech-Language Pathology, 12*, 400-415.

Corfield, D.R., Murphy, K., Josephs, O., Fink, G.R., Frackowiak, R.S., Guz, A., et al. (1999). Cortical and subcortical control of tongue movements in humans: a functional neuroimaging study using fMRI. *Journal of Applied Physiology, 86*, 1468-1477.

Decety, J., & Grezes, J. (1991). Neural mechanisms subserving the perception of human actions. *Trends in Cognitive Sciences, 3*, 172-178.

Desmond, J.E., & Glover, G.H. (2002). Estimating sample size in functional MRI (fMRI) neuroimaging studies: statistical power analyses. *Journal of Neuroscience Methods, 118*, 115-128.

Donnan, G.A., Carey, L.M., & Saling, M.M. (1999). More (or less) on Broca. *Lancet, 353*(9158), 1031-1032.

Dresel, C., Castrop, F., Haslinger, B., Wohlschlaeger, A.M., Hennenlotter, A., & Ceballos-Baumann, A.O. (2005). The functional neuroanatomy of coordinated orofacial movements: Sparse sampling fMRI of whistling. *NeuroImage, 28*, 588-597.

Drew, T. (1993). Motor cortical activity during voluntary gait modifications in the cat. I. Cells related to the forelimbs. *Journal of Neurophysiology, 70*, 179-199.

Drew, T., Prentice, S., & Schepens, B. (2004). Cortical and brainstem control of locomotion. *Progress in Brain Research, 143*, 251-261.

Dronkers, N.F. (1996). A new brain region for coordinating speech articulation. *Nature, 384*, 159-161.

Duffy, J.R. (2005). *Motor speech disorders: Substrates, differential diagnosis, and management.* Edited by K. Falk, and C. Hart. Elsevier Health Sciences.

Dworkin, J.P., Abkarian, G.G., & Johns, D.F. (1988). Apraxia of speech: the effectiveness of a treatment regimen. *The Journal of Speech and Hearing Disorders, 53*, 280-294.

Eden, G.F., Joseph, J.E., Brown, H.E., Brown, C.P., & Zeffiro, T.A. (1999). Utilizing hemodynamic delay and dispersion to detect fMRI signal change without auditory interference: the behavior interleaved gradients technique. *Magnetic Resonance in Medicine, 41*, 13-20.

Edmister, W.B., Talavage, T.M., Ledden, P.J., & Weisskoff, R.M. (1999). Improved auditory cortex imaging using clustered volume acquisitions. *Human Brain Mapping, 7*, 89-97.

Estep, M., & Barlow, S.M. (2007). Modulation of the trigeminofacial pathway during syllabic speech. *Brain Research, 1171*, 67-74.

Fay, R.A., & Norgren, R. (1997a). Identification of rat brainstem multisynaptic connections to the oral motor nuclei using pseudorabies virus. I. Masticatory muscle motor systems. *Brain Research. Brain Research Reviews, 25*, 255-275.

Fay, R.A., & Norgren, R. (1997b). Identification of rat brainstem multisynaptic connections to the oral motor nuclei using pseudorabies virus. II. Facial muscle motor systems. *Brain Research. Brain Research Reviews, 25*, 276-290.

Fay, R.A., & Norgren, R. (1997c). Identification of rat brainstem multisynaptic connections to the oral motor nuclei using pseudorabies virus. III. Lingual muscle motor systems. *Brain Research. Brain Research Reviews, 25*, 291-311.

Foki, T., Geissler, A., Gartus, A., Pahs, G., Deecke, L., & Beisteiner, R. (2007). Cortical lateralization of bilateral symmetric chin movements and clinical relevance in tumor patients – a high field BOLD-fMRI study. *NeuroImage, 37*, 26-39.

Folkins, J.W., Moon, J.B., Luschei, E.S., Robin, D.A., Tye-Murray, N., & Moll, K.L. (1995). What can nonspeech tasks tell us about speech motor disabilities? *Journal of Phonetics, 23,* 139-147.

Forrest, K., Weismer, G., & Turner, G.S. (1989). Kinematic, acoustic, and perceptual analyses of connected speech produced by Parkinsonian and normal geriatric adults. *Journal of the Acoustical Society of America, 85,* 2608-2622.

Frackowiak, R.S., Friston, K.J., Frith, C.D., Dolan, R.J., & Mazziotta, J.C. (1997). *Human brain function.* San Diego: Academic Press.

Friston, K.J., Jezzard, P.J., & Turner, R. (1994). Analysis of functional MRI time-series. *Human Brain Mapping, 1*, 153-171.

Friston, K.J., Mechelli, A., Turner, R., & Price, C.J. (2000). Nonlinear responses in fMRI: the Balloon Model, Volterra kernels, and other hemodynamics. *NeuroImage, 12*, 466-477.

Friston, K.J., Penny, W.D., & Glaser, D.E. (2005). Conjunction revisited. *NeuroImage, 25*, 661-667.

Friston, K.J., Price, C.J., Fletcher, P., Moore, C., Frackowiak, R.S., & Dolan, R.J. (1996). The trouble with cognitive subtraction. *NeuroImage, 4*, 97-104.

Fu, C.H.Y., Morgan, K., Suckling, J., Williams, S.C.R., Andrew, C., Vythelingum, G.N., et al. (2002). A functional magnetic resonance imaging study of overt letter verbal fluency using a

clustered acquisition sequence: greater anterior cingulate activation with increased task demand. *NeuroImage, 17*, 871-879.

Galati, G., Committeri, G., Spitoni, G., Aprile, T., Di Russo, R., Pitzalis, S., et al. (2008). A selective representation of the meaning of actions in the auditory mirror system. *NeuroImage, 40*, 1274-1286.

Garraux, G., McKinney, C., Wu, T., Kansaku, K., Nolte, G., & Hallett, M. (2005). Shared brain areas but not functional connections controlling movement timing and order. *The Journal of Neuroscience, 25*, 5290-5297.

Ganushchak, L.Y., & Schiller, N.O. (2006). Effects of time pressure on verbal self-monitoring: an ERP study. *Brain Research, 1125*, 104-115.

Gentil, M. (1990). Dysarthria in Friedreich disease. *Brain and Language, 38*, 438-448.

Gerhring, W.J., & Knight, R.T. (2000). Prefrontal-cingulate interactions in action monitoring. *Nature Neuroscience, 3*, 516-520.

Gil-da-Costa, R., Braun, A., Lopes, M., Hauser, M.D., Carson, R.E., Herscovitch, P., & Martin, A. (2004). Toward an evolutionary perspective on conceptual representation: species-specific calls activate visual and affective processing systems in the macaque. *Proceedings of the National Academy of Sciences of the United States of America, 101*, 17516-17521.

Glover, G.H. (1999). Deconvolution of impulse response in event-related BOLD fMRI. *NeuroImage, 9*, 416-429.

Gracco, V.L., Tremblay, P., & Pike, B. (2005). Imaging speech production using fMRI. *NeuroImage, 26*, 294-301.

Grafton, S.T., & Hamilton, A.F. (2007). Evidence for a distributed hierarchy of action representation in the brain. *Human Movement Science, 26*, 590-616.

Greicius, M.D., Supekar, K., Menon, V., & Dougherty, R.F. (2008). Resting-state functional connectivity reflects structural connectivity in the default mode network. *Cerebral Cortex, 19*, 72-78.

Grillner, S. (1981). Control of locomotion in bipeds, tetrapods, and fish. In V.B. Brooks (Ed.), *Handbook of physiology* (pp. 1179-1236). Bethesda, MD: American Physiological Society.

Grillner, S. (1991). Recombination of motor pattern generators. *Current Biology, 1*, 231-233.

Grillner, S., Georgopoulos, A.P., & Jordan, L. (1997). Selection and initiation of motor behavior. In: P.S.G. Stein, S. Grillner, A.I. Selverston, and D.G. Stuart, (Eds.), *Neurons, networks, and motor behavior* (pp. 3-19). Cambridge: MIT Press.

Grillner, S., Hellgren, J., Menard, A., Saitoh, K., & Wikstrom, M.A. (2005). Mechanisms for selection of basic motor programs – roles for the striatum and pallidum. *Trends in Neurosciences, 28*, 364-370.

Grillner, S., & Wallen, P. (2004). Innate versus learned movements – a false dichotomy? *Progress in Brain Research, 143*, 3-12.

Grodd, W., Hulsmann, E., Lotze, M., Wildgruber, D., & Erb, M. (2001). Sensorimotor mapping of the human cerebellum: fMRI evidence of somatotopic organization. *Human Brain Mapping, 13*, 55-73.

Guenther, F.H. (2006). Cortical interactions underlying the production of speech sounds. *Journal of Communication Disorders, 39*, 350-365.

Guenther, F.H., Ghosh, S.S., & Tourville, J.A. (2006). Neural modeling and imaging of the cortical interactions underlying syllable production. *Brain and Language, 96*, 280-301.

Hage, S.R., & Jurgens, U. (2006). On the role of the pontine brainstem in vocal pattern generation: a telemetric single-unit recording study in the squirrel monkey. *Journal of Neuroscience, 26*, 7105-7115.

Hageman, C.F., Robin, D.A., Moon, J.B., & Fokins, J.W. (1994). Oral motor tracking in normal and apraxic speakers. *Clinical Aphasiology, 22,* 219-229.

Hall, D.A., Haggard, M.P., Akeroyd, M.A., Palmer, A.R., Summerfield, A.Q., Elliott, M.R., et al. (1999). "Sparse" temporal sampling in auditory fMRI. *Human Brain Mapping, 7*, 213-223.

Halpern, A.R. & Zatorre, R.J. (1999). When the tune runs through your head: a PET investigation of auditory imagery for familiar melodies. *Cerebral Cortex, 9*, 697-704.

Hamdy, S., Xue, S., Valdez, D., & Diamant, N.E. (2001). Induction of cortical swallowing activity by transcranial magnetic stimulation in the anaesthetized cat. *Neurogastroenterology and Motility, 13*, 65-72.

Hanakawa, T., Parikh, S., Bruno, M.K., & Hallett, M. (2005). Finger and face representations in the ipsilateral precentral motor areas in humans. *Journal of Neurophysiology, 93*, 2950-2958.

Handwerker, D.A., Ollinger, J.M., & D'Esposito, M. (2004). Variation of BOLD hemodynamic responses across subjects and brain regions and their effects on statistical analyses. *NeuroImage, 21*, 1639-1651.

Hartsuiker, R.J., & Kolk, H.H.J. (2001). Error monitoring in speech production: a computation test of the perceptual loop theory. *Cognitive Psychology, 42*, 113-157.

Haughton, V., & Biswal, B. (1998). Clinical application of basal regional cerebral blood flow fluctuation measurements by fMRI. *Advances in Experimental Medicine and Biology, 454,* 583-590.

Herholz, K., Thiel, A., Wienhard, K., Pietrzyk, U., von Stockhausen, H.M., Karbe, H., et al. (1996). Individual functional anatomy of verb generation. *NeuroImage, 3*, 185-194.

Hesselmann, V., Sorger, B., Lasek, K., Guntinas-Lichius, O., Krug, B., Sturm, V., et al. (2004). Discriminating the cortical representation sites of tongue and lip movement by functional MRI. *Brain Topography, 16*, 159-167.

Hickok, G. (2001). Functional anatomy of speech perception and speech production: psycholinguistic implications. *Journal of Psycholinguistic Research, 30*, 225-235.

Hidaka, O., Morimoto, T., Masuda, Y., Kato, T., Matsuo, R., Inoue, T., et al. (1997). Regulation of masticatory force during cortially induced rhythmic jaw movements in the anesthetized rabbit. *Journal of Neurophysiology, 77*, 3168-3179.

Hikosaka, O. (2007). GABAergic output of the basal ganglia. *Progress in Brain Research, 160*, 209-226.

Hirano, S., Kojima, H., Naito, Y., Honjo, I., Kamoto, Y., Okazawa, H., et al. (1997). Cortical processing mechanism for vocalization with auditory verbal feedback. *NeuroReport, 8*, 2379-2382.

Holroyd, C.B., & Coles, M.G.H. (2002). The neural basis of human error processing: reinforcement learing, dopamine and the error-related-negativity. *Psychological Review, 109*, 679-709.

Hooper, S.L., & Moulins, M. (1989). Switching of a neuron from one network to another by sensory-induced changes in membrane properties. *Science, 244*, 1587-1589.

Hoshiyama, M., Gunji, A., & Kakigi, R. (2001). Hearing the sound of silence: a magnetoencephalographic study. *NeuroReport, 12*, 1097-1102.

Hulvershorn, J., Bloy, L., Gualtieri, E., Redmann, C., Leigh, J., & Elliott, M.. (2005). Temporal resolving power of spin echo and gradient echo fMRI at 3T with apparent diffusion coefficient compartmentalization. *Human Brain Mapping, 25*, 247-258.

Hunter, M.D., Eickhoff, S.B., Miller, T.W.R., Farrow, T.F.D., Wilkinson, I.D., & Woodruff, W.R. (2006). Neural activity in speech-sensitive auditory cortex during silence. *Proceedings of the National Academy of Sciences of the United States of America, 103*, 189-194.

Hwang, E.J., & Shadmehr, R. (2005). Internal models of limb dynamics and the encoding of limb state. *Journal of Neural Engineering, 2*, S266-S278.

Indefrey, P., & Levelt, W.J.M. (2004). The spatial and temporal signatures of word production components. *Cognition, 92*, 101-144.

Iriki, A., Nozaki, S., & Nakamura, Y. (1988). Feeding behavior in mammals: corticobulbar projection is reorganized during conversion from sucking to chewing. *Brain Research. Developmental Brain Research, 44*, 189-196.

Islam, S.S., Zelenin, P.V., Orlovsky, G.N., Grillner, S., & Deliagina, T.G. (2006). Pattern of motor coordination underlying backward swimming in the lamprey. *Journal of Neurophysiology, 96*, 451-460.

Janczewski, W.A., & Karczewski, W.A. (1984). Respiratory effects of pontine, medullary and spinal cord midline sections in the rabbit. *Respiration Physiology, 57*, 293-305.

Johnson, M.T., & Ebner, T.J. (2000). Processing of multiple kinematic signals in the cerebellum and motor cortices. *Brain Research Reviews, 33*, 155-168.

Johnson-Frey, S.H., Newman-Norlund, R., & Grafton, S.T. (2005). A distributed left hemisphere network active during planning of everyday tool use skills. *Cerebral Cortex, 15*, 681-695.

Jones, J.A., & Munhall, K.G. (2000). Perceptual calibration of F0 production: evidence from feedback perturbation. *The Journal of the Acoustical Society of America, 108*, 1246-1251.

Jurgens, U. (2002). Neural pathways underlying vocal control. *Neuroscience and Biobehavioral Reviews, 26*, 235-258.

Kastner, S. & Ungerleider, L.G. (2000). Mechanisms of visual attention in the human cortex. *Annual Review of Neuroscience, 23*, 315-341.

Kelso, J.A.S., & Tuller, B. (1983). Compensatory articulation: under reduced conditions of afferent information: a dynamic formulation. *Journal of Speech and Hearing Research, 26,* 217-224.

Kent, R.D., Duffy, J.R., Slama, A., Kent, J.F., & Clift, A. (2001). Clinicoanatomic studies in dysarthria: review, critique, and directions for research. *Journal of Speech, Language, and Hearing Research, 44*, 535-551.

Kent, R.D., Mitchell, P.R., & Sancier, M. (1991). Evidence and role of rhythmic organization in early vocal development in human infants. In J. Fagard and P. Wolff (Eds.), *The development of timing control and temporal organization in coordinated action* (pp. 135-149). Amsterdam: Elsevier.

Kiehl, K.A., Liddle, P.F., & Hopfinger, J.B. (2000). Error processing and the rostral anterior cingulated: An event-related fMRI study. *Psychophysiology, 37*, 216-223.

Kimura, D., & Watson, N. (1989). The relation between oral movement control and speech. *Brain and Language, 37*, 565-590.

Kirzinger, A., & Jurgens, U. (1991). Vocalization-correlated single-unit activity in the brain stem of the squirrel monkey. *Experimental Brain Research, 84*, 545-560.

Koizumi, H., Nomura, K., Yokota, Y., Enomoto, A., Yamanishi, T., Iida, S., Ishihama, K., & Kogo, M. (2009). Regulation of trigeminal respiratory motor activity in the brainstem. *Journal of Dental Research, 88I, 1048-1053.*

Kolta, A., Westberg, K.G., & Lund, J.P. (2000). Identification of brainstem interneurons projecting to the trigeminal motor nucleus and adjacent structures in the rabbit. *Journal of Chemical Neuroanatomy, 19*, 175-195.

Komisaruk, B.R., Mosier, K.M., Liu, W., Criminale, C., Zaborszky, L., Whipple, B., et al. (2002). Functional localization of brainstem and cervical spinal cord nuclei in humans with fMRI. *American Journal of Neuroradiology, 23*, 609-617.

Kraemer, D.J., Macrae, C.N., Green, A.E., & Kelley, W.M. (2005). Musical imagery: sound of silence activates auditory cortex. *Nature, 434*, 158.

Kubina, B., Ristic, D., Weber, J., Stracke, C.P., Forster, C., & Ellrich, J. (2009). Bilateral brainstem activation by thermal stimulation of the face in healthy volunteers. *Journal of Neurology* [epub ahead of print]. DOI: 10.1007/s00415-009-5307-z

Kuriki, S., Mori, T., & Hirata, Y. (1999). Motor planning center for speech articulation in the normal human brain. *NeuroReport, 10*, 765-769.

Kuypers, H.G.J.M. (1958). Corticobulbar connections to the pons and lower brain-stem in man: an anatomical study. *Brain, 81*, 364-388.

Langers, D.R., van Dijk, P., & Backes, W.H. (2005). Lateralization, connectivity and plasticity in the human central auditory system. *NeuroImage, 28*, 490-499.

Levelt, W.J.M. (1989). *Speaking: from intention to articulation.* Cambridge, MA: MIT Press.

Levelt, W.J. M. (2001). Spoken word production: a theory of lexical access. *Proceedings of the National Academy of Sciences of the United States of America, 98*, 13464-13471.

Li, Y.Q., Takada, M., Kaneko, T., & Mizuno, N. (1996). GABAergic and glycinergic neurons projecting to the trigeminal motor nucleus: a double labeling study in the rat. *The Journal of Comparative Neurology, 373*, 498-510.

Liberman, A.M. (1996). *Speech: A special code.* Cambridge, MA: MIT Press.

Lo, Y.L., & Ratnagopal, P. (2007). Cortico-hypoglossal and corticospinal conduction abnormality in Bickerstaff's brainstem encephalitis. *Clinical Neurology and Neurosurgery, 109*, 523-525.

Logothetis, N.K. (2008). What we can do and what we cannot do with fMRI. *Nature, 453*, 869-878.

Logothetis, N.K., Murayama, Y., Augath, M., Steffen, T., Werner, J., & Oeltermann, A. (2009). How not to study spontaneous activity. *NeuroImage, 45*, 1080-1089.

Lotze, M., Seggewies, G., Erb, M., Grodd, W., & Birbaumer, N. (2000). The representation of articulation in the primary sensorimotor cortex. *NeuroReport, 11*, 2985-2989.

Lowe, M.J., Dzemidzic, M., Lurito, J.T., Mathews, V.P., & Phillips, M.D. (2000). Correlations in low-frequency BOLD fluctuations reflect cortico-cortical connections. *NeuroImage, 12*, 582-587.

Ludlow, C.L., Connor, N.P., & Bassich, C.J. (1987). Speech timing in Parkinson's and Huntington's disease. *Brain and Language, 32*, 195-214.

Ludlow, C.L., Hoit, J., Kent, R., Ramig, L.O., Shrivastav, R., Strand, E., et al. (2008). Translating principles of neural plasticity into research on speech motor control recovery and rehabilitation. *Journal of Speech Language and Hearing Research, 51*, S240-S258.

Lund, J.P., & Kolta, A. (2006a). Brainstem circuits that control mastication: do they have anything to say during speech? *Journal of Communication Disorders, 39*, 381-390.

Lund, J.P., & Kolta, A. (2006b). Generation of the central masticatory pattern and its modification by sensory feedback. *Dysphagia, 21*, 167-174.

Maillard, L., Ishii, K., Bushara, K., Waldvogel, D., Schulman, A.E., & Hallett, M. (2000). *Neurology, 55*, 377-383.

Mainero, C., Zhang, W.T., Kumar, A., Rosen, B.R., & Sorensen, A.G. (2007). Mapping the spinal and supraspinal pathways of dynamic mechanical allodynia in the human trigeminal system using cardiac-gated fMRI. *NeuroImage, 35*, 1201-1210.

Masaki, H., Tanaka, H., Takasawa, N., & Yamazaki, K. (2001). Error-related brain potentials elicited by vocal errors. *NeuroReport, 12*, 1851-1855.

McAuliffe, M.J., Ward, E.C., Murdoch, B.E., & Farrell, A.M. (2005). A nonspeech investigation of tongue function in Parkinson's disease. *The Journals of Gerontology, Series A, Biological Sciences and Medical Sciences, 60*, 667-674.

McGuigan, F.J., & Winstead, C.L. (1974). Discriminative relationship between covert oral behavior and the phonemic system in internal information processing. *Journal of Experimental Psychology, 103,* 885-890.

McGuire, P.K., Silbersweig, D.A., Murray, R.M., David, A.S., Frackowiak, R.S., & Frith, C.D. (1996). Functional anatomy of inner speech and auditory verbal imagery. *Psychological Medicine, 26*, 29-38.

McIntosh, A.R., Rajah, M.N., & Lobaugh, N.J. (2003). Functional connectivity of the medial temporal lobe relates to learning and awareness. *The Journal of Neuroscience, 23*, 6520-6528.

McKay, L.C., Adams, L., Frackowiak, R.S., & Corfield, D.R. (2008). A bilateral cortico-bulbar network associated with breath holding in humans, determined by functional magnetic resonance imaging. *NeuroImage, 40*, 1824-1832.

McNeil, M.R., & Kent, R.D. (1990). Motoric characteristics of adult aphasic and apraxic speakers. In G.E. Hammond (Ed.), *Cerebral control of speech and limb movements* (pp. 349-386). Amsterdam: Elsevier Science Publishers.

Menard, A. & Grillner, S. (2008). Diencephalic locomotor region in the lamprey – afferents and efferent control. *Journal of Neurophysiology, 100*, 1343-1353.

Menard, A., Auclair, F., Bourcier-Lucas, C., Grillner, S., & Dubuc, R. (2007). Descending GABAergic projections to the mesencephalic locomotor region in the lamprey Petromyzon marinus. *The Journal of Comparative Neurology, 501*, 260-273.

Mentel, T., Cangiano, L., Grillner, S., & Buschges, A. (2008). Neuronal substrates for state-dependent changes in coordination between motoneuron pools during fictive locomotion in the lamprey spinal cord. *The Journal of Neuroscience, 28*, 868-879.

Mentel, T., Krause, A., Pabst, M., El Manira, A., & Buschges, A. (2006). Activity of fin muscles and fin motoneurons during swimming motor pattern in the lamprey. *The European Journal of Neuroscience, 23*, 2012-2026.

Meyrand, P., Simmers, J., & Moulins, M. (1991). Construction of a pattern-generating circuit with neurons of different networks. *Nature, 351*, 60-63.

Meyrand, P., Simmers, J., & Moulins, M. (1994). Dynamic construction of a neural network from multiple pattern generators in the lobster stomatogastric nervous system. *The Journal of Neuroscience, 14*, 630-644.

Middleton, F.A., & Strick, P.L. (2000). Basal ganglia and cerebellar loops: motor and cognitive circuits. *Brain Research Reviews, 31*, 236-250.

Mink, J.W. (1996). The basal ganglia: focused selection and inhibition of competing motor programs. *Progress in Neurobiology, 50*, 381-425.

Moore, C.A., Smith, A., & Ringel, R.L. (1988). Task-specific organization of activity in human jaw muscles. *Journal of Speech and Hearing Research, 31*, 670-680.

Morecraft, R.J., Stilwell-Morecraft, K.S., & Rossing, W.R. (2004). The motor cortex and facial expression: new insights from neuroscience. *The Neurologist, 10*, 235-249.

Muellbacher, W., Artner, C., & Mamoli, B. (1999). The role of the intact hemisphere in recovery of midline muscles after recent monohemispheric stroke. *Journal of Neurology, 246*, 250-256.

Muller, R.A., Rothermel, R.D., Behen, M.E., Muzik, O., Mangner, T.J., & Chugani, H.T. (1997). Receptive and expressive language activations for sentences: a PET study. *NeuroReport, 8*, 3767-3770.

Munhall, K.G. (2001). Functional imaging during speech production. *Acta Psychologica, 107*, 95-117.

Murphy, K., Corfield, D.R., Guz, A., Fink, G.R., Wise, R.J., Harrison, J., et al. (1997). Cerebral areas associated with motor control of speech in humans. *Journal of Applied Physiology, 83*, 1438-1447.

Nakamura, Y., & Katakura, N. (1995). Generation of masticatory rhythm in the brainstem. *Neuroscience Research, 23*, 1-19.

Nakamura, S., Muramatsu, S., & Yoshida, M. (1990). Role of the basal ganglia in manifestation of rhythmical jaw movements in rats. *Brain Research, 535*, 335-338.

Nakano, K. (2000). Neural circuits and topographic organization of the basal ganglia and related regions. *Brain and Development, 22*, S5-S16

Nambu, A., Tokuno, H., & Takada, M. (2002). Functional significance of the cortico-subthalamo-pallidal 'hyperdirect' pathway. *Neuroscience Research, 43*, 111-117.

Nestor, P.J., Graham, N.L., Fryer, T.D., Williams, G.B., Patterson, K., & Hodges, J.R. (2003). Progressive non-fluent aphasia is associated with hypometabolism centered on the left anterior insula. *Brain 126*, 2406-2418.

Nozaki, S., Iriki, A., & Nakamura, Y. (1986). Role of corticobulbar projection neurons in cortically induced rhythmical masticatory jaw-opening movement in the guinea pig. *Journal of Neurophysiology, 55*, 826-845.

Nozaki, S., Iriki, A., & Nakamura, Y. (1993). Trigeminal premotor neurons in the bulbar parvocellular reticular formation participating in induction of rhythmical activity of trigeminal motoneurons by repetitive stimulation of the cerebral cortex in the guinea pig. *Journal of Neurophysiology, 69*, 595-608.

Obermann, M., Pleger, B., de Greiff, A., Stude, P., Kaube, H., Diener, H.C., et al. (2009). Temporal summation of trigeminal pain in human anterior cingulate cortex. *NeuroImage, 46*, 193-200.

Onozuka, M., Fujita, M., Watanabe, K., Hirano, Y., Niwa, M., Nishiyama, K., et al. (2002). Mapping brain region activity during chewing: a functional magnetic resonance imaging study. *Journal of Dental Research, 81*, 743-746.

Ostry, D.J., & Munhall, K.G. (1994). Control of jaw orientation and position in mastication and speech. *Journal of Neurophysiology, 71*, 1528-1545.

Ozdemir, E., Norton, A., & Schlaug, G. (2006). Shared and distinct neural correlates of singing and speaking. *NeuroImage, 33*, 628-635.

Paradiso, G., Cunic, D., Saint-Cyr, J.A., Hoque, T., Lozano, A.M., Lang, A.E., et al. (2004). Involvement of human thalamus in the preparation of self-paced movement. *Brain, 127*, 2717-2731.

Paxinos, G., & Huang, X-F. (1995). *Atlas of the human brainstem*. San Diego, CA: Academic Press.

Pickett, E.R., Kunihom, E., Protopapas, A., Friedman, J., & Liedberman, P. (1998). Selective speech motor, syntax and cognitive deficits associated with bilateral damage to the putamen and the head of the caudate nucleus: A case study. *Neuropsychologia, 36*, 173-188.

Pope, P., Wing, A.M., Praamstra, P., & Miall, R.C. (2005). Force related activations in rhythmic sequence production. *NeuroImage, 27*, 909-918.

Poremba, A., Malloy, M., Saunders, R.C., Carson, R.E., Herscovitch, P., & Mishkin, M. (2004). Species-specific calls evoke asymmetric activity in the monkey's temporal poles. *Nature, 427*, 448-451.

Price, C.J., & Friston, K.J. (1997). Cognitive conjunction: A new approach to brain activation experiments. *NeuroImage, 5,* 261-270.

Price, C.J., Wise, R.J., & Frackowiak, R.S. (1996). Demonstrating the implicit processing of visually presented words and pseudowords. *Cerebral Cortex, 6*, 62-70.

Ray, J. (2003). Effects of orofacial myofunctional therapy on speech intelligibility in individuals with persistent articulatory impairments. *The International Journal of Orofacial Myology, 29,* 5-14.

Ricci, M., Magarelli, M., Todino, V., Bianchini, A., Calandriello, E., & Tramutoli, R. (2008). Progressive apraxia of speech presenting as isolated disorder of speech articulation and prosody: a case report. *Neurocase, 14*, 162-168.

Riecker, A., Ackermann, H., Wildgruber, D., Meyer, J., Dogil, G., Haider, H., et al. (2000). Articulatory/phonetic sequencing at the level of the anterior perisylvian cortex: a functional magnetic resonance imaging (fMRI) study. *Brain and Language, 75*, 259-276.

Riecker, A., Brendel, B., Ziegler, W., Erb, M., & Ackermann, H. (2008). The influence of syllable onset complexity and syllable frequency on speech motor control. *Brain and Language, 107*, 102-113.

Riecker, A., Kassubek, J., Groschel, K., Grodd, W., & Ackermann, H. (2006). The cerebral control of speech tempo: opposite relationship between speaking rate and BOLD signal changes at striatal and cerebellar structures. *NeuroImage, 29*, 46-53.

Riecker, A., Wildgruber, D., Dogil, G., Grodd, W., & Ackermann, H. (2002). Hemispheric lateralization effects of rhythm implementation during syllable repetitions: an fMRI study. *NeuroImage, 16*, 169-176.

Riecker, A., Mathiak, K., Wildgruber, D., Erb, M., Hertrich, I., Grodd, W., et al. (2005). fMRI reveals two distinct cerebral networks subserving speech motor control. *Neurology, 64*, 700-706.

Rimol, L.M., Specht, K., Weis, S., Savoy, R., & Hugdahl, K. (2005). Processing of sub-syllabic speech units in the posterior temporal lobe: An fMRI study. *NeuroImage, 26*, 1059-1067.

Rocca, M.A., Gatti, R., Agosta, F., Tortorella, P., Riboldi, E., Broglia, P., et al. (2007). Influence of body segment position during in-phase and antiphase hand and foot movements: a kinematic and functional MRI study. *Human Brain Mapping, 28*, 218-227.

Saitoh, K., Menard, A., & Grillner, S. (2007). Tectal control of locomotion, steering, and eye movements in lamprey. *Journal of Neurophysiology, 97*, 3093-3108.

Sakamoto, K., Nakata, H., Honda, Y., & Kakigi, R. (2009). The effect of mastication on human motor preparation processing: a study with CNV and MRCP. *Neuroscience Research, 64*, 259-266.

Salmelin, R., Hari, R., Lounasmaa, O.V., & Sams, M. (1994). Dynamics of brain activation during picture naming. *Nature, 368*, 463-465.

Salmelin, R., & Sams, M. (2002). Motor cortex involvement during verbal versus non-verbal lip and tongue movements. *Human Brain Mapping, 16*, 81-91.

Schaal, S., Sternad, D., Osu, R., & Kawato, M. (2004). Rhythmic arm movement is not discrete. *Nature Neuroscience, 7*, 1136-1143.

Schiller, N.O. (2005). Verbal self-monitoring. In A. Cutler (Ed.), *Twenty-first century psycholinguistics: Four cornerstones* (pp. 245-261). Hillsdale, NJ: Lawrence Erlbaum Associates.

Schroeder, C. & Foxe, J. (2005). Multisensory contributions to low-level 'unisensory' processing. *Current Opinion in Neurobiology, 15*, 454-458.

Shuster, L.I., & Lemieux, S.K. (2005). An fMRI investigation of covertly and overtly produced mono- and multisyllabic words. *Brain and Language, 93*, 20-31.

Sigalovsky, I.S., & Melcher, J.R. (2006). Effects of sound level of fMRI activation in human brainstem, thalamic and cortical centers. *Hearing Research, 215*, 67-76.

Simonyan, K., Ludlow, C.L., & Vortmeyer, A.O. (2009). Brainstem pathology in spasmodic dysphonia. *The Laryngoscope* [epub ahead of print] DOI: 10.1002/lary.20677

Solomon, N.P., Robin, D.A., & Luschei, E.S. (2000). Strength, endurance, and stability of the tongue and hand in Parkinson disease. *Journal of Speech Language and Hearing Research, 43*, 256-267.

Soros, P., Sokoloff, L.G., Bose, A., McIntosh, A.R., Graham, S.J., & Stuss, D.T. (2006). Clustered functional MRI of overt speech production. *NeuroImage, 32*, 376-387.

Spencer, K.A., & Rogers, M.A. (2005). Speech motor programming in hypokinetic and ataxic dysarthria. *Brain and Language, 94*, 347-366.

Stankewitz, A., Voit, H.L., Bingel, U., Peschke, C., & May, A. (2009). A new trigemino-nociceptive stimulation model for event-related fMRI. *Cephalagia* [epub ahead of print] DOI: 10.1111/j.1468-2982.2009.01968.x

Svensson, P., Henningson, C., & Karlsson, S. (1993). Speech motor control in Parkinson's disease: a comparison between a clinical assessment protocol and a quantitative analysis of mandibular movements. *Folia Phoiatrica, 45*, 157-164.

Takahashi, T., Miyamoto, T., Terao, A., & Yokoyama, A. (2007). Cerebral activation related to the control of mastication during changes in food hardness. *Neuroscience, 145*, 791-794.

Talairach, J., & Tournoux, P. (1988). *Co-planar stereotaxic atalas of the human brain*. New York, NY: Thieme.

Taniwaki, T., Okayama, A., Yoshiura, T., Togao, O., Nakamura, Y., Yamasaki, T., et al. (2006). Functional network of the basal gaglia and cerebellar motor loops in vivo: Different activation patterns between self-initiated and externally triggered movements. *NeuroImage, 31,* 745-753.

Terao, Y., Ugawa, Y., Yamamoto, T., Sakurai, Y., Masumoto, T., Abe, O., et al. (2007). Primary face motor area as the motor representation of articulation. *Journal of Neurology, 254*, 442-447.

Terumitsu, M., Fujii, Y., Suzuki, K., Kwee, I.L., & Nakada, T. (2006). Human primary motor cortex shows hemispheric specialization for speech. *NeuroReport, 17*, 1091-1095.

Tononi, G., Sporns, O., & Edelman, G.M. (1999). Measures of degeneracy and redundancy in biological networks. *Proceedings of the National Academy of Sciences of the United States of America, 96*, 3257-3262.

Tuller, B., & Kelso, J.A. (1984). The timing of articulatory gestures: evidence for relational invariants. *The Journal of the Acoustical Society of America, 76*, 1020-1036.

Tunik, E., Rice, N.J., Hamilton, A., & Grafton, S.T. (2007). Beyond grasping: representation of action in human anterior intraparietal sulcus. *NeuroImage, 36*(S2), T77-T86.

Voisin, J., Bidet-Caulet, A., Bertrand, O., & Fonlupt, P. (2006). Listening in silence activates auditory areas: a functional magnetic resonance imaging study. *The Journal of Neuroscience, 26*, 273-278.

Von Krosigk, M., & Smith, A.D. (1991). Descending projections from the substantia nigra and retrorubral field to the medullary and pontomedullary reticular formation. *The European Journal of Neuroscience, 3*, 260-273.

Weismer, G. (2006). Philosophy of research in motor speech disorders. *Clinical Linguistics and Phonetics, 20*, 315-349.

Wildgruber, D., Ackermann, H., & Grodd, W. (2001). Differential contributions of motor cortex, basal ganglia, and cerebellum to speech motor control: effects of syllable repetition rate evaluated by fMRI. *NeuroImage, 13*,101-109.

Wise, R.S.J., Green, J., Buchel, C., & Scott, S.K. (1999). Brain regions involved in articulation. *Lancet, 353*, 1057-1061.

Zelenin, P.V., Grillner, S., Orlovsky, G.N., & Deliagina, T.G. (2003). The pattern of motor coordination underlying the roll in the lamprey. *The Journal of Experimental Biology, 206*, 2557-2566.

Zhang, S.P., Davis, P.J., Bandler, R., & Carrive, P. (1994). Brain stem integration of vocalization: role of the midbrain periaqueductal gray. *Journal of Neurophysiology, 72*, 1337-1356.

Zhang, Y.T., Geng, Z.J., Zhang, Q., Li, W., & Zhang, J. (2006). Auditory cortical responses evoked by pure tones in healthy and sensorineural hearing loss subjects: functional MRI and magnetoencephalography. *Chinese Medical Journal, 1191*, 1548-1554.

Ziegler, W. (2002). Task-related factors in oral motor control: Speech and oral diadochokinesis in dysarthria and apraxia of speech. *Brain and Language, 80,* 556-575.

Ziegler, W. (2003). Speech motor control is task-specific: evidence from dysarthria and apraxia of speech. *Aphasiology, 17,* 3-36.

Ziegler, W., & von Cramon, D. (1986a). Disturbed coarticulation in apraxia of speech: acoustic evidence. *Brain and Language, 29*, 34-47.

Ziegler, W., & von Cramon, D. (1986b). Timing deficits in apraxia of speech. *European Archives of Psychiatry and Neurological Sciences, 236*, 44-49.

Ziegler, W., & von Cramon, D. (1986c). Spastic dysarthria after acquired brain injury: an acoustic study. *The British Journal of Disorders of Communication, 21*, 173-187.

Zimmerman, E., & Barlow, S.M. (2008). Pacifier stiffness alters the dynamics of the suck central pattern generator. *Journal of Neonatal Nursing, 14*, 79-86.